

Lorents Ebbesvik Flygansvær

Mathias Berg Rønning

Effect of boundary conditions and connection modelling in a nonlinear finite element analysis of a concrete dam

Master's thesis in Civil and Environmental Engineering

Supervisor: Max Hendriks and Morten Engen

June 2019

Lorents Ebbesvik Flygansvær

Mathias Berg Rønning

Effect of boundary conditions and connection modelling in a nonlinear finite element analysis of a concrete dam

Master's thesis in Civil and Environmental Engineering
Supervisor: Max Hendriks and Morten Engen
June 2019

Norwegian University of Science and Technology
Faculty of Engineering
Department of Structural Engineering





MASTER THESIS 2019

SUBJECT AREA: Computational Mechanics Concrete Structures	DATE: 11.06.2019	NO. OF PAGES: 140
---	---------------------	----------------------

TITLE:

Effect of boundary conditions and connection modelling in a nonlinear finite element analysis of a concrete dam

Effekt av randbetingelser og kontaktmodellering i en ikke-lineær elementanalyse av en damkonstruksjon i betong

BY:

Lorents Ebbesvik Flygansvær

Mathias Berg Rønning



SUMMARY:

The objective for this thesis is to assess the importance of realistic modelling of boundary conditions and connections when performing a nonlinear finite element analysis (NLFEA) of a specific concrete dam. This is done by making four FE-models of the dam, where the models have an increasing compliance with the physical problem. Only the modelling of boundary conditions and connections is varied, and the effect on displacement, crack, and stress response are then studied. The thesis also provides a method of verifying the displacement results from the FE-model of an arch dam. The displacement response of the dam is increased about 17 % from the most simplified to the most realistic model. The largest increase in displacement response is caused by modelling details in the connection between dam and bedrock. Here, the global response were notably affected when avoiding all modelled cohesion. The results show that local crack pattern and stress field near connections will be effected by how these are modelled. However, the global effect of boundary conditions and connections is damped due to the redistribution of forces allowed when using a nonlinear material model. The most realistic model includes bedrock and a connection between dam and bedrock consisting of interface elements simulating no-slip-contact in addition to a translation line constraint. It is concluded that realistic modelling of boundary conditions and connections is of importance when analyzing dam structures using NLFEA. A recommended procedure is that the most important properties of the physical problem should be listed as criteria for realistic modelling. Further, the results from the FE-model should be checked for compliance with these criteria.

RESPONSIBLE TEACHERS/
SUPERVISORS:

Professor Max Hendriks (NTNU and TU Delft)
Associate Professor Morten Engen (NTNU and Multiconsult)

CARRIED OUT AT: Department of Structural Engineering, NTNU Gløshaugen

Preface

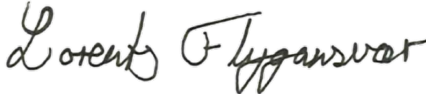
This master thesis has been written at the Norwegian University of Science and Technology (NTNU) at the Department of Structural Engineering (KT) in the first half of 2019. It concludes two years of studying in the great city of Trondheim.

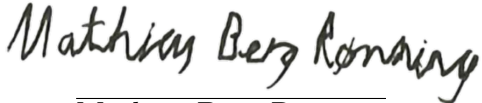
The main motivation for the present work is the desire to model structures as accurate as possible. Our interest for nonlinear finite element analysis (NLFEA) is thus not so surprising. Both of us are fascinated by large concrete structures. As a consequence of this, the thesis concerns realistic modelling of boundary conditions and connections in a NLFEA of a concrete dam. Also, with the extensive use of large concrete structures in society, a better understanding of these will be favourable in future employment.

We would like to thank our supervisors, Professor Max Hendriks (NTNU and TU Delft) and Associate Professor Morten Engen (NTNU and Multiconsult), for helpful guidance and interesting discussions. We also thank Professor Max Hendriks for giving us the possibility to present our work at the DIANA Users Meeting. Further, we extend our gratitude to Professor Jan Arve Øverli (NTNU) for help with the software used, and to Ph.D. Richard Malm (KTH) for providing the geometry files for the benchmark dam analyzed. DIANA Support have also been very helpful with modelling questions and providing background literature.

We would like to thank our parents for all the support. Lorents especially thank his father (Svein Flygansvær) for his strict logic and reasoning, and dedicate the thesis to his grandfather (Osvald Flygansvær, 1928-2019).

Trondheim 11.06.2019


Lorents Ebbesvik Flygansvær


Mathias Berg Rønning

Abstract

The objective for this thesis is to assess the importance of realistic modelling of boundary conditions and connections when performing a nonlinear finite element analysis (NLFEA) of a specific concrete dam. This is done by making four FE-models of the dam, where the models have an increasing compliance with the physical problem. Only the modelling of boundary conditions and connections is varied, and the effect on displacement, crack, and stress response are then studied. The thesis also provides a method of verifying the displacement results from the FE-model of an arch dam. The verification model is based on a hybrid solution of arch and plate theory.

The displacement response of the dam is increased by approximately 17 % from the most simplified to the most realistic model. The largest increase in displacement response is caused by modelling details in the connection between the dam and the bedrock. Here, the global response was notably affected when avoiding all modelled cohesion. The results show that the local crack pattern and the stress field near connections will be affected by how these are modelled. However, the global effect of boundary conditions and connections is damped due to the redistribution of forces allowed when using a nonlinear material model.

The most realistic model includes bedrock and a connection between dam and bedrock consisting of interface elements simulating no-slip-contact, in addition to a translation line constraint. It is concluded that realistic modelling of boundary conditions and connections is of importance when analyzing dam structures using NLFEA. A recommended procedure is that the most important properties of the physical problem should be listed as criteria for realistic modelling. Further, the results from the FE-model should be checked for compliance with these criteria.

Sammendrag

Målet med denne masteroppgaven er å vurdere viktigheten av realistisk modellering av randbetingelser og kontakt i en ikkelineær elementanalyse av en damkonstruksjon i betong. Dette er utført ved å etablere fire elementmodeller av dammen, der modellene har en økende overenstemmelse med virkeligheten. Bare modellering av randbetingelser og kontakt varierer. Dens påvirkning på forskyvning, rissmønster og spenningsfelt kan dermed vurderes. Det blir også presentert en metode for å kontrollere forskyvningsresultat fra en FE-modell av en hvelvdam. Denne verifiseringsmetoden er en hybrid av bue- og plateteori.

Forskyvningen til demningen økte med rundt 17 % fra den mest forenklede til den mest realistiske modellen. Den største økningen i forskyvning var forårsaket av detalj modellering av kontakten mellom dam og fjell. Her ble den globale responsen merkbart påvirket ved å unngå all modellert heft. Resultatene viser at lokalt rissmønster og spenningsfelt nær kontaktflater vil avhenge av hvordan interaksjonen her er modellert. Globale effekter blir derimot noe dempet ved bruk av en ikkelineær materialmodell. Dette skyldes omfordeling av krefter.

Den mest realistiske modellen inkluderer omliggende fjell og en kontaktflate mellom dam og fjell bestående av interface-element som simulerer ingen glidning ved kontakt, i tillegg til en linje-fastholdning. Det konkluderes med at modellering av randbetingelser og kontakt er viktig i ikkelineær analyse av damkonstruksjoner. En anbefalt prosedyre er å liste opp kriterier for realistisk modellering basert på den faktiske utførelsen av demningen. Videre bør resultatene fra elementmodellen kontrolleres opp mot disse kriteriene.

Contents

Preface	iii
Abstract	v
Sammendrag	vii
Abbreviations and Nomenclatures	xii
List of Figures	xiv
List of Tables	xvi
1 Introduction	1
1.1 Background and previous research	1
1.2 Problem description	2
1.3 Approach	3
1.4 Structure of the thesis	4
2 Principles and framework	5
2.1 Design of dams	5
2.2 Presentation of the dam	7
2.2.1 Geometry	7
2.2.2 Material properties	9
2.2.3 Dam-bedrock connection	10
3 Concepts of nonlinear finite element analysis of concrete dams	11
3.1 Nonlinear concrete material models	12
3.1.1 Numerical concrete models	12
3.1.2 Total Strain Crack Model	13
3.1.3 <i>fib</i> Model Code 2010	15
3.2 Geometric nonlinearities	16
3.3 Numerical solution methods	18
3.4 Boundary Conditions and Contact Properties	20
3.4.1 Interface Elements	21
3.4.2 Coulomb Friction	25

4	Solution strategy	26
4.1	Material models	26
4.1.1	Concrete material model	26
4.1.2	Verifying the concrete model	27
4.1.3	Reinforcement material model	29
4.2	Loads	31
4.2.1	Hydrostatic pressure and water intrusion	32
4.2.2	Ice-Load	33
4.2.3	Remaining Loads	33
4.2.4	Load Sequence	34
4.3	Boundary Conditions and Connections	35
4.3.1	Criteria for realistic modelling	35
4.3.2	The FE-models	37
4.3.3	Common properties of the FE-models	40
4.3.4	Verifying the interface elements	42
4.4	Finite element discretization	46
4.5	Numerical solution method	49
4.6	Geometric nonlinearities	50
4.7	Summary of modelling approach	51
5	Verification of the FE-model	53
5.1	Arch Theory	53
5.2	Plate Theory	57
5.3	Verification model	61
6	Results	63
6.1	Model I : Dam with fixed boundary conditions	63
6.2	Model II : Dam with boundary interface	67
6.3	Model III : Dam and bedrock with interface	70
6.4	Model IV : Dam and bedrock with contact interface	73
6.5	Comparison of Results	76
7	Discussion of individual analyses	82
7.1	Model I : Dam with fixed boundary conditions	83
7.2	Model II : Dam with boundary interface	85
7.3	Model III : Dam and bedrock with interface	88

7.4	Model IV : Dam and bedrock with contact interface	90
8	Discussion of results comparison	92
8.1	Comparison of displacement response	92
8.2	Comparison of stress fields	95
8.3	Comparison of crack pattern	96
9	Conclusion	98
10	Limitations and further research	100
	References	101
 Appendix		
A	MATLAB code for the verification model	106
B	DIANA Users Meeting presentation	112

Abbreviations and Nomenclatures

Abbreviations

DOF	Degree of freedom
FE	Finite element
FEM	Finite Element Method
FEA	Finite Element Analysis
NLFEA	Nonlinear Finite Element Analysis
NVE	The Norwegian Water Resources and Energy Directorate
EC-2	Eurocode-2 NS-EN-1992-1-1
ICOLD	International Commission on Large Dams
FIB	The International Federation for Structural Concrete
CAD	Computer Aided Design

Nomenclatures

Φ	Reinforcement Diameter
$\{\epsilon_{xyz}\}$	Strain vector in global coordinate system
$\{\epsilon_{nst}\}$	Strain vector in crack coordinate system
$[\mathbf{T}]$	Transformation matrix from global to crack coordinate system
$[\mathbf{D}]$	Material stiffness matrix
$\{\mathbf{x}\}$	Vector in C_n
$\{\mathbf{X}\}$	Vector in C_0
$[\mathbf{F}]$	Deformation gradient
$[\epsilon_G]$	Green strain matrix
$[\mathbf{I}]$	Identity matrix
$\{\sigma_{PK}\}$	Second Piola-Kirchhoff stress measure
V_0	Volume in C_0
$[\mathbf{K}]$	Global stiffness matrix
$\{\mathbf{R}\}$	Global load vector
$\{\mathbf{u}\}$	Displacement vector
s	Tangential arch coordinate

$\{\mathbf{a}\}$	Nodal displacement vector
$[\mathbf{N}]$	Shape function matrix
$\{\mathbf{v}\}$	Relative displacement vector
$[\mathbf{L}]$	Absolute to relative displacement transformation matrix
$[\mathbf{C}]$	Interface constitutive matrix
t_t	Tangential stress traction
t_n	Normal stress traction
c	Cohesion
ϕ	Friction angle
f_t	Maximum tensile strength
P	Pressure
g	Gravity acceleration
H	Height of dam
K_t	Tangential stiffness
K_n	Normal stiffness
μ	Coulomb friction coefficient
w	Radial arch displacement
v	Tangential arch displacement
R	Arch radius
z	Radial arch coordinate
θ	Current arch opening angle
α	Total arch opening angle
q	Radial line load
ϵ_s	Strain in an arch
κ	Curvature
σ_s	Stress in an arch
E	Young's Modulus for concrete B30
A	Cross section area of an arch
I	Second moment of area for an arch
a	Length of the plate simulating the dam
b	Height of the plate simulating the dam
u	Normal deflection of the plate simulating the dam
D	Plate stiffness for the dam
ν	Poisson's ratio
q_0	Maximum hydrostatic pressure
t	Thickness of the dam

List of Figures

1	Load carrying in shells versus plates.	5
2	Geometry of the model [16].	7
3	Reinforcement layout [15].	8
4	The real and simplified geometric form according to formulators [15].	10
5	Vertical section of the dam [17].	10
6	Discrete crack model and smeared crack model, respectively [1]. . .	13
7	Local axis in the crack plane [23].	14
8	Fixed versus rotating crack model, respectively [1].	15
9	Stress-strain relation according to <i>fib</i> Model Code 2010 [22].	15
10	Movement of a solid body [25].	16
11	Illustration of the different approaches when modelling boundary conditions. Figure inspired by reference [30].	20
12	Interface element CQ48I in DIANA [33].	21
13	Illustration of interface element configuration [31].	22
14	Relation between normal and tangential traction using the Coulomb Friction model [22].	25
15	Setup of material test in DIANA	27
16	Stress-Strain relation for the FIB Model Code 2010 Total Strain Crack Model from a material test in DIANA	28
17	Reinforcement stress-strain relation given as input in DIANA	29
18	The surfaces defined as reinforcement grids in DIANA	30
19	Illustration of the applied loads in the model. Hydrostatic-pressure and ice-load are highlighted in white and red, respectively.	31
20	The analysis set-up in DIANA	34
21	Model I versus Model II	37
22	Model III versus Model IV	38
23	Illustration of the boundary conditions applied to the bedrock	40
24	The simplified dam first considered, to validate the interface	42
25	Slide validation model in DIANA	43
26	Tangential stress plotted against tangential displacement.	43
27	Cauchy stress in z-direction for the first and the last load step, respectively.	44
28	Normal stress plotted against normal displacement for both tension and compression	45

29	The CHX60 element in DIANA [33]	46
30	The mesh used in the analyses seen from downstream	47
31	The mesh used in the analyses seen from upstream	48
32	Static model of an arch [40]	53
33	Deformation of an arch [18].	54
34	Polar plot of a clamped arch, deformed and undeformed.	56
35	Plate model resembling the dam structure [41]	57
36	Dam deformation along a centered vertical section, according to plate theory.	60
37	Part of the dam considered in the numerical validation.	62
38	MATLAB-plot of the deformed and undeformed dam given as col- ored and transparent graph, respectively.	62
39	Total displacement contour plot for Model I.	63
40	Total displacement of dam bottom for Model I.	63
41	Reinforcement stresses in global Z-direction for Model I.	64
42	Scaled reinforcement stresses in global Z-direction for Model I.	64
43	Crack strains on the downstream side in Model I.	65
44	Crack strains on the upstream side in Model I.	65
45	Principal stress field on the downstream side in Model I.	66
46	Principal stress field on the upstream side in Model I.	66
47	Total displacement contour plot for Model II.	67
48	Interface relative displacement for Model II.	67
49	Principal stress field on the downstream side for Model II.	68
50	Principal stress field on the upstream side for Model II.	68
51	Crack strains on the downstream side for Model II.	69
52	Crack strains on the upstream side for Model II.	69
53	Total displacement contour plot for Model III.	70
54	Interface relative displacement for Model III.	70
55	Principal stress field on the downstream side for Model III.	71
56	Principal stress field on the upstream side for Model III.	71
57	Crack strains on the downstream side in Model III.	72
58	Crack strains on the upstream side in Model III.	72
59	Total displacement contour plot for Model IV.	73
60	Interface relative displacement for Model IV.	73
61	Principal stress field on the downstream side in Model IV.	74

62	Principal stress field on the upstream side in Model IV.	74
63	Crack strains on the downstream side in Model IV.	75
64	Crack strains on the upstream side in Model IV.	75
65	Global X-displacement along the dam crest for the different models. The spillway is at the origin.	76
66	Global X-displacement along a vertical section for the different models.	77
67	The displacement-load relationship for the different models.	78
68	Crack pattern from Model IV (a) and the real crack pattern [17] (b).	79
69	Stress comparison, downstream.	80
70	Stress comparison, upstream.	81
71	False anchoring	86
72	Discretization of the interface to isolate radial and circumferential properties	88

List of Tables

1	Material properties [15].	9
2	Summary of mesh information	48
3	Summary of analysis input	52
4	The deflection normal to the plate for different b/a ratios [41].	59

1 Introduction

1.1 Background and previous research

Concrete structures are often used in civil engineering. Many of which with an impressive size and load carrying capacity. In the present work, the focus will be on a concrete dam. Design of such structures is challenging, and a thorough approach is of great importance to ensure reliability. In finite element analyses of dams, an important aspect is the modelling of boundary conditions and connections. There exist guidelines with recommended procedures for this [1]. However, it was difficult to find research concerning the actual response effect of this modelling. The main motivation for this thesis is a desire to shed light on and assess the importance of realistic modelling of boundary conditions and connections.

Dams have been built since ancient times, and the oldest dams are almost 5 000 years. In those times, the main propose of dams was to ensure water supply and irrigation. When civilizations became larger, dams could also serve the need for flood control and energy production. In the late nineteenth century, the first hydroelectric power plants for generation of electricity were established. They have steadily increased in use, and today 24 % of all electricity is produced by such power plants [2] [3].

As a consequence of society's increasing demand for reliable and effective dams, the *International Commission of Large Dams* (ICOLD) was formed. ICOLD's main goal is to share knowledge concerning project design and analyses, and extensive research makes the organization able to set standards and make guidelines for dam design [4] [5]. The numerical examples in the present work are based on a former benchmark dam presented by ICOLD.

1.2 Problem description

The objective for this thesis is to assess the effect of different degrees of realistic modelling of boundary conditions and connections when performing an NLFEA of a specific concrete dam.

The research questions considered are:

- How should the boundary conditions and connections of the dam be modelled most realistic?
- How do different degrees of realistic modelling of boundary conditions and connections affect the response of the dam?
- How to verify the results from the FE-model of dam structures?

1.3 Approach

In the present work, the following approach has been made:

- Make criteria for realistic modelling of boundary conditions and connections in an FE-model of the dam. These criteria are based solely on the real execution of the dam.
- Make four different FE-models with an increasing level of realistic modelling of boundary conditions and connections.
- Make a procedure to verify the results from the FE-model of the dam.
- Assess the analyses results to see how the models fulfill the criteria for realistic modelling.
- Assess the effect of different degrees of realistic modelling of boundary conditions and connections. This is done by comparing the results from the different models.

The FEA-software DIANA [6] is exclusively used in all analyses in the present work.

1.4 Structure of the thesis

This master thesis is divided into ten chapters.

- *Chapter 2* gives an introduction to design of arch dams and presents the specific dam considered.
- *Chapter 3* presents all the necessary theory to solve the problem description.
- *Chapter 4* concerns the approach in the design of the FE-models.
- *Chapter 5* comprises the verification of the FE-model.
- *Chapter 6* presents the results from the analyses.
- *Chapter 7* contains a discussion of the results from the individual analyses and determine how each model fulfill the criteria for realistic modelling.
- *Chapter 8* contains a discussion of the effect of different degrees of realistic modelling.
- *Chapter 9* is the conclusions draw from the study.
- *Chapter 10* contains limitations of the present study, and suggestion for further work.

2 Principles and framework

In this chapter, the principle behind load carrying of arch dams is presented. Further, some general framework for designing of dams is reviewed. The chapter ends with presenting the specific dam used as basis for all numerical simulations in the present work.

2.1 Design of dams

Arch dams are constructed in a way that utilizes the best quality of concrete; compression capacity. The geometric shape will cause membrane action to dominate rather than plate action, as illustrated in figure 1. This yields lower displacement response and stress amplitudes in the structure, thus allowing for less material use or larger loads. This effect of arches and shells is ancient knowledge and is excellent when large loads should be carried by relatively slender structures. However, such types of structures depend highly on the integrity and execution of the supports. Shell structures will tend to straighten out, and if this is not prohibited by the supports, the membrane action will be lost.

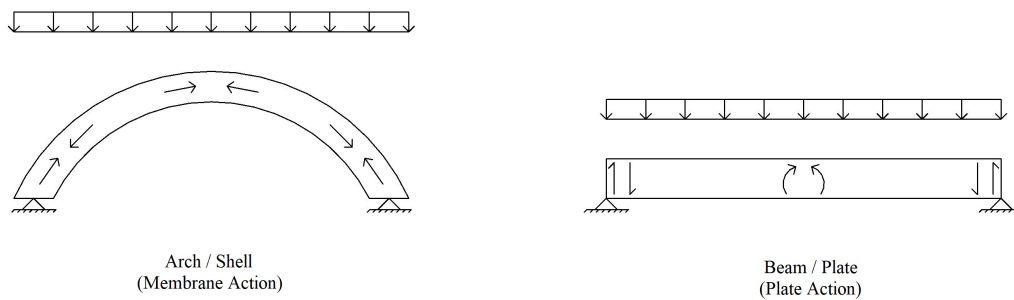


Figure 1: Load carrying in shells versus plates.

Even though arches and shells are well known, this is not to say that these are straightforward structures to analyze. On the contrary, the geometric shape makes shell design challenging. Arch dams are therefore complex and require careful analysis and design. Dams are usually designed with an FEA using linear material models, combined with post-processing tools to determine the required reinforcement [7]. An example of a post-processing tool is the iteration method [8]. Many analysts, for instance in Multiconsult [9], include some contact formulation between dam and bedrock, which requires a nonlinear finite element analysis. With the computational power presently available, a complete analysis including a nonlinear formulation of all of the most important aspects for the structural response can be executed. With the possibility NLFEA gives in capturing the real response of the structure, this almost serves as a computer-simulated experiment.

In Norway, The Norwegian Water Resources and Energy Directorate (NVE) is the responsible authority for control of dam safety. All aspects of building dams are given in Norwegian laws [10], and NVE controls the project's compliance with these. NVE also provides informative guidelines on the design of dam facilities [11]. Since most dam structures are made of reinforced concrete, Eurocode-2 [12] gives the overall guidelines for the structural design and detailing. The International Federation for Structural Concrete (*fib*) has also made a standard for design of concrete structures [13]. This Model Code focuses on numerical simulation of concrete, where several material models are presented. The *fib* Model Code also present several methods for assessing the structural reliability of concrete structures.

Although the finite element method is dominating in structural analysis and design today, many dams were constructed before the present computer power was available. As a consequence of this, there exist several approximate methods for dam design. Many of these methods are developed on behalf of The United States Government [14]. Verification of the numerical model by such methods are beneficial. Hence, careful checking of the results by simplified and well-based theoretical approaches should be emphasized in any structural design.

2.2 Presentation of the dam

The dam analyzed in the present work is from a previous benchmark workshop hosted by the ICOLD. This was the 14th benchmark workshop and took place in Sweden in 2017. Here, several case studies of dams had been prepared, including a nonlinear finite element analysis of a concrete arch dam. In this case, the goal was to assess the response in terms of displacement and cracking, due to temperature variation. The CAD-geometry and other necessary information were given to the participants to make comparable numerical models [15]. One of the challenges in the benchmark was the handling of boundary conditions and connections. Therefore, this case study seemed appropriate to use as the basis for the numerical simulations in this thesis, despite that the present work has different goals than the benchmark. The rest of this section presents the geometry and information provided by the formulators of the benchmark, which is used in the design of the different FE-models in the present work.

2.2.1 Geometry

Figure 2 shows the geometry of the dam, provided as a geometry input-file.

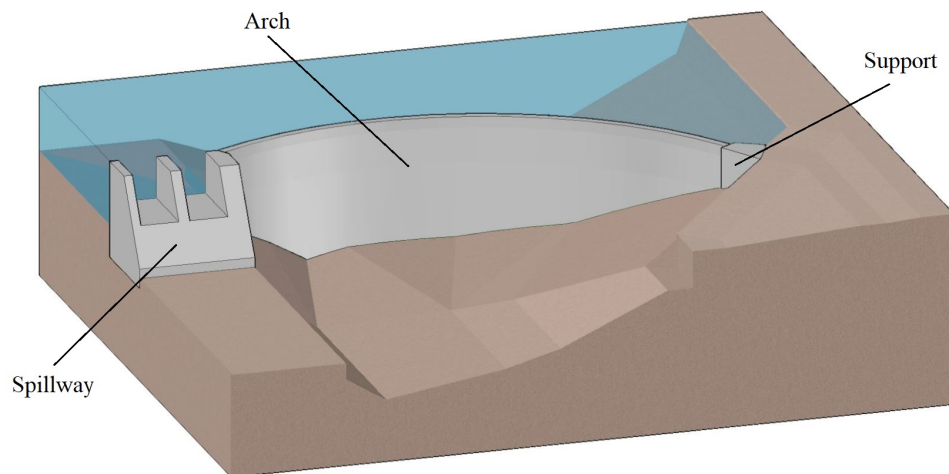


Figure 2: Geometry of the model [16].

The crest length of the arch is approximately 170 m, and the radius is 110 m. The maximum height of the dam is about 40 m. The height and the width of the spillway are 30 m and 35 m, respectively. As shown in figure 2, the spillway consists of two open sections. The width of these is 12 m. The thickness of the arch part of the dam varies from 2.5 m at the crest to 5 m at the bottom. The bedrock has an area of 193 x 225 m in the horizontal plane, and the height varies from 20 to 60 m.

Figure 3 shows the reinforcement in the arch part of the dam, seen from above.

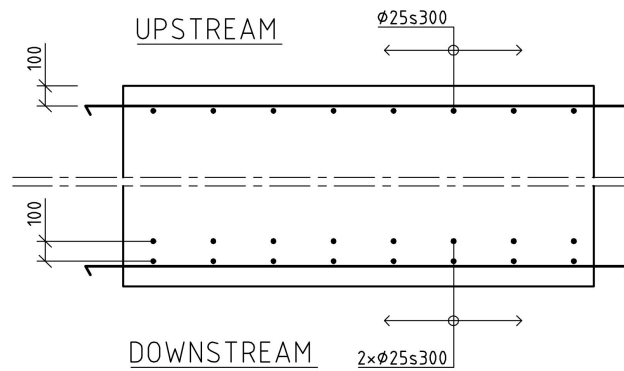


Figure 3: Reinforcement layout [15].

The reinforcement consists of a grid at the upstream and the downstream side and one layer of vertical bars at the downstream side. The concrete cover and distance between reinforcement layers are 100 mm. The spacing between the bars is 300 mm, and all the reinforcing bars have a diameter of 25 mm. No information about reinforcement in the spillway and support is provided.

2.2.2 Material properties

The given parameters for the concrete, reinforcement, and bedrock are given in table 1. This is the only material information provided by the formulators.

Property	Unit	Concrete	Reinforcement	Bedrock
Young's Modulus	GPa	33	200	40
Poisson's ration	-	0.2	0.3	0.15
Density	kg/m ³	2300	7800	2700
Compression strength	MPa	38	-	-
Tensile strength	MPa	2.9	-	-
Yield stress	MPa	-	360	-
Ultimate stress	MPa	-	600	-
Ultimate strain	-	-	0.15	-

Table 1: Material properties [15].

The concrete properties correspond to B30 concrete according to Eurocode-2. No effects of creep or shrinkage are modelled in the present work. Due to limited information, linear elastic material properties of the bedrock is assumed.

2.2.3 Dam-bedrock connection

In reality, the bottom of the arch part of the dam is excavated into the rock, as seen in figure 4 and 5.

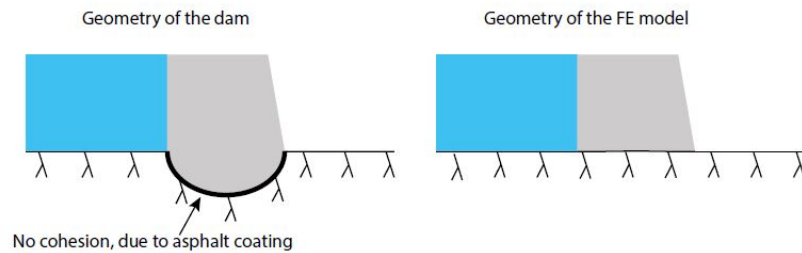


Figure 4: The real and simplified geometric form according to formulators [15].

Only the information in figure 4 is provided regarding the dam-bedrock connection. Under construction, asphalt coating was applied at the bedrock surface to avoid cohesion and reduce friction in the connection. The geometry file provided by the formulators is simplified by ignoring the excavated bulge in the bedrock, as illustrated in figure 4.

According to the benchmark information, the participants should decide on their own how to model the boundary conditions and connections.

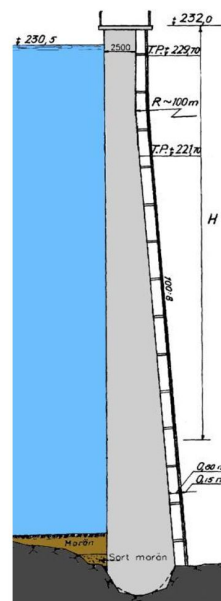


Figure 5: Vertical section of the dam [17].

3 Concepts of nonlinear finite element analysis of concrete dams

This chapter contains the theory used to solve the problem description. The theory mainly concerns nonlinear finite element analyses, and can be categorized as follows [18]:

- **Material nonlinearity.** The material properties are dependent on the state of stress or strain and are not constant. An example is the cracking of concrete.
- **Geometric nonlinearity.** The equilibrium equations are written with respect to the deformed state of the structure. An example is the determination of buckling load.
- **Contact nonlinearity.** The interaction between bodies is dependent on the relative position. Here, the simplification of translation or rotation fixed connections is unrealistic.

3.1 Nonlinear concrete material models

In this section, some theory behind the numerical simulation of concrete will be presented. The focus will be on the *fib* Model Code 2010 material model, which is solely used in the proceeding.

3.1.1 Numerical concrete models

Concrete is characterized by a low tensile strength. In a uniaxial tensile test, concrete shows a linear stress-strain curve up to 90 % of the maximum tensile stress [19]. Failure does not occur when the highest level of tensile stress is reached; the material shows a softening behaviour. Hence, concrete should not be treated as a perfect-brittle material, but rather as a quasi-brittle material. Uniaxial test of concrete in compression displays a highly nonlinear stress-strain curve. Only up to 30 % of the ultimate compressive strength can be considered as linear. The stiffness will then decrease, and at 70-75 % cracking will occur. After the maximum stress is reached, some softening behaviour is observed [20].

In numerical simulations of concrete, there are mainly two approaches for crack modelling; the discrete and the smeared crack model. The discrete method is less used because it demands a loss of connectivity in the mesh and cracks are restricted to form at given locations. In the smeared crack model, the cracks are modelled by reducing the stiffness where the crack forms, but not altering the connectivity of the mesh. This is not consistent with the discontinuity of a crack, but is more suited for numerical simulation and gives all necessary information about the cracks. The *fib* Model Code 2010 material model is based on the smeared crack approach.

Figure 6 illustrates both the smeared and discrete crack approach.

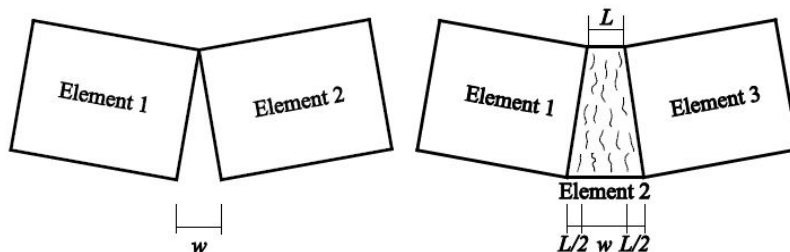


Figure 6: Discrete crack model and smeared crack model, respectively [1].

3.1.2 Total Strain Crack Model

The Total Strain Crack Model was proposed by Vecchio and Collins [21] and is based on modified compression field theory. The theory that follows is mainly adopted from DIANA User's Manual [22], Rots and Blaauwendraad [23] and the Energiforsk Guidelines [1].

The Total Strain Crack Model evaluates the strain in a coordinate system defined by the crack and establishes the constitutive relation in the same coordinate system. It starts with incrementally updating the global element strain vector, $\{\epsilon_{xyz}\}$:

$$\{\epsilon_{xyz}\}_{i+1} = \{\epsilon_{xyz}\}_i + \{\Delta\epsilon_{xyz}\} \quad (1)$$

Further, the strain is transformed to the direction given by the crack. This direction is assumed to coincide with the principal strain direction, which is evaluated by finding the eigenvectors of the strain tensor. The strain tensor and the eigenvalue problem are defined as:

$$[\epsilon_{xyz}] = \begin{bmatrix} \epsilon_{xx} & \epsilon_{xy} & \epsilon_{xz} \\ \epsilon_{yx} & \epsilon_{yy} & \epsilon_{yz} \\ \epsilon_{zx} & \epsilon_{zy} & \epsilon_{zz} \end{bmatrix}, \quad [\epsilon_{xyz}]\{\mathbf{x}\} = \lambda\{\mathbf{x}\} \quad (2)$$

Where $\{\mathbf{x}\}$ and λ are the eigenvectors and eigenvalues, respectively. The new coordinate system, nst , is then spanned by the eigenvectors, as seen from figure 7:

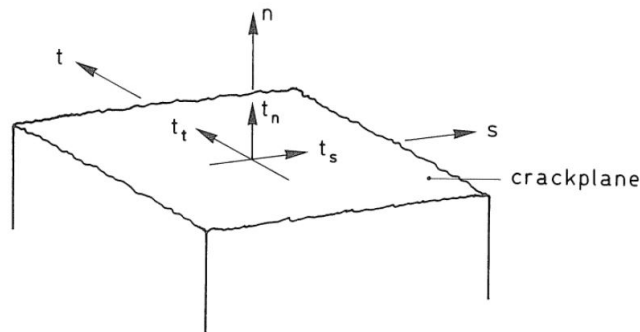


Figure 7: Local axis in the crack plane [23].

The transformation matrix, $[\mathbf{T}]$, which defines a transition from strain in the global coordinate system to strain in the coordinate system spanned by the eigenvectors, can be defined [22]:

$$\{\epsilon_{nst}\} = [\mathbf{T}] \{\epsilon_{xyz}\} \quad (3)$$

Further, the stiffness material matrix can be stated in the following form:

$$[\mathbf{D}] = [\mathbf{T}]^T [\mathbf{D}_{tangent}] [\mathbf{T}] \quad (4)$$

$[\mathbf{D}_{tangent}]$ is the tangent material stiffness matrix in the nst -coordinate system. This matrix can be divided into four submatrices in the form:

$$[\mathbf{D}_{tangent}] = \begin{bmatrix} [\mathbf{D}_{nn}] & [\mathbf{D}_{n\theta}] \\ [\mathbf{D}_{\theta n}] & [\mathbf{D}_{\theta\theta}] \end{bmatrix} \quad (5)$$

$[\mathbf{D}_{nn}]$ describes the normal stiffness, while $[\mathbf{D}_{\theta\theta}]$ describes the shear stiffness. $[\mathbf{D}_{n\theta}]$ and $[\mathbf{D}_{\theta n}]$ represent the coupling terms between the normal and shear stiffness. These four matrices are evaluated in the nst -coordinate system.

There are two ways of calculating the transformation matrix, $[T]$. In both approaches, the cracks initiate in the integration points when the maximum principal stress is equal to the tensile strength. In the first approach, the crack direction is fixed in the direction of the first initiated crack, regardless of change in stress or strain state caused by further loading. This is called fixed crack, and the $[T]$ -matrix is constant. In the other model, the crack direction is updated according to the current principal strain direction. Hence, the $[T]$ -matrix will be updated during loading. This is the rotating crack model, which is most conservative and recommended by the Dutch Guidelines [24]. Figure 8 illustrates both approaches.

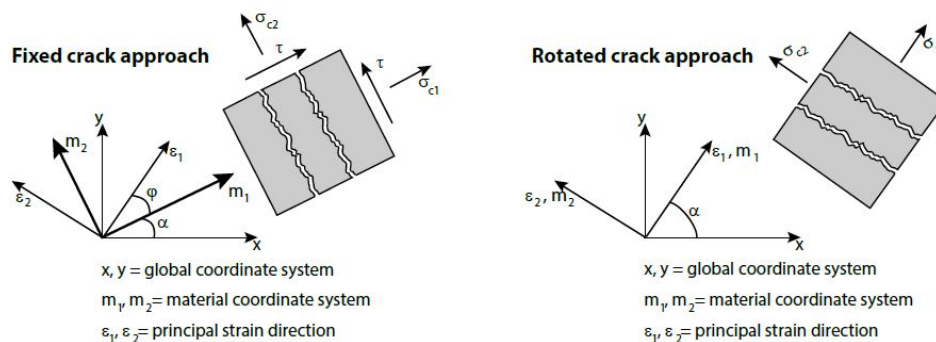


Figure 8: Fixed versus rotating crack model, respectively [1].

3.1.3 *fib* Model Code 2010

The *fib* Model Code 2010 material model in DIANA is a smeared crack and crushing, rotating crack model. The only input is the concrete grade according to Eurocode-2, B30 in this case. The stress-strain relation in figure 9 is then used by DIANA as the basis for the concrete properties in the crack coordinate system.

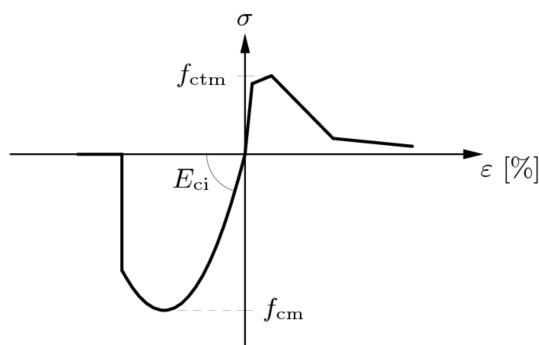


Figure 9: Stress-strain relation according to *fib* Model Code 2010 [22].

3.2 Geometric nonlinearities

The theory that follows is mainly adopted from Mathisen [25], Cook et al. [18], and the DIANA User Manual [26].

Figure 10 shows a transition from a reference state, C_0 , to a current state, C_n , of a solid body in physical space.

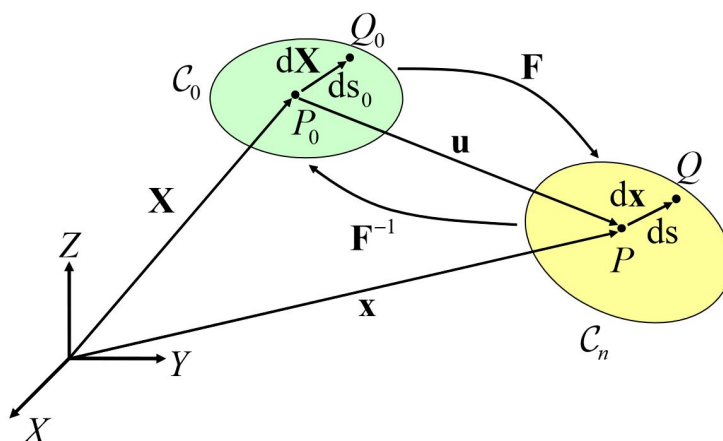


Figure 10: Movement of a solid body [25].

In the proceedings, it is assumed that a Lagrangian approach is used, where all field variables are referred to the initial condition, C_0 . This is opposed to Eulerian/Updated Lagrange approach, where the field variables are referred to the current state, C_n . The Lagrangian approach is default in DIANA and is also stated as most attractive for structural mechanics problems by Mathisen [25].

The mapping from the reference state to the current state of a vector, between the same two points in a solid body, is given by the deformation gradient, $[\mathbf{F}]$:

$$\{d\mathbf{x}\} = [\mathbf{F}] \{d\mathbf{X}\} \quad \text{where} \quad [\mathbf{F}] = \begin{bmatrix} \frac{\partial x}{\partial X} & \frac{\partial x}{\partial Y} & \frac{\partial x}{\partial Z} \\ \frac{\partial y}{\partial X} & \frac{\partial y}{\partial Y} & \frac{\partial y}{\partial Z} \\ \frac{\partial z}{\partial X} & \frac{\partial z}{\partial Y} & \frac{\partial z}{\partial Z} \end{bmatrix} \quad (6)$$

By using the Green strain measure:

$$[\boldsymbol{\epsilon}_G] = \frac{1}{2}([\mathbf{F}]^T[\mathbf{F}] - [\mathbf{I}]) \quad (7)$$

which is dependent on the deformation gradient, this will give a more exact representation of strain compared to the engineering strain measure. The difference between these measures is that the Green strain will include a more accurate change of length between two points. An example of this is when one point is subjected to a displacement normal to the vector between the points. The Green strain takes the length change of this movement into account, while the engineering measure ignores it. The inclusion of nonlinear geometry is necessary for problems where the deformation can affect the stress state significantly, such as large deformation or buckling analyses.

When establishing the weak form of the problem, an increment in the internal energy of the body becomes:

$$\delta U = \int_{V_0} \{\delta \boldsymbol{\epsilon}_G\}^T \{\boldsymbol{\sigma}_{PK}\} dv_0 \quad (8)$$

Here, $\{\delta \boldsymbol{\epsilon}_G\}$ is an increment in the Green strain, and $\{\boldsymbol{\sigma}_{PK}\}$ is the Second Piola-Kirchhoff stress measure, work-conjugate to the Green strain. Both are arranged as 6×1 matrices. Note that the Cauchy stress measure is used in DIANA, which is defined as force per deformed area. The Piola-Kirchhoff stress is thus transformed to the Cauchy stress. When using the Green strain measure in the weak form, the resulting internal force vector will be nonlinear dependent on the nodal displacements.

For more thorough information on geometrically nonlinear problems, it is referred to Chatzi [27].

3.3 Numerical solution methods

The theory that follows is mainly adopted from Mathisen [28].

A significant difference between linear and nonlinear finite element analysis is the numerical solution method. A nonlinear problem yields the following equation to solve:

$$[\mathbf{K}(\mathbf{u})]\{\mathbf{u}\} = \{\mathbf{R}(\mathbf{u})_{ext}\} \quad (9)$$

Here, $[\mathbf{K}(\mathbf{u})]$ is the global stiffness matrix, $\{\mathbf{u}\}$ is the nodal displacement vector and $\{\mathbf{R}(\mathbf{u})_{ext}\}$ is the global external force vector. This problem cannot be solved by inverting $[\mathbf{K}(\mathbf{u})]$, as in a linear analysis. The problem has to be iteratively solved by requiring equilibrium between internal and external forces:

$$\{\mathbf{R}(\mathbf{u})_{int}\} = \{\mathbf{R}(\mathbf{u})_{ext}\} \quad (10)$$

where the internal load vector $\{\mathbf{R}(\mathbf{u})_{int}\} = [\mathbf{K}(\mathbf{u})]\{\mathbf{u}\}$. Equation 10 has to be iteratively solved for $\{\mathbf{u}\}$. This is done by dividing the external load vector into several parts, called increments. By successfully adding increments and updating the displacement to satisfy equation 10 for each one, the final configuration can be achieved.

To satisfy equation 10 within a load step, the residual, or out-of-balance force, is linearized around a point on the equilibrium function:

$$\{\mathbf{R}(\mathbf{u})_{res}\}_{i+1} = \{\mathbf{R}(\mathbf{u})_{ext} - \mathbf{R}(\mathbf{u})_{int}\}_{i+1} \approx \{\mathbf{R}(\mathbf{u})_{res}\}_i + \left[\frac{\partial \mathbf{R}_{res}}{\partial \mathbf{u}} \right]_i \{\Delta \mathbf{u}\}_i \quad (11)$$

By requiring the residual in step $i + 1$ to be zero, the incremental update in nodal displacement can be found:

$$\{\mathbf{R}(\mathbf{u})_{res}\}_i = - \left[\frac{\partial \mathbf{R}_{res}}{\partial \mathbf{u}} \right]_i \{\Delta \mathbf{u}\}_i = [\mathbf{K}_t]_i \{\Delta \mathbf{u}\}_i \quad (12)$$

In equation 12, $[\mathbf{K}_t]_i$ is the tangential stiffness matrix. Equation 12 can be solved for $\{\Delta \mathbf{u}\}_i$ just like in linear analyses, and iterated until the required accuracy in the load step is reached. This accuracy can be specified in NLFEA programs as numerical convergence criteria. The convergence criteria are usually related to the residual force or out-of-balance energy. These are defined in DIANA as [26]:

$$\text{Force norm ratio} = \frac{\sqrt{\mathbf{R}_{res,i}^T \mathbf{R}_{res,i}}}{\sqrt{\mathbf{R}_{int,1}^T \mathbf{R}_{int,1}}} \quad (13)$$

$$\text{Energy norm ratio} = \frac{\Delta \mathbf{u}_i^T (\mathbf{R}_{int,i+1} + \mathbf{R}_{int,i})}{\Delta \mathbf{u}_0^T (\mathbf{R}_{int,1} + \mathbf{R}_{int,0})} \quad (14)$$

In equations 13 and 14, the notation $i = 0$ is used for the configuration before the load step is applied and $i = 1$ are the first equilibrium iteration in the load step. The force norm in equation 13 is the ratio of the force residual over the internal force. The energy norm in equation 14 can be considered as the ratio between the internal energy added in the last iteration over the internal energy added in the first iteration. Convergence with a reasonable size of the norms is always preferred to get accurate results, but no convergence in some increments are usually not critical and will not affect the final result.

The above discussion focuses on finding the nodal displacement by a Newton-Raphson procedure *within* a load step. The load step, or predictor step, can be done in several ways. Increments of the external load can be applied, and this method is called load control. Another way is to prescribe the displacement, which is called displacement control. It is possible to combine these two methods in different ways. The Arc-Length Method is an example of such a combination [29].

3.4 Boundary Conditions and Contact Properties

Contact between bodies is a very complex phenomenon. In this chapter, the necessary theory used in the present work for modelling boundary conditions and connections is presented.

According to guidelines from Energiforsk [1], there are three different ways of handling the boundary conditions in analyses of concrete dams:

- Boundary conditions directly applied to the dam:
Here, translation/rotational degrees of freedom is directly suppressed.
- Implicit modelling of the bedrock:
Here, the dam is spring supported to simulate the bedrock.
- Direct modelling of the bedrock:
The bedrock is included in the FE-model, and connection properties between dam and bedrock are defined.

The different approaches are illustrated in figure 11.

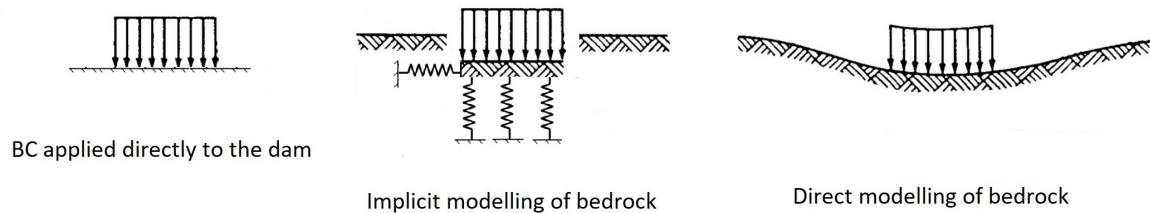


Figure 11: Illustration of the different approaches when modelling boundary conditions. Figure inspired by reference [30].

In the proceedings of this section, special finite elements called interface element are presented. These can be used in modelling the two approaches to the right in figure 11, and are used to simulate all contact in the present work.

3.4.1 Interface Elements

Interface elements are essential in the present work to simulate the connection properties between the dam and the bedrock and between the dam and a fixed boundary. In the following, the theory behind these elements will be presented. The theory is mainly adopted from the work of de Borst, Crisfield, Remmers and Verhoosel [31], Schellekens and de Borst [32], and the DIANA User's Manual [33].

Figure 12 shows the 16 node interface element CQ48I in DIANA.

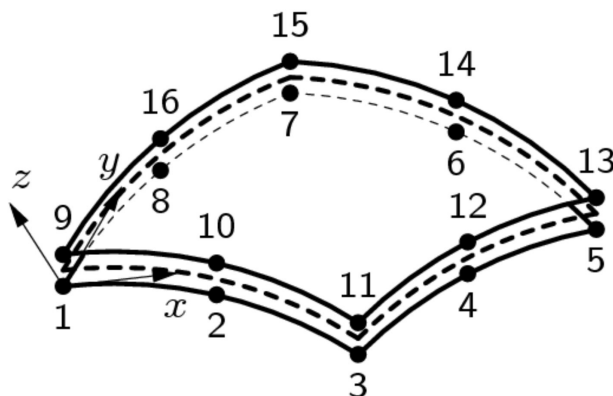


Figure 12: Interface element CQ48I in DIANA [33].

One interface element consists of two independent surface elements, as shown in figure 12. In the present work, when using the DIANA element CQ48I, the surface elements are the 8-node Serendipity. The shape functions for the surface elements are derived in a standard manner [34].

One of the node pairs in figure 12 is isolated, and the x, y, z - axis are renamed to the s, t, n - axis, respectively. Further, the nodal displacements is denoted by the letter a , and subscript corresponding to direction (s, t, n) and superscript corresponding to upper (+) or lower (-) element is used. Figure 13 will then illustrate the interface configuration.

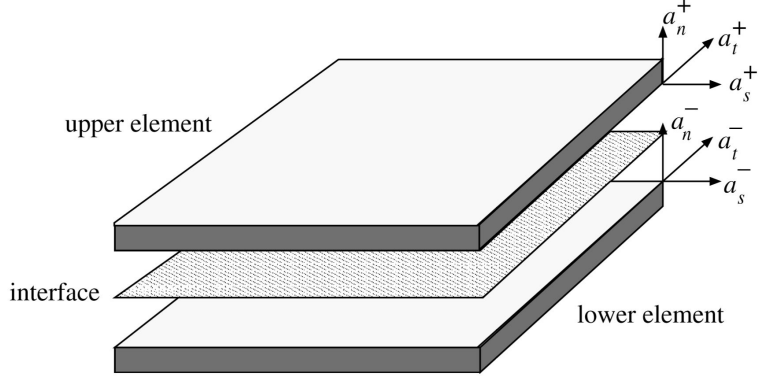


Figure 13: Illustration of interface element configuration [31].

The displacements of the upper and lower surface of the interface element are related to the nodal displacements in a standard manner, by the shape functions:

$$\{\mathbf{u}\} = [\mathbf{N}] \{\mathbf{a}\} \quad (15)$$

Where:

$$\{\mathbf{u}(n, s, t)\}^T = [u_n^- \quad u_n^+ \quad u_s^- \quad u_s^+ \quad u_t^- \quad u_t^+] \quad (16)$$

is the displacement vector function of the interface elements upper (+) and lower (-) surface. Note that each of the components of $\{\mathbf{u}\}$ is a function of the position in the interface element. Further, the nodal displacement vector must be arranged as follows, where i denotes the node pair:

$$\{\mathbf{a}\}^T = [(a_n^-)_1, \dots, (a_n^-)_{i=8}, (a_s^-)_1, \dots, (a_s^-)_{i=8}, (a_t^-)_1, \dots, (a_t^-)_{i=8}, (a_n^+)_1, \dots, (a_n^+)_{i=8}, (a_s^+)_1, \dots, (a_s^+)_{i=8}, (a_t^+)_1, \dots, (a_t^+)_{i=8}] \quad (17)$$

The matrix containing the shape functions is displayed in equation 18. In the present work, $\{\mathbf{n}\}$ is the 1×8 matrix containing the eight Serendipity shape functions.

$$[\mathbf{N}] = \begin{bmatrix} \{\mathbf{n}\} & \{\mathbf{0}\} & \{\mathbf{0}\} & \{\mathbf{0}\} & \{\mathbf{0}\} & \{\mathbf{0}\} \\ \{\mathbf{0}\} & \{\mathbf{n}\} & \{\mathbf{0}\} & \{\mathbf{0}\} & \{\mathbf{0}\} & \{\mathbf{0}\} \\ \{\mathbf{0}\} & \{\mathbf{0}\} & \{\mathbf{n}\} & \{\mathbf{0}\} & \{\mathbf{0}\} & \{\mathbf{0}\} \\ \{\mathbf{0}\} & \{\mathbf{0}\} & \{\mathbf{0}\} & \{\mathbf{n}\} & \{\mathbf{0}\} & \{\mathbf{0}\} \\ \{\mathbf{0}\} & \{\mathbf{0}\} & \{\mathbf{0}\} & \{\mathbf{0}\} & \{\mathbf{n}\} & \{\mathbf{0}\} \\ \{\mathbf{0}\} & \{\mathbf{0}\} & \{\mathbf{0}\} & \{\mathbf{0}\} & \{\mathbf{0}\} & \{\mathbf{n}\} \end{bmatrix} \quad (18)$$

The properties of the interface element should be related to the relative displacements between the upper and lower surface of the element. The relative displacements can be found by a straightforward transformation of the interface displacements:

$$\{\mathbf{v}\} = [\mathbf{L}] \{\mathbf{u}\} \Rightarrow \begin{bmatrix} v_n \\ v_s \\ v_t \end{bmatrix} = \begin{bmatrix} -1 & 1 & 0 & 0 & 0 & 0 \\ 0 & 0 & -1 & 1 & 0 & 0 \\ 0 & 0 & 0 & 0 & -1 & 1 \end{bmatrix} \begin{bmatrix} u_n^- \\ u_n^+ \\ u_s^- \\ u_s^+ \\ u_t^- \\ u_t^+ \end{bmatrix} \quad (19)$$

The constitutive matrix is introduced as:

$$[\mathbf{C}] = \begin{bmatrix} c_n & 0 & 0 \\ 0 & c_s & 0 \\ 0 & 0 & c_t \end{bmatrix} \quad (20)$$

Here, the inputs along the diagonal are the interface stiffnesses in $(\text{N}/\text{m}^2)/\text{m}$. The constitutive matrix relates the stress to the relative motion between the upper and lower surface of the interface element.

The element stiffness matrix can be found from the internal virtual work in the interface element:

$$\tilde{U} = \iint_S \{\tilde{\mathbf{v}}\}^T [\mathbf{C}] \{\mathbf{v}\} ds dt = \{\tilde{\mathbf{a}}\}^T \left(\iint_S ([\mathbf{L}] [\mathbf{N}])^T [\mathbf{C}] ([\mathbf{L}] [\mathbf{N}]) ds dt \right) \{\mathbf{a}\} \quad (21)$$

Thus, the stiffness matrix for the interface element in terms of the nodal displacements is:

$$[\mathbf{K}] = \iint_S ([\mathbf{L}] [\mathbf{N}])^T [\mathbf{C}] ([\mathbf{L}] [\mathbf{N}]) ds dt \quad (22)$$

The stiffness matrix for the interface element, based on the nodal displacements of the upper and lower elements that should be connected, is thus derived. This derivation is done by giving constitutive relations for the relative displacements between the upper and lower surface of the interface element. These surface elements are coincident with the elements that should be connected. Different constitutive relations in equation 20 can be used to simulate various contact formulations. In all four FE-models in the present work, a nonlinear elasticity material model has been used. This constitutive model can specify the normal interface stiffness in compression, in tension and the interface tangential stiffness in two orthogonal directions. The tangential stiffnesses can be taken differently depending on whether there is tension or compression in the interface.

3.4.2 Coulomb Friction

A Coulomb Friction model is used as the material model for the interface in the verification in this thesis since it addresses all properties needed in the present work. Coulomb Friction is regarded as sufficient for many engineering problems [35].

Figure 14 shows the properties of the Coulomb Friction model in DIANA.

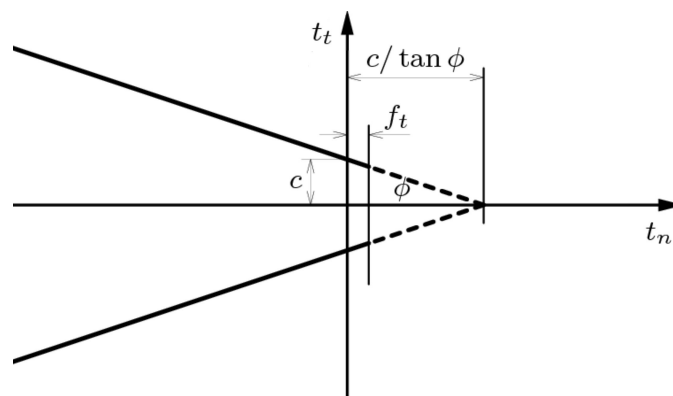


Figure 14: Relation between normal and tangential traction using the Coulomb Friction model [22].

Here, the following notations have been used:

t_t = Tangential stress traction

t_n = Normal stress traction

c = Cohesion

ϕ = Friction angle, where the friction coefficient = $\mu = \tan \phi$

f_t = Maximum tensile strength before gap occurs

The input in DIANA is the tangential and normal stiffnesses of the interface, in addition to the relation in figure 14. This yield a versatile description of the interface behaviour.

4 Solution strategy

This chapter contains the approach, or solution strategy, made in the design of the FE-models of the dam. Simple tests of important aspects are also done in order to verify the approach. According to Engen [7], a solution strategy comprises all choices made regarding kinematic compatibility, constitutive relations and equilibrium, in a numerical simulation. More specifically this can be the material models used, the nature of the loads applied and how they are acting on the structure, evaluation of the mesh and type of finite element used, and modelling of boundary connections and connections. Due to limited time, all aspects cannot be treated as thoroughly. However, all of the most important choices will be addressed to some extent. The emphasis is on the modelling of boundary conditions and connections, which is the only part of the solution strategy that varies between the four FE-models of the dam.

4.1 Material models

4.1.1 Concrete material model

The material model used in all analyses is presented in chapter 3.1. This is based on smeared cracking and crushing; the FIB Model Code 2010 Total Strain Crack Model. The reason for this choice is the international recognition FIB Model Code holds in numerical simulation of concrete. This makes it a suitable alternative to the Eurocode-2, whose material model seems too conservative concerning the fracture energy/tension softening. Eurocode-2 assumes a brittle tensile failure, as opposed to the FIB Model Code. It is considered important to use a realistic material model, not too conservative or non-conservative, as both might change the response of the entire structure in an unknown way.

4.1.2 Verifying the concrete model

To be aware of the actual behavior of the chosen concrete material model in DIANA, a simple uniaxial prescribed displacement test have been performed. This gives the stress-strain curve for the concrete, which is the only input in the Total Strain Crack Model. The extension to a 3D stress state is based on this uniaxial relation.

Figure 15 shows the set-up of the material test in DIANA, where the load is applied to the top of the cylinder as a prescribed displacement in the Z-direction. The bottom of the cylinder is modelled with interface elements between the test specimen and a fixed boundary. This is called a boundary interface in DIANA and simulates a spring support. The material model for the interface is non-linear elasticity. Here, a high normal stiffness are modelled to almost fix the base in the load direction. Further, a very low tangential stiffness is modelled to allow for lateral contraction and expansion while preventing rigid body motion. Elements with linear interpolation of displacements are used.

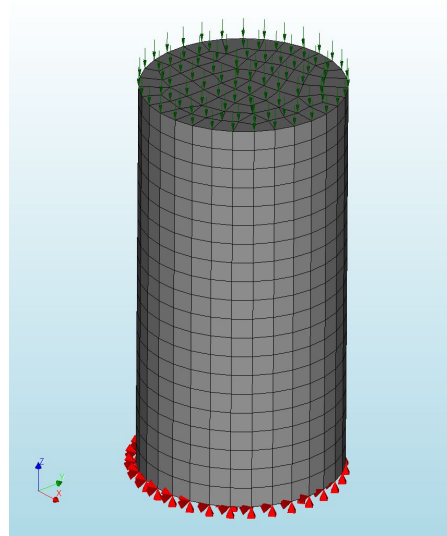


Figure 15: Setup of material test in DIANA

Figure 16 shows the resulting stress-strain relation for a centered element at the top of the test cylinder.

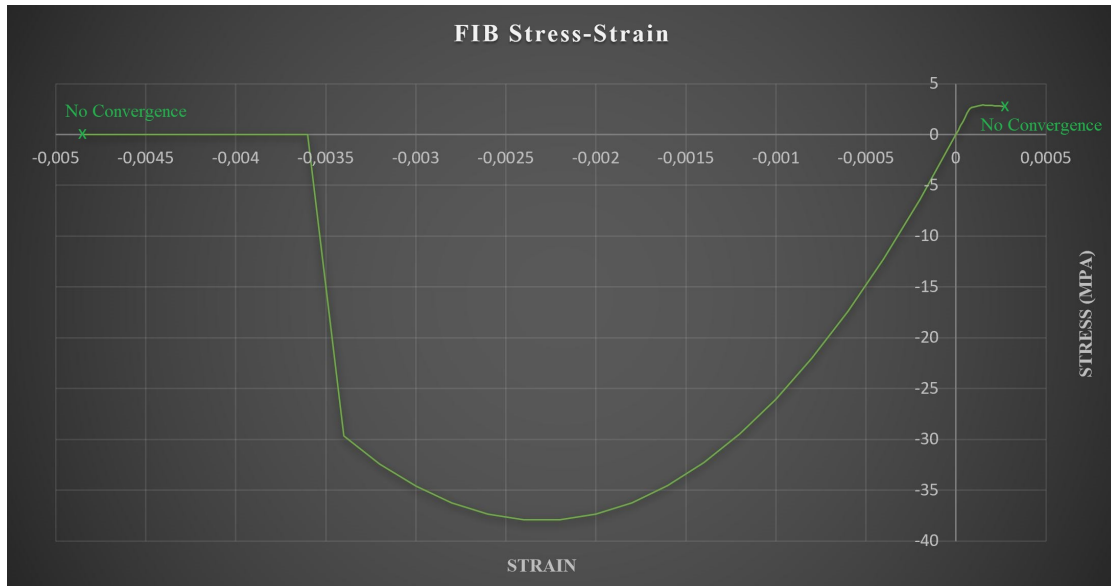


Figure 16: Stress-Strain relation for the FIB Model Code 2010 Total Strain Crack Model from a material test in DIANA

The material used is equivalent to concrete grade B30 from Eurocode-2. From figure 16, the properties in compression is very similar to the theoretical stress-strain curve from figure 9. The compressive stress reaches 38 MPa, which is the mean compressive strength of B30 concrete. It is noted that a quite large strain is possible in compression before no convergence occurs. In tension, however, the properties shown in figure 16 differs somewhat from the theoretical curve in figure 9. The test specimen exhibit tension softening after reaching the theoretical tensile strength of 2.9 MPa. However, it was expected a drop in stress before no convergence occurred. The reason for the discrepancy might be that the test specimen will show total failure after the capacity is reached. If the test was designed such that some redistribution of forces were allowed, for instance in a reinforced beam, it might be easier to trace the tension softening of the elements first prone to cracking. Despite of this discrepancy, the most important result is that some tension softening occur, which is consistent with the theoretical FIB concrete model.

4.1.3 Reinforcement material model

In the present work, embedded reinforcement in DIANA is used. This means that the reinforcement does not have degrees of freedom, so the response in the reinforcement is calculated from the displacement field of the concrete element. This implies a perfect bond between reinforcement and concrete. However, it is possible to specify bond slip in DIANA, but this is not done in the present work.

For the reinforcement steel, the uniaxial nonlinear elasticity material model in DIANA is used. In this model, the stress-strain curve for the reinforcement is the only input. This curve is based on the material properties in table 1, in combination with the recommended shape of the stress-strain curve from the Dutch Guidelines [24]. The stress-strain curve used for the reinforcement is shown in figure 17.



Figure 17: Reinforcement stress-strain relation given as input in DIANA

In the material model used in DIANA, no failure criterion is implemented. A failure criterion is necessary when assessing the ultimate capacity of the dam, but no failure is assumed in the present work. This is because the loads are applied with-

out any load factors and since the maximum strain capacity of the reinforcement is high. The information needed for the more sophisticated reinforcement material models in DIANA, such as hardening parameters, are not given in the benchmark information. Note that the stress-strain curve given in figure 17 simulates isotropic hardening after yield, but without any plasticity.

In DIANA, the reinforcement is modelled by extracting the upstream and downstream surfaces of the arch part of the dam. These are then moved radially into the dam section a length corresponding to the reinforcement cover. To simulate top and bottom cover, the surfaces are moved slightly up and trimmed by a horizontal plane at the top. The surfaces are then modelled as reinforcement grids in DIANA by giving the spacing and diameters of the reinforcing bars from figure 3. The reinforcing grid surfaces are shown in figure 18. There are three layer in total, two at the downstream and one at the upstream.

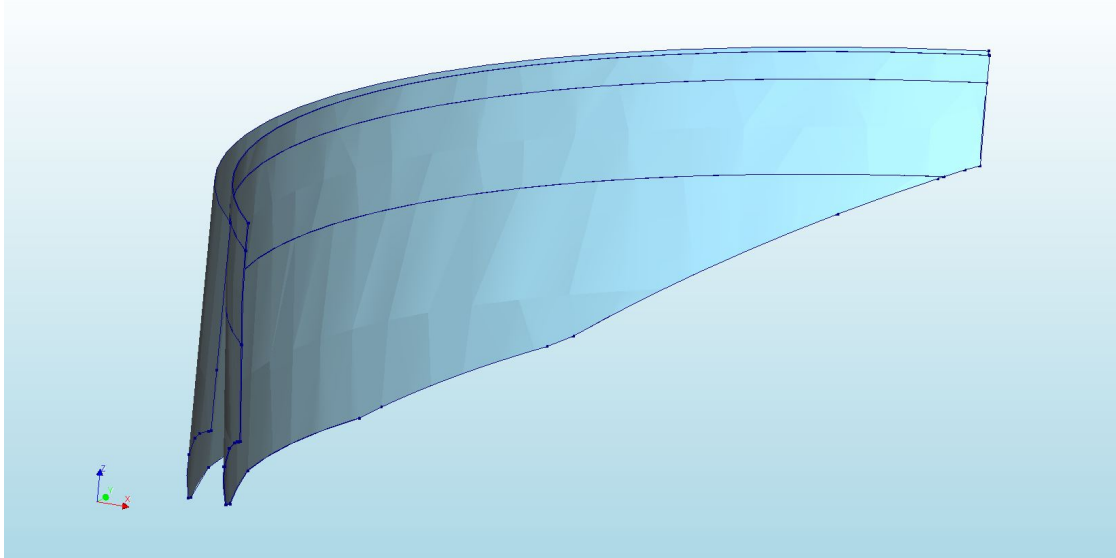


Figure 18: The surfaces defined as reinforcement grids in DIANA

4.2 Loads

In this section, the loads applied to the FE-model are presented. Only static loads without safety factors are applied; self-weight, hydrostatic-pressure and ice-load. These are chosen since they represent a common load state of the dam. It would thus be a good basis for assessing the effect of boundary conditions and connections. Temperature load was focused on in the original benchmark, but this is not included in the present work.

The self-weight is included for all shapes in the model, the hydrostatic-pressure is applied to all surfaces upstream, and the ice-load is modelled as a uniform radial surface load at the crest of the dam. Hydrostatic pressure is also applied underneath the arch part of the dam and on the entire vertical side of the spillway and support to simulate water intrusion.

Figure 19 illustrates the loads applied to the FE-model. Note that the self-weight is not shown explicitly.

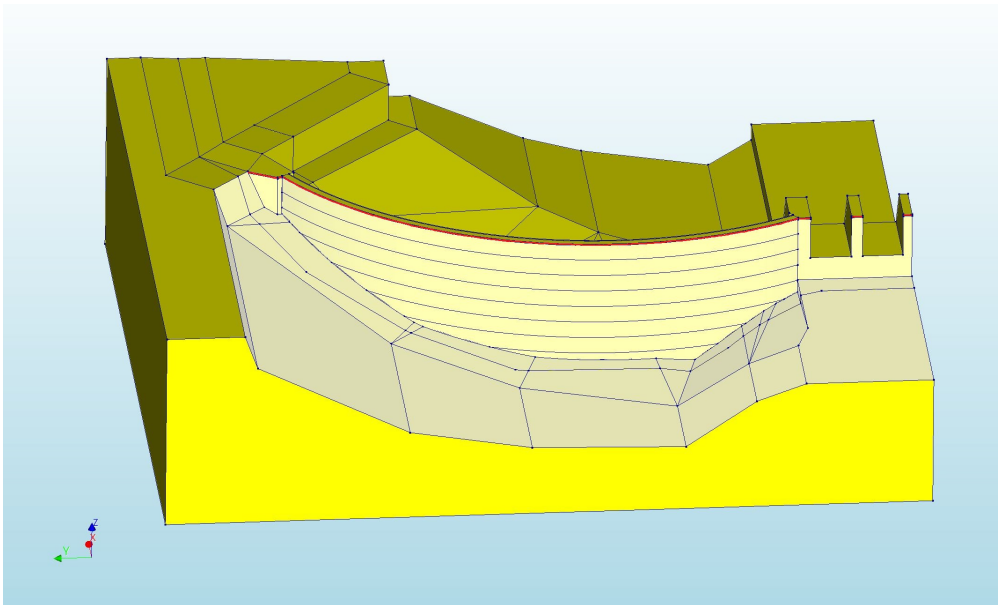


Figure 19: Illustration of the applied loads in the model. Hydrostatic-pressure and ice-load are highlighted in white and red, respectively.

4.2.1 Hydrostatic pressure and water intrusion

Only the static water pressure are taken into account, any occurrence of flood is neglected. The water level is assumed to be at the crest, as stated in the benchmark description. Thus, the hydrostatic load is given as:

$$P = \rho g (H - Z) \quad (23)$$

Where:

$$\rho = 1000 \text{ kg/m}^3$$

$$g = 9.81 \text{ m/s}^2$$

H = Vertical height of dam given in meters

Z = Vertical coordinate with origin at the dam base, given in meters

P = Pressure given in Pa = N/m²

The water does not cause any shear buoyancy, but since concrete is an imperfect material with pores, the water may enter the concrete. This can cause splitting of the concrete and expansion of the connections between dam and bedrock. NVE gives guidelines for assessing this effect [36], which is dependent on the whether there is tension or compression in the connection. This is simplified in the present work by assuming a uniform pressure from water intrusion, independent of the state of the connections. The water intrusion is modelled by applying the hydrostatic pressure to the connections. The water intrusion is only applied under the arch part of the dam and the vertical upstream side of the spillway and support. It is noted that water intrusion is not modelled on the bedrock part of the connection. This is to avoid load cancelling when the bedrock and the dam share nodes.

4.2.2 Ice-Load

NVE states that the ice-load can be treated as a line load acting 250 mm below the highest water level [36]. The size of the ice load ranges from 100 kN/m up to 150 kN/m. To find the actual load, several criteria have to be considered, which will not be done in the present work. The Swedish Standard [37] and the Energiforsk Guidelines [1] state that the ice-load in Northern Sweden should be applied as a surface load equivalent to a line load of 200 kN/m with a distribution dependent on the ice thickness. It is found that the latter approach is much more suited for NLFEA since it avoids singularities associated with a line load, and seems more realistic. Thus, the ice-load is taken as an evenly distributed radial load of 400 kN/m² applied from the crest and 0.5 meters down, and acting along the entire crest, as shown in figure 19. The ice thickness is taken as 0.5 meters to fulfill NVEs requirement for where the ice load resulting force should act.

4.2.3 Remaining Loads

To calculate the gravity load, the densities of concrete and bedrock given in table 1 are used. When these are provided in the material properties in DIANA, the self-weight is automatically evaluated when the global load case called "dead weight" is added. Note that the gravity axis in DIANA is by default the negative global Z-axis as it should be in this case.

Many loads are neglected in this thesis. These could be temperature load, wind and wave loads, and maybe traffic load on top of the dam. Temperature load was found to affect the dam response significantly in the original benchmark workshop [17]. Dynamic analysis of the dam is also necessary to assure that it can withstand an earthquake for instance. Here, one would have to include dam-bedrock-water interaction in the dynamic equilibrium. If this becomes a nonlinear problem the solution would have to be numerically solved, by the HHT- α Method for instance [25]. Dynamic analyses are not included in the present work.

4.2.4 Load Sequence

When performing a nonlinear analysis the load sequence is important [18]. First, the self-weight is applied, then the hydrostatic-pressure, and finally the ice-load. The hydrostatic-pressure is applied to the structure such that a percentage of the total load is applied sequentially. This is not entirely realistic, as this means that the hydrostatic pressure acts from bottom to crest in all load steps, and is not modelled as a gradually increasing hydraulic head. This difference is assumed negligible for the purpose of the present work. Figure 20 shows the analysis set-up in DIANA.

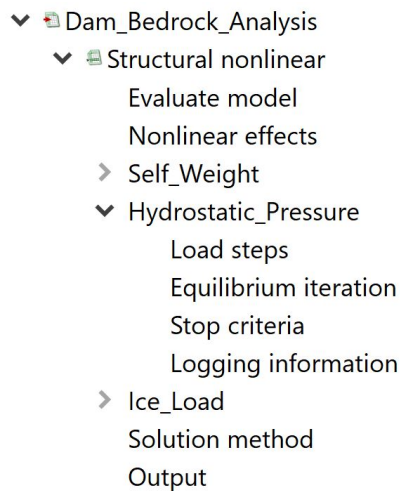


Figure 20: The analysis set-up in DIANA

4.3 Boundary Conditions and Connections

This section starts with establishing criteria for realistic modelling. These criteria are based on the physical problem, which is described in chapter 2. Then, four FE-models are established, where only the modelling of boundary conditions and connections are varied. Further, common approaches for all the FE-models are elaborated. The section ends with a verification of the interface elements.

4.3.1 Criteria for realistic modelling

The spillway and support have a large weight and are surrounded by bedrock in the bottom. So even though no information on the detailing between the spillway/support and the bedrock is given, it is assumed low bottom displacement of these. However, the bedrock will provide an elastic support. The bedding is probably small, since the extensive size and relatively high Young's modulus of the bedrock make its contact stiffness large. This discussion give criteria 1 and 2 at the next page.

The asphalt layer under the arch part of the dam is applied to avoid cohesion between concrete and bedrock. This will also contribute to reduce friction and thus lowering the resistance for circumferential motion of the bottom of the arch part of the dam. Here, the dam will also be restrained against relative radial motion. This is due to the unlikeliness that the displacements are so large that the dam transverses the excavated bulge in the bedrock, seen in figure 4. This discussion give criteria 3, 4, 5.

Since the bottom of the arch part of the dam is idealized as flat in the geometry files, measures should be taken to approximate the real stress field in this area. For instance, the support forces will likely concentrate on the downstream side of the bottom. However, since the bottom is curved, the support forces will be more evenly distributed over the bottom than just concentrated on the downstream edge. This gives criterion 6.

From the above discussion, the criteria for realistic modelling is summarized:

1. Spillway and support should be elastically supported at the bottom, but is close to rigid at the base.
2. Low, but present, bedding of dam in bedrock.
3. No cohesion in the connection between the dam arch and the bedrock.
4. Reduced resistance for circumferential displacement of the dam in the connection between the dam arch and the bedrock.
5. No relative radial displacement of the dam in the connection between the dam arch and the bedrock.
6. The real stress field in the bottom of the dam arch should be approximated since the idealized geometric shape of the bottom is used.

4.3.2 The FE-models

The differences between **Model I** and **Model II** are shown in figure 21.

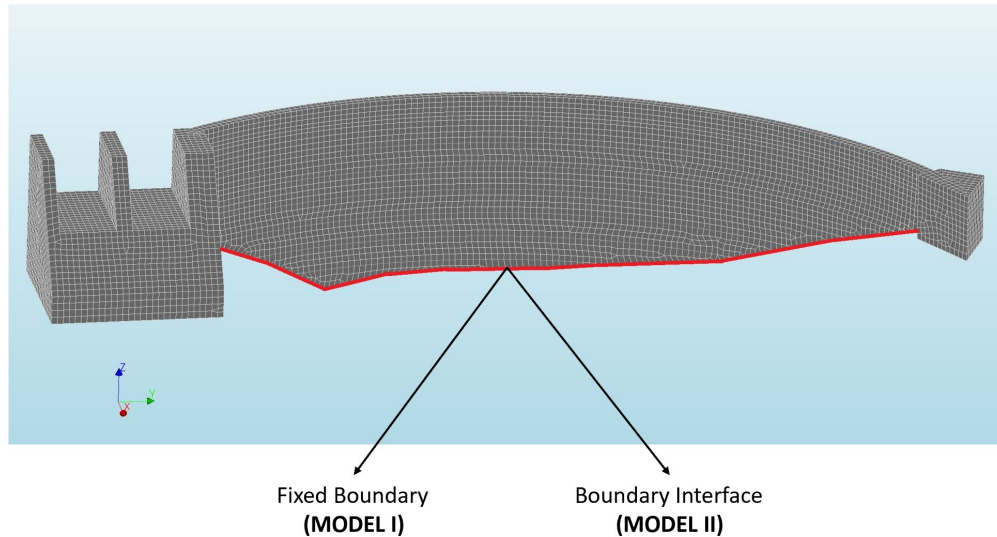


Figure 21: Model I versus Model II

MODEL I is a simple and basic model concerning boundary conditions. In this model, the bedrock is excluded. All dam faces shared by the bedrock and the dam are fixed from all translation. Rotational DOFs need not be constrained since they are not present when using 3D solid elements. The bedrock has been imprinted on the dam, such that the faces shared by the bedrock and the dam are possible to isolate. This is assumed to be a less realistic model since it only fulfills the no radial displacement criterion. Model I will probably underestimate the displacement of the dam. This is because the bottom of the dam is fixed from all translation, which is not consistent with the no-cohesion and the bedding criteria. Extensive cracking in the dam bottom will probably also occur, since the bottom of the dam arch act as a clamped support rather than a pinned one.

MODEL II is almost identical to Model I, the only difference is the inclusion of a boundary interface under the arch part of the dam, as illustrated in figure 21. The boundary interface simulates nonlinear springs between the dam and a translation fixed boundary. The boundary interface allows the dam to detach from the fixed boundary, but only in a direction normal to the dam bottom. The other

displacements components of the dam bottom are close to fixed. These interface properties are simulated by modelling the interface with a very high normal compression stiffness, but the normal tension stiffness is close to nothing. This is the only nonlinear property of the connection. The tangential stiffnesses in the two local interface directions are taken equal and linearly elastic with high values. This model should fulfill the no-cohesion and no radial displacement criterion. It is expected that this analysis will give an uplift where the interface is applied, yielding a larger displacement response than model I.

The differences between **Model III** and **Model IV** are shown in figure 22.

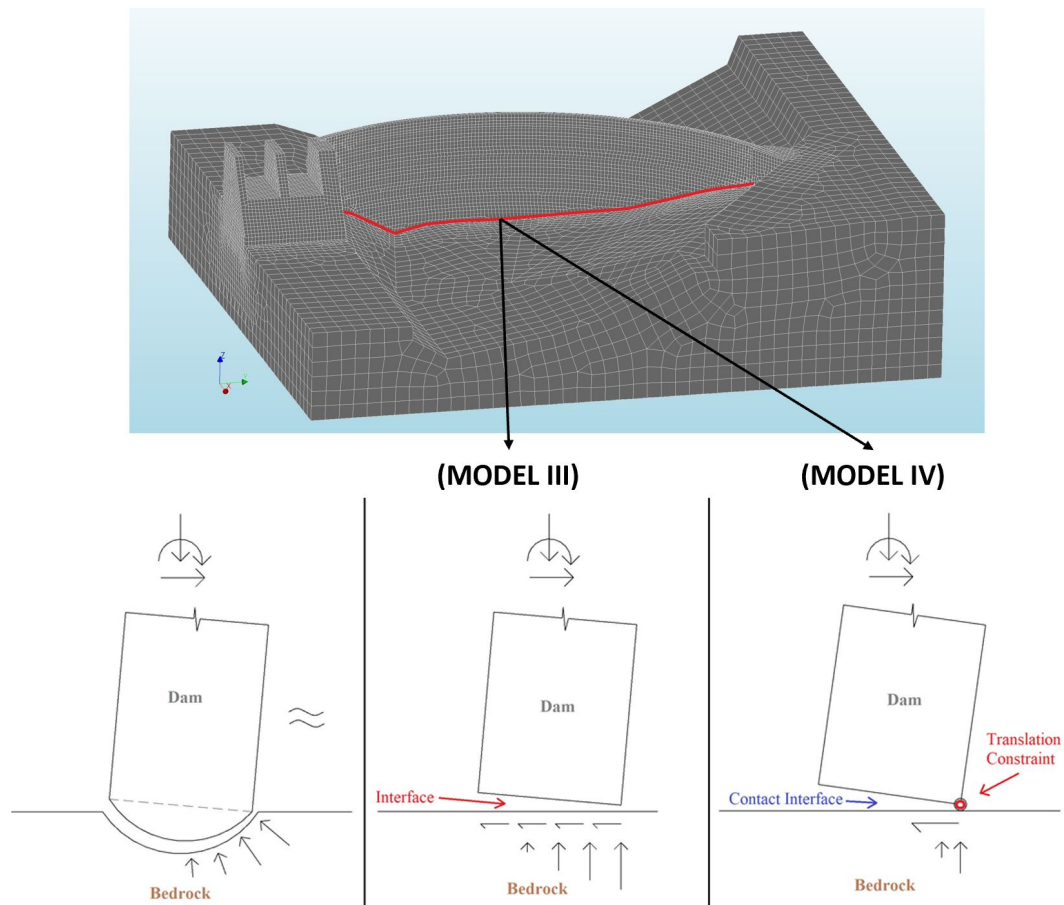


Figure 22: Model III versus Model IV

MODEL III includes the bedrock. The spillway and support are fixed to the bedrock; they share nodes. By default in DIANA, all coincident shapes are connected by sharing nodes. However, it is necessary to ensure that the tolerances in the geometry input file have a lower value than the tolerance used by DIANA. Between the arch part of the dam and the bedrock, an interface is applied, as shown in figure 22. The interface properties are the same as in Model II. Thus, the approach in Model III is equivalent to bracing the spillway and support to the bedrock, and almost bracing the arch part of the dam to the bedrock in all directions, except allowing for a gap normal to the interface surface. It is expected that this analysis will be close to Model II, but will give higher displacement response due to softer dam support when including the bedrock. Thus, Model III will likely satisfy the criteria about elastic support of the spillway and support and inclusion of bedding, in addition to the criteria satisfied by Model II.

MODEL IV differ only from Model III in the properties of the connection between the dam arch and the bedrock, as shown in figure 22. The interface used in this model simulates contact behaviour while not losing connectivity. This means that the normal compression stiffness of the interface is very high to simulate no penetration of the dam into bedrock. Further, the normal tension stiffness is very low to simulate no cohesion. The tangential stiffnesses in both local directions in the interface surface are very high, but reduces to almost nothing where interface tension occurs. This interface is very close to a no-slip-contact formulation. A translation constraint applied between the downstream bottom dam edge and the bedrock was used to avoid unrealistic radial slip. This restrain all relative translation between the dam edge and the bedrock, but does not resist any rotation. The interface used will allow for concentrations of support forces at the downstream bottom edge, which is more realistic. The other models will probably show a more evenly distributed support forces due to the constant tangential stiffness and fixed boundary. This model will probably also satisfy the no cohesion and low circumferential resistance criterion better than Model II and III, due to the contact interface. Thus, this model is expected to fulfill all the criteria.

4.3.3 Common properties of the FE-models

The boundary conditions applied to the cut-planes of the bedrock are not varied. These boundary conditions are assumed to be of less importance for the dam response when enough bedrock is included in the model. The foundation will then have to transfer the support forces from the dam through a lot of solid rock, and by Saint-Venant's principle, the effect of the boundary conditions at the cut planes should then be damped. In the provided geometry, a reasonable amount of bedrock is in fact included, except on one side of the spillway. It seems unrealistic that the lack of bedrock here is the case in the physical problem as well, see figure 23. This assumed exclusion of some bedrock in the geometry files could be unfortunate with respect to the sensitivity of the bedrock boundary conditions. Measures to correct this is not taken due to the lack of information on the physical problem.

Despite the damped effect of bedrock boundary conditions when including enough bedrock in the model, reasonable boundary conditions should be applied. After recommendations in the Energiforsk Guidelines [1], the bedrock cut planes should be constrained against displacement normal to the cut-plane and otherwise free. This is also done in the present work, and is shown in figure 23.

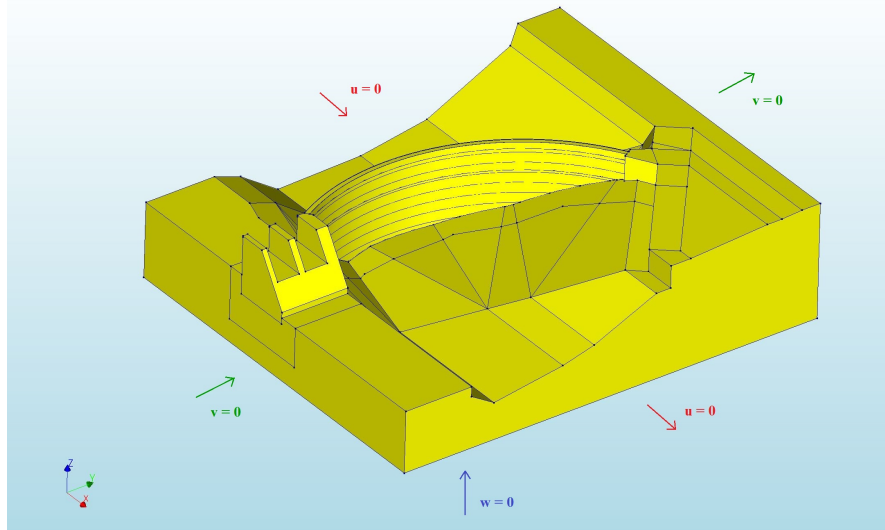


Figure 23: Illustration of the boundary conditions applied to the bedrock

In figure 23, u , v and w are the displacements in global X, Y, and Z direction, respectively. This approach for the boundary conditions of the bedrock seems realistic. The bedrock usually has a large extent in the normal direction to the cut faces which could indicate plane strain in the face surface. This is similar to not allowing for displacement in the normal direction. Also, normal stiffness is larger than shear stiffness for the rock. So, when referring to figure 23, it seems appropriate to neglect the $u = 0$ faces tangential properties because all load will be taken as normal action by the $w = 0$ face, for instance. In reality, the bedrock may also have low shear stiffness due to cracks.

Interface elements, as formulated in chapter 3, is exclusively used to simulate both the connection between dam and bedrock and nonlinear springs. These elements can simulate contact, but they never loose mesh connectivity as opposed to contact elements. Thus, interface elements can only be used in contact problems with low relative motion [33]. Based on the criteria for realistic modelling, the relative motion in the connection between dam and bedrock is likely small in this case. The use of interface elements are also justified by the robust and simple approach in DIANA. This modelling of the connections will also reduce computational effort, compared to the use of contact elements. This is because there is no searching for where the contact occurs, which is necessary when using contact elements.

4.3.4 Verifying the interface elements

To be aware of the properties of the interface elements, and to get familiar with the modelling, simple verification tests has been performed.

There are two aspects of the interfaces that needs to be verified; tangential and normal properties. At first, a simplified model of the dam, supported only by a boundary interface at the bottom, were considered. The initial idea was to apply the hydrostatic pressure and assess the tilting and sliding response. Figure 24 show the simplified dam.

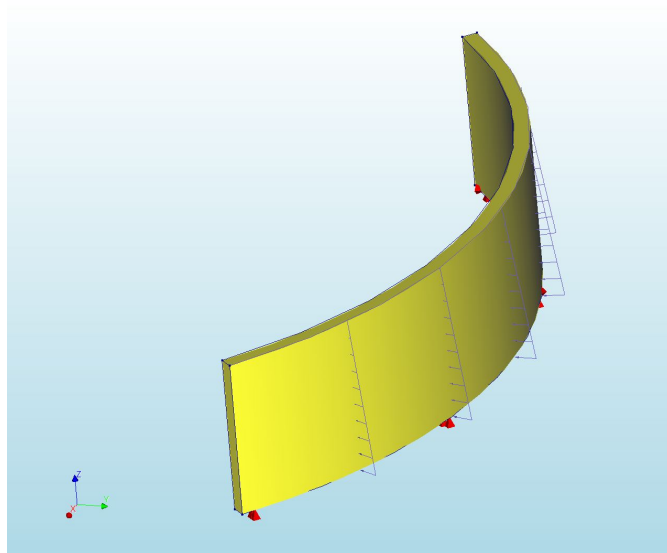


Figure 24: The simplified dam first considered, to validate the interface

It soon became evident that it was difficult to isolate the different properties of the interface with this model. The global maximum load supported by the boundary could, to some extent, be calculated by hand and compared with results from DIANA. However, the properties of the interface would be tainted by the geometry of, and load applied to, the model considered. Therefore, two simple models with geometry and load suited to trace the properties of the interface were considered instead.

To validate the tangential properties, the model in figure 25 was used.

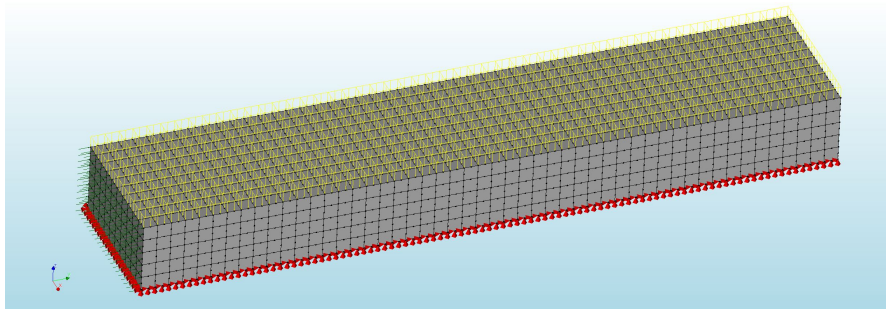


Figure 25: Slide validation model in DIANA

Figure 25 depicts a low concrete wall with a boundary interface at the bottom and subjected to downward normal pressure at the top and a prescribed displacement at the left end. The boundary interface simulate nonlinear springs with the properties of the Coulomb Friction Model. The prescribed displacement is used to trace the post-peak behavior of the equilibrium curve in the tangential direction. Figure 26 shows the relation between tangential stress and tangential displacement extracted from DIANA:

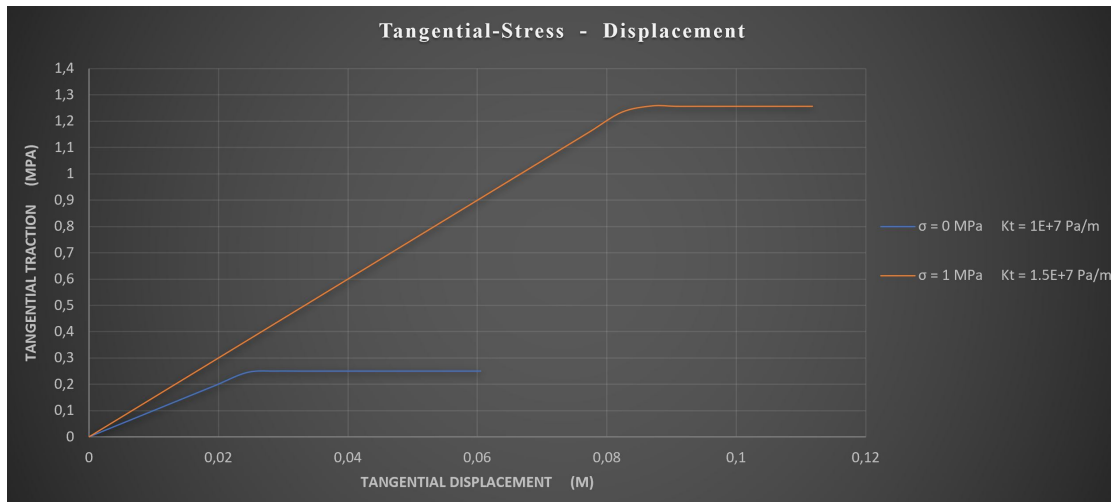


Figure 26: Tangential stress plotted against tangential displacement.

Two different tangential stiffnesses, K_t , with different normal pressures, σ , are evaluated. The cohesion and the coefficient of friction are the same in both cases, respectively $c = 0.25$ MPa and $\mu = 1$. The results from figure 26 are very consistent with the modelled properties. It is evident that the tangential stiffness is linear until it becomes singular when reaching the maximum tangential stress. At this point sliding will occur. An interesting result from figure 26 is that there is no reduction of the tangential stress when transversing from static to sliding friction.

The normal properties of the boundary interface with Coulomb Friction properties is verified by the use of a cantilever wall subjected to a prescribed displacement of the top face in the global X-direction. The propagation of tension failure in the boundary interface is shown in figure 27.

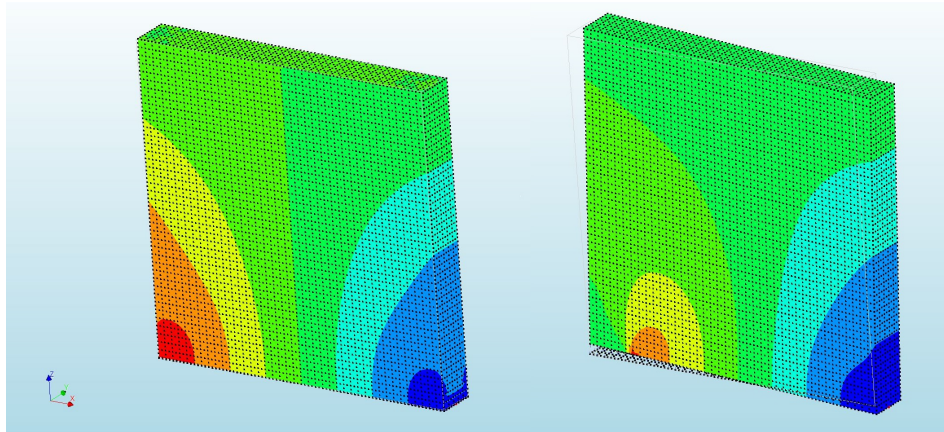


Figure 27: Cauchy stress in z-direction for the first and the last load step, respectively.

The maximum normal stress of the boundary interface is set to 0.1 MPa, with brittle failure. The normal stress versus normal displacement for the two points with the highest stresses is given in figure 28 on the next page. Note that the absolute value of the displacement is used.

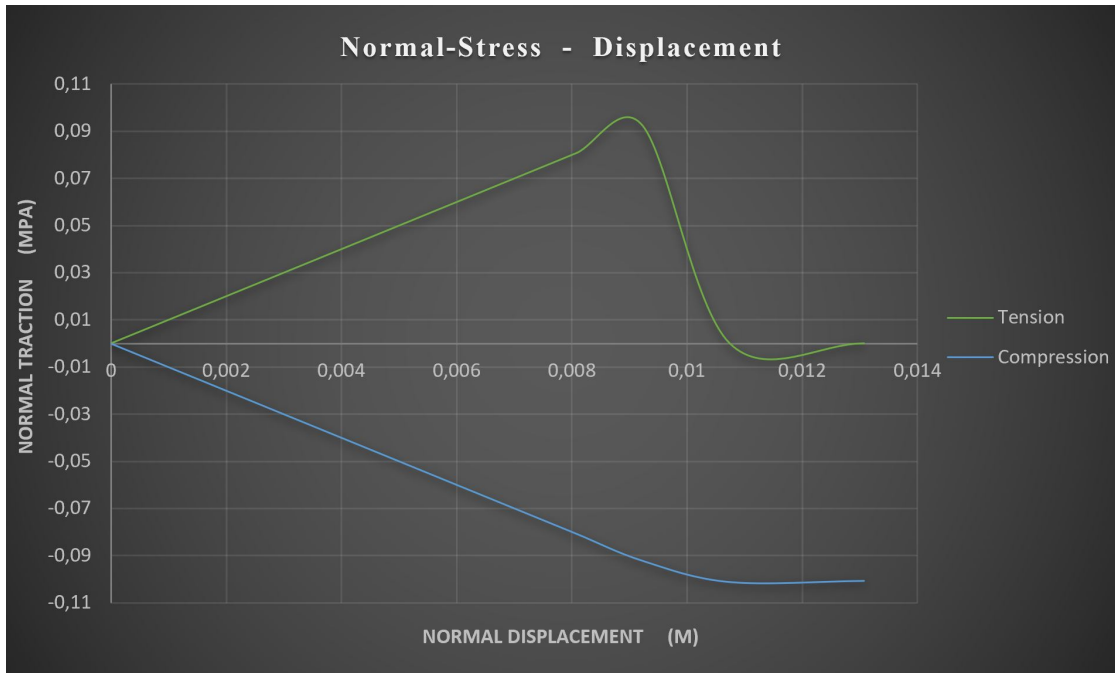


Figure 28: Normal stress plotted against normal displacement for both tension and compression

Both tension and compression behave as expected. The failure for tension is about 0.1 MPa, as given in the input. The slight tension softening is not consistent with the brittle failure, but is advantageous as it will increase numerical stability [24]. Note that the compression stress will stabilize when the maximum resisted moment is reached by the cantilever. However, in a uniaxial test the tension would behave as depicted in figure 28, but the compression would go "infinite" as a linear relation is assumed here.

It should be mentioned that the properties of the boundary interface and the test specimens are chosen somewhat arbitrary for testing reasons, and are used only to understand the behavior of the interface. A very fine mesh is used in the tests. This is due to the desire of multiple elements over the interface thickness, and the element size are equal in all three directions to avoid distortions. The tests are performed with negligible CPU-time.

4.4 Finite element discretization

In general, the mesh should be refined until the field variables vary in an adequately small degree with the element size. In the present work, a reasonable discretization is done based on the meshes used in the original benchmark [17] [38]. The finest mesh possible is chosen, limited by the hardware used and a reasonable analysis time. Mesh sensitivity studies has not been performed, which is justified by the fact that the same mesh is used in all analyses. Thus, when only assessing the effect of boundary conditions and connections, the discretization will be less important. However, a reasonable discretization is decisive.

3D solid finite elements are exclusively used in the present work. This is to include all stress components, which is not possible when using shell elements. However, shell element have the advantage of showing resulting forces rather than stresses, such that the required reinforcement is easier to determine. Elements with quadratic interpolation of displacements are used. This is to overcome the difficulties associated with lower order elements, such as spurious strain energy. Also, the higher order elements will describe more challenging modes, such as bending, more accurately and are less prone to decrease in accuracy due to distortions [34] [39]. The geometry of the finite elements are chosen to be hexahedron rather than tetrahedron. This is recommended by the Dutch Guidelines [24], and is due to the more robust formulation of hexahedron shaped elements. However, tetrahedron is a more versatile geometry, such that more effort is required to get a regular mesh when using hexahedron shaped elements. The dominating element used to mesh the dam is shown in figure 29.

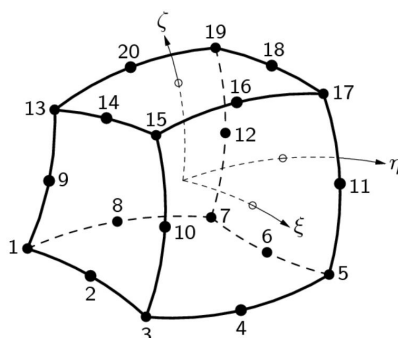


Figure 29: The CHX60 element in DIANA [33]

An effort has been made to make a regular good looking mesh with minimum distortions. The focus has been on the dam; the bedrock mesh has not been optimized. The spillway and support were meshed quite good by the automatic mesh generator, but the arch part of the dam required attention. First, a dividing of the dam surface into smaller regular shaped surfaces was considered. When seeding the dam with respect to these regular surfaces, improvement on the mesh quality was achieved. However, this approach could not guarantee a regular mesh throughout the thickness of the dam. Therefore, the geometry of the dam arch was cut with horizontal planes 5 meters apart. This corresponds to an integer number of elements. When the dam was divided into these shapes, a regular good quality mesh was achieved. This approach was used in all analysis, and the resulting mesh is shown in figure 30 and 31.

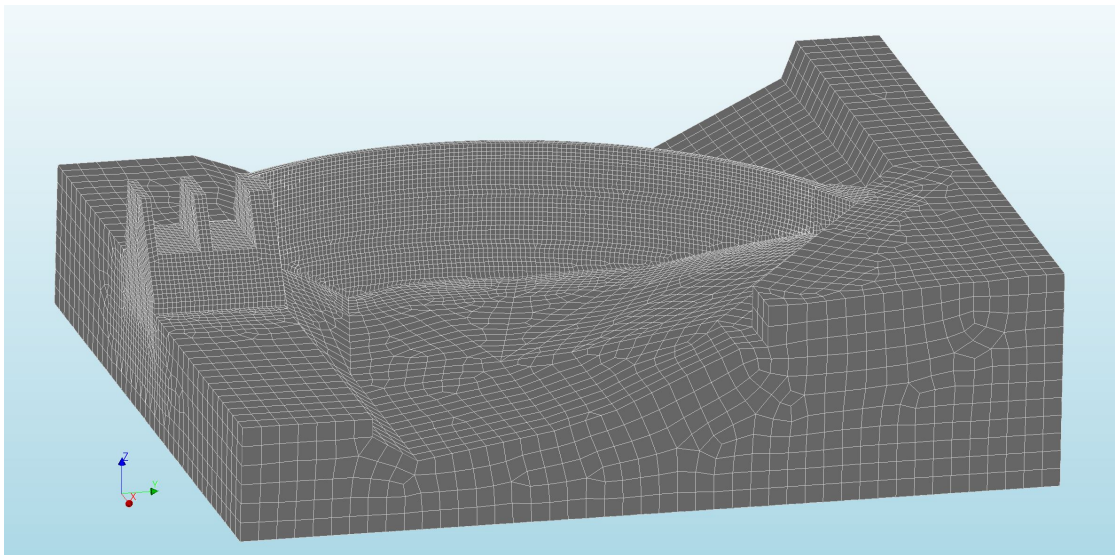


Figure 30: The mesh used in the analyses seen from downstream

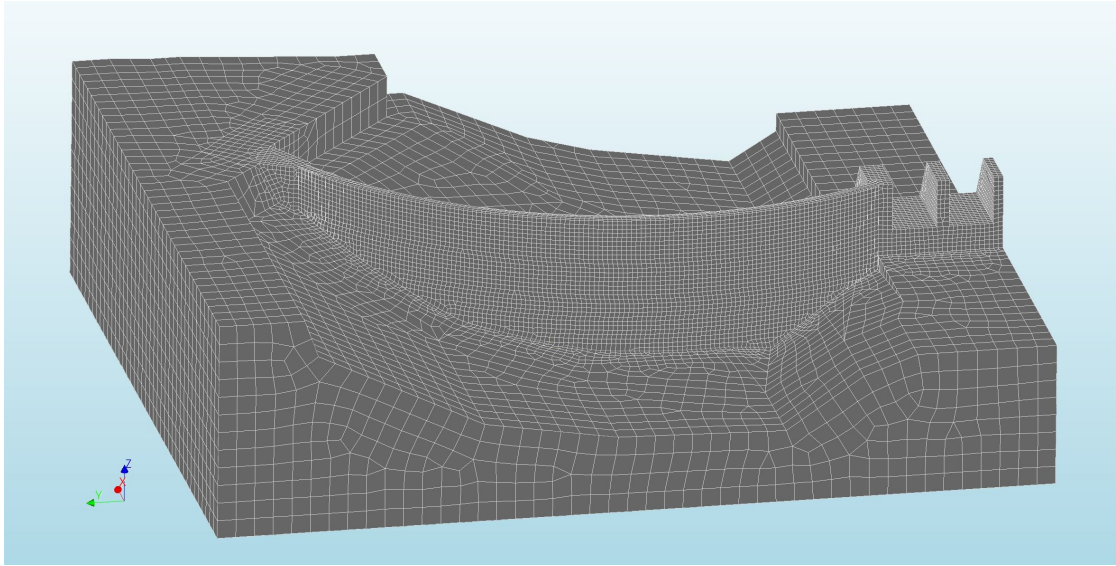


Figure 31: The mesh used in the analyses seen from upstream

There are some distorted elements in the bottom of the dam. However, these distortions are limited both in magnitude and extent and are therefore accepted. A gradual increase from the element size in the dam to the foundation and finally to the overall bedrock are applied. This is done by doubling the seeding size from the first to the latter.

A summary of the mesh information is given in table 2. Note that it is the dominant element type that is stated. Some tetrahedron/triangular elements occur in the mesh by default in DIANA to reduce distortions, but these are a minority.

Shape	Element Type	Seed Size (m)	Number of Elements
Entire Dam	CHX60	1.25	26944
Rock Foundation	CHX60	2.5	34450
Bedrock	CHX60	5	36642
Reinforcement	Grid	Not relevant	3
Interface	CQ48I	1.25	530

Table 2: Summary of mesh information

4.5 Numerical solution method

To decide which solution algorithm to use on the problem, it can be advantageous to roughly predict the global equilibrium path of the dam. When assessing the ultimate capacity, the equilibrium path would likely transverse a limit point, mainly due to a ductile behaviour caused by the reinforcement. A turning point may also be passed. Thus, to trace the equilibrium path all the way to failure, the Arc-Length Method is probably necessary. In the present work, the dam is only subjected to a normal load state. It should be designed to withstand this with ease. Thus, using the Arc-Length Method is not necessary. The automatic size of the load steps in the Arc-Length Method in DIANA could also have problems transversing points with a sudden change in stiffness, for instance caused by cracking. The Newton-Raphson method is more controllable and is sufficient for the present purpose. Thus, a regular Newton-Raphson solution method is used.

The convergence criteria for the numerical solution method is taken as recommended by the Dutch Guidelines [24]:

- Force Norm : 0.01
- Energy Norm : 0.001

4.6 Geometric nonlinearities

The first question that arises is whether geometric nonlinearities effect the response of the dam to an extent that it should be included. This effect should be included were large displacements or buckling stresses is expected. Displacements are assumed to be small. Since most of the load in the water pressure direction is carried by membrane action rather than plate action, as seen in figure 1, the structure could buckle. However, it is very unlikely that this will happen since the dam should be design strong enough to avoid this. The axial force in the vertical direction, caused by the self weight and maybe a load on the crest, is not likely to make geometric higher order effects substantial either.

Even though geometric nonlinear effects are not assumed to be decisive in the present problem, it can alter the dam response somewhat. Thus, geometric nonlinearities are included in all analyses to increase the accuracy of the results. The increase in CPU-time caused by this is not expected to be too large.

4.7 Summary of modelling approach

So far in this chapter, many different aspects of the FE-model design have been dealt with. In this section, the most important properties of the four different models are summarized. Note that the only thing varied between the models are the boundary conditions and connections.

- **MODEL I : Fixed boundary conditions.** Only the dam geometry is included, and the bottom of the dam are fixed from all translation.
- **MODEL II : Boundary interface.** Similar to Model I, but a boundary interface is included under the dam arch.
- **MODEL III : Bedrock interface.** In this model both the bedrock and dam are included. An interface between the dam arch and the bedrock is applied.
- **MODEL IV : Bedrock contact interface.** This model is similar to Model III, but the interface simulates no-slip-contact and a translation constraint is added.

Table 3 summarizes the input of the analyses.

Property	Model I	Model II	Model III	Model IV
Mesh	Dam Standard Mesh		Dam + Bedrock Standard Mesh	
Load	Self-Weight, Hydrostatic-Pressure and Ice-load			
Material Model Concrete	FIB Model Code 2010 Total Strain Rotating Crack			
Material Model Reinforcement	Nonlinear Elasticity			
Boundary Conditions (Arch Part of Dam)	Translation Fixed	Boundary Interface	Interface	Interface + Translation Constraint
	-	1000	1000	1000
	-	0.000001	0.000001	0.000001
	-	1000	1000	1000
Tangential Stiffness (Contact) (GPa/m)	-	1000	1000	0.000001
Tangential Stiffness (No Contact) (GPa/m)	-	1000	1000	0.000001
Boundary Conditions (Spillway and Support)	Translation Fixed			
Boundary Conditions (Bedrock)	-		Fixed Translation	Fixed Translation
Geometric Nonlinearities	-		Normal to Cut-Planes	
Solution Method	On			
Maximum Iterations Allowed	Regular Newton-Raphson			
Load-Steps	75			
Convergence Criterion	1 + 10 + 4			
	Energy: 0.001 and/or Force: 0.01			

Table 3: Summary of analysis input

5 Verification of the FE-model

This chapter concerns a verification model for checking the numerical results. Verification is important when analyzing large and complex structures, to avoid errors.

In the following, a simplified analytic model for verifying the displacement response is presented. The verification model is made by using an arch shape function for the dam in the horizontal plane, and interpolate this vertically by a plate shape function. This gives a 3D displacement field for the dam. The chapter starts with presenting the necessary background theory, before the verification model and results are given. In the discussion in chapter 8, the accordance between the verification model and the numerical results is assessed.

5.1 Arch Theory

The objective in this section is to derive the radial shape function for the arch representing the dam crest in the horizontal plane. Figure 32 shows the static system of a clamped arch subjected to a radial load. Here, w is the radial displacement, v is the tangential displacement, R is the center arch radius and z is the radial coordinate. θ and α are the current and total opening angle, respectively. The radial load is denoted q .

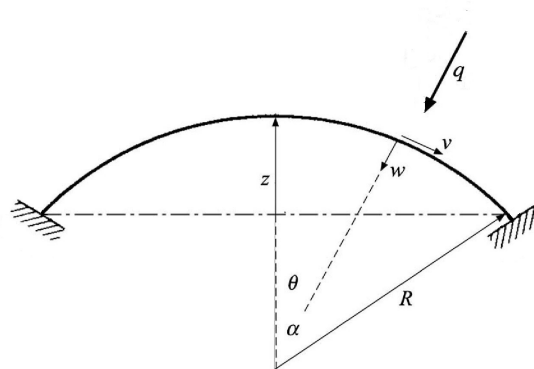


Figure 32: Static model of an arch [40]

By considering the dam in the horizontal plane, it is possible to make an idealized 2D model of the dam arch. In this particular case, the arch part of the dam is monolithic connected to the very stiff spillway and support. Hence, it is reasonable to idealize the arch with clamped endpoints. This yields the static system shown in figure 32. The theory that follows is mainly adopted from Dym and Williams [40] and Cook, Malkus, Plesha and Witt [18].

If the arch is assumed slender, the transverse shear strain radial to the arch can be neglected. The displacement of the arch can be decomposed into three cases, as shown in figure 33. Here, the hoop strain, ϵ_s , and v are positive when extended, and w is positive inwards. Further, s and z are the tangential and radial coordinates, respectively.

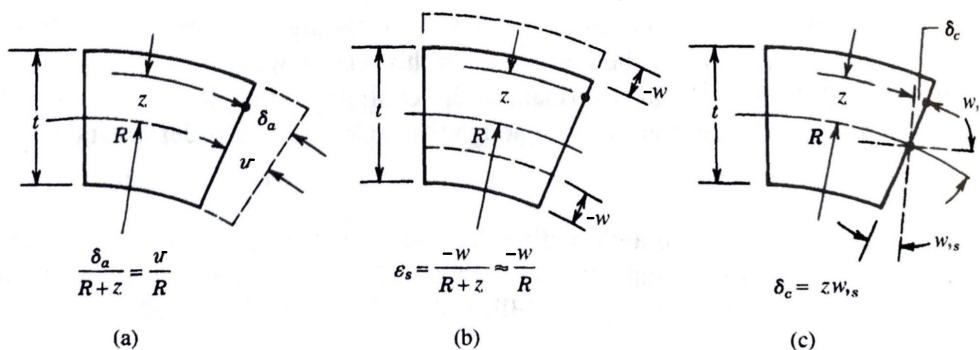


Figure 33: Deformation of an arch [18].

The expression in figure 33 (a) follows directly from the definition of radians. Writing δ_a explicit gives:

$$\delta_a = v + \frac{vz}{R} \quad (24)$$

The relation in figure 33 (b) can be derived from the engineering strain measure directly by considering the change in tangential length. When ignoring the arch thickness, this gives:

$$\epsilon_{s(b)} = \frac{d\theta(R-w) - d\theta R}{d\theta R} = \frac{-w}{R} \quad (25)$$

The expression in figure 33 (c) follows directly from the figure if a small angle of the radial displacement curve, $w_{,s}$, is assumed:

$$\delta_c = zw_{,s} = z \frac{dw}{ds} \quad (26)$$

The only strain component is the hoop strain, and by using the engineering definition of strain, the expression for this becomes:

$$\epsilon_s = \frac{d}{ds}(\delta_a + \delta_c) - \frac{w}{R} \quad (27)$$

When inserting the expressions for δ_a and δ_c , and by utilizing the chain rule after noting the relation $s = R\theta$, the hoop strain can be expressed as:

$$\epsilon_s(\theta, z) = \epsilon_m + z\kappa = \left[\frac{1}{R} \left(\frac{dv(\theta)}{d\theta} - w(\theta) \right) \right] + z \left[\frac{1}{R^2} \left(\frac{d^2w(\theta)}{d\theta^2} + \frac{dv(\theta)}{d\theta} \right) \right] \quad (28)$$

Note the distinguishing in equation 28 between membrane strain (axial force) and curvature (bending moment). In a plane problem, the hoop strain is the only component. Thus, by the principle of virtual displacements, equilibrium is achieved if:

$$\int_V \sigma_s \tilde{\epsilon}_s dv - \int_S q\tilde{w} ds = 0 \quad (29)$$

A linear elastic material is assumed in equation 29 and it is distinguished between the work done by axial forces and bending moments. Then, after integrating over the cross section area, equation 29 becomes:

$$\int_{-\alpha}^{\alpha} (EA\epsilon_m \tilde{\epsilon}_m + EI\kappa \tilde{\kappa} - q\tilde{w}) R d\theta = 0 \quad (30)$$

When using the sign convention $N = EA\epsilon_m$ and $M = -EI\kappa$, and inserting the expression for the strain and curvature, equation 30 can be written as:

$$\int_{-\alpha}^{\alpha} \left(\frac{N}{R} \left[\frac{d\tilde{v}}{d\theta} - \tilde{w} \right] - \frac{M}{R^2} \left[\frac{d^2\tilde{w}}{d\theta^2} + \frac{d\tilde{v}}{d\theta} \right] - q\tilde{w} \right) R d\theta = 0 \quad (31)$$

By using integration by parts and collecting terms, equation 31 can be rewritten:

$$\int_{-\alpha}^{\alpha} \left(\left[\frac{1}{R} \frac{dN}{d\theta} - \frac{1}{R^2} \frac{dM}{d\theta} \right] \tilde{v} + \left[\frac{N}{R} + \frac{1}{R^2} \frac{d^2M}{d\theta^2} + q \right] \tilde{w} \right) R d\theta = 0 \quad (32)$$

For the virtual work to vanish for an arbitrary virtual displacement, both of the expressions in the brackets must vanish, which is the condition for equilibrium. The differential equations in the brackets are simultaneously solved for N and M . When using the relations $N = EA\epsilon_m$ and $M = -EI\kappa$ and inserting the kinematic relations in equation 28, it can be shown that the radial displacement is on the following form [40]:

$$w(\theta) = \frac{qR^4}{EI} \left[\left(\frac{1 + \bar{I}}{2} \theta \sin \theta \right) C_1 - C_2 + (\bar{I} \cos \theta) C_3 + \bar{I} \right] \quad (33)$$

Here, $\bar{I} = I/(AR^2)$, where I is the second moment of area and A is the cross section area. E is Young's modulus, while C_1 , C_2 and C_3 is constants. These constants are found by invoking the boundary conditions:

$$w = 0, \quad v = 0, \quad \frac{dw}{d\theta} = 0 \quad \text{for } \theta = \pm\alpha \quad (34)$$

It is referred to the MATLAB script in appendix A for the calculation of the radial displacement for the dam. A more thorough solution of the differential equations can be found from Dym and Williams [40]. Figure 34 illustrates the resulting deformation mode of a clamped arch subjected to a uniform radial load.

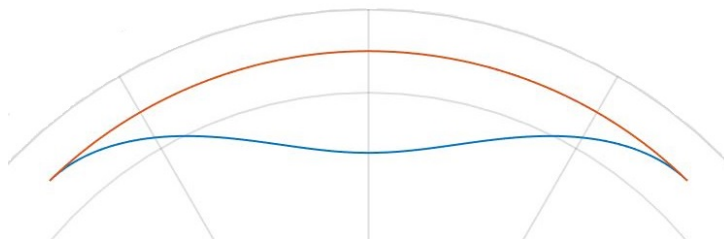


Figure 34: Polar plot of a clamped arch, deformed and undeformed.

5.2 Plate Theory

The goal in this section is to derive the vertical shape function for the dam. This shape function is assumed equal to the center deflection in y -direction of plate shown in figure 35. In this figure, three edges are simply supported, the last edge is free, and the plate is subjected to hydrostatic pressure. Note that the boundary conditions along $y = 0$ and $y = b$ are the most important ones, since the deflection of the plate center in the y -direction is the goal. Thus, the boundary conditions along $x = 0$ and $x = a$ are not so critical. So even though these two edges are simply supported, in stead of fixed as assumed in the previous section, this is considered to be of less importance.

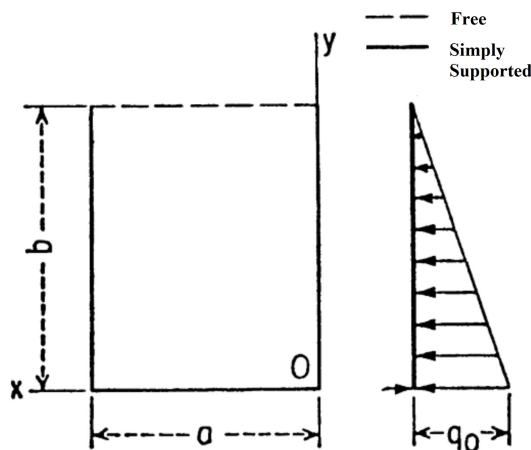


Figure 35: Plate model resembling the dam structure [41]

Timoshenko and Woinowsky-Krieger have already derived a function for the displacement of this plate problem [41]. The deflection normal to the plate, u , has to satisfy Kirchhoff's plate differential equation:

$$\frac{\partial^4 u_i}{\partial x^4} + 2 \frac{\partial^4 u_i}{\partial^2 x \partial^2 y} + \frac{\partial^4 u_i}{\partial^4 y} = \frac{q}{D} \quad (35)$$

The boundary conditions for this configuration becomes:

$$u = 0 \quad \frac{\partial^2 u}{\partial x^2} = 0 \quad \text{for } x = 0 \text{ and } x = a \quad (36)$$

$$u = 0 \quad \left(\frac{\partial^2 u}{\partial y^2} + \nu \frac{\partial^2 u}{\partial x^2} \right) = 0 \quad \text{for } y = 0 \quad (37)$$

$$\frac{\partial^2 u}{\partial y^2} + \nu \frac{\partial^2 u}{\partial x^2} = 0 \quad \left(\frac{\partial^3 u}{\partial y^3} + (2 - \nu) \frac{\partial^3 u}{\partial y \partial x^2} \right) = 0 \quad \text{for } y = b \quad (38)$$

Equations 36 and 37 require no deflection along, and no moment normal to, the edges stated. The reason why equation 36 expresses the moment in x-direction as $\frac{\partial^2 u}{\partial x^2} = 0$ and not as $\left(\frac{\partial^2 u}{\partial x^2} + \nu \frac{\partial^2 u}{\partial y^2} \right) = 0$ is because requiring $u = 0$ along a line parallel to the y-axis would also demand $\frac{\partial^2 u}{\partial y^2} = 0$ along the same line. Hence, the term associated with Poisson's ratio can be neglected. This is also true for equation 37, but this simplification is not done in the theory adopted in the present work. Equation 38 expresses no moment and no shear force along the free edge, respectively. Note that the Kirchhoff shear force is stated in the last expression in equation 38, which combine the effect of shear force and twisting moment.

According to Timoshenko et al. [41], the deflection can be written as a sum of two parts: u_1 and u_2 . The first component can be written:

$$u_1 = \frac{4q_0(1 - y/b)a^4}{\pi^5 D} \sum_{m=1,3,5,\dots}^{\infty} \frac{1}{m^5} \sin \frac{m\pi x}{a} \quad (39)$$

This part represents the deflection of a uniformly loaded and simply supported strip, which is parallel to the x-axis. The boundary conditions in equation 36 are thus fulfilled. The second component is stated as:

$$u_2 = \sum_{m=1,3,5,\dots}^{\infty} f(y)_m \sin \frac{m\pi x}{a} \quad (40)$$

By inserting u_1 and u_2 in equation 35 and invoking the boundary conditions in equations 36-38, $f(y)_m$ can be found. The full derivations are omitted in the present work, and it is referred to Timoshenko and Woinowsky-Krieger [41] for a more thorough presentation.

In table 4, the resulting displacement, u , is given for two points on the plate for several b/a ratios. Here, q_0 is the hydrostatic load at the dam bottom, $D = Et^3/12(1 - \nu^2)$ is the plate stiffness and b/a is the height/length ratio of the plate representing the dam. The deflection is evaluated at $x=a/2$ with $\nu = 0.3$.

b/a	$y = b$	$y = b/2$
1/2	$0.00230 q_0 a^4 / D$	$0.00135 q_0 a^4 / D$
2/3	$0.00304 q_0 a^4 / D$	$0.00207 q_0 a^4 / D$
1	$0.00368 q_0 a^4 / D$	$0.00313 q_0 a^4 / D$
1.5	$0.00347 q_0 a^4 / D$	$0.00445 q_0 a^4 / D$
2	$0.00291 q_0 a^4 / D$	$0.00533 q_0 a^4 / D$
∞	0	$0.00651 q_0 a^4 / D$

Table 4: The deflection normal to the plate for different b/a ratios [41].

Figure 36 shows a plot of the deflection curves in y -direction of the plate center, for different b/a ratios. These curves represent the displacement along a vertical section of the dam and are made by regression. The curves are second order polynomials, which demand three points for each curve. Two of the points were extracted from table 4 and the last point, at the bottom of the dam, has zero deflection. In figure 36 it is assumed an average dam height of 30 meters.

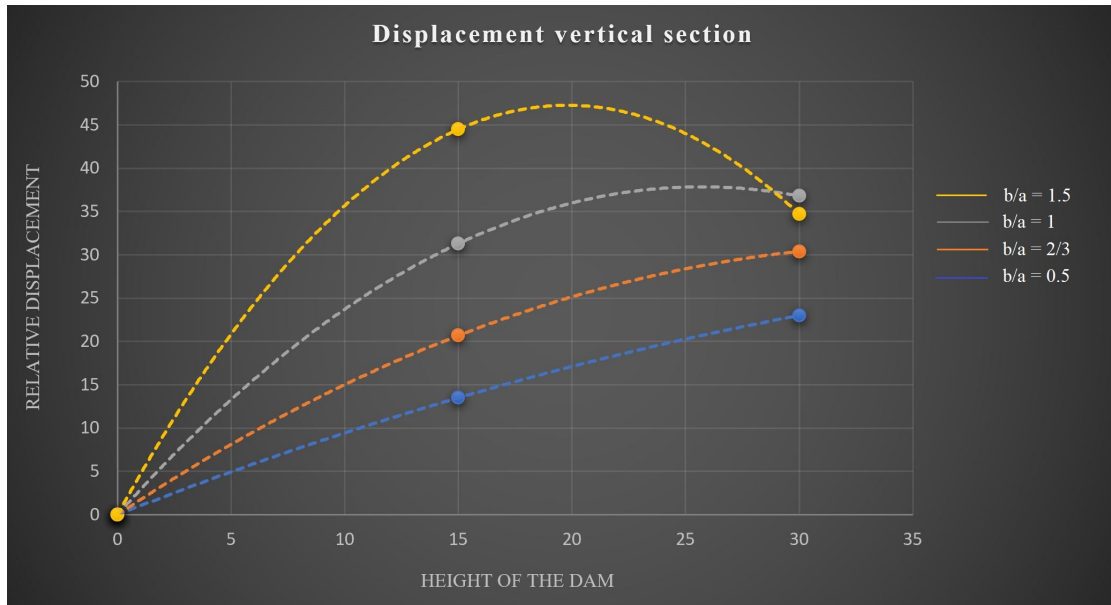


Figure 36: Dam deformation along a centered vertical section, according to plate theory.

5.3 Verification model

To verify the displacement response from the FE-models, it is proposed to use the radial shape function of the arch in the horizontal plane and interpolate this vertically by the mid deflection of the plate from the previous section. This yields a 3D deformation plot of the dam.

The choosing of the correct vertical shape function from figure 36, depends on the b/a ratio. When the dam is idealized as the plate shown in figure 35, the height/width ratio is approximately 30 m/150 m which is 0.2. However, since the dam is curved, it is much stiffer in the width direction than in the height direction, compared to a plane plate with uniform thickness. The latter situation is assumed in the derivation in section 5.2. This difference in stiffness can be accounted for by increasing the b/a ratio. This is set equal to 1 in the further calculations, and the $b/a = 1$ curve is chosen as the shape function for the dam in the vertical direction.

To get numerical results from the verification, it is considered that load carrying by arch effect dominates at the highlighted part of the dam shown in figure 37. That is, the effect of the boundary conditions at the bottom of the dam is assumed to have no effect here. The gradually decreasing influence of boundary conditions is also described by Engen [42]. Hence, this part of the dam carries the load on it independently from the bottom of the dam, and it becomes a 2D problem if the variation of the load in the vertical direction is neglected. As a consequence, the radial displacement function found in section 5.1 can describe the displacement of the dam in this area. This displacement function is then scaled vertically by the $b/a = 1$ curve in figure 36, to extend it to three dimensional space.

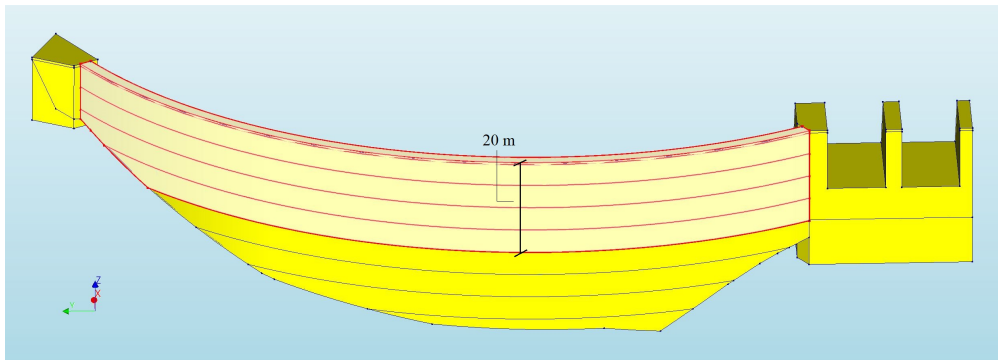


Figure 37: Part of the dam considered in the numerical validation.

It is referred to appendix A for the full numerical calculations. The resulting displacement field for the dam is shown in figure 38. A maximum displacement of 24.5 mm occurs at the center of the crest. Note that only the radial displacement is included, the circumferential displacement is neglected.

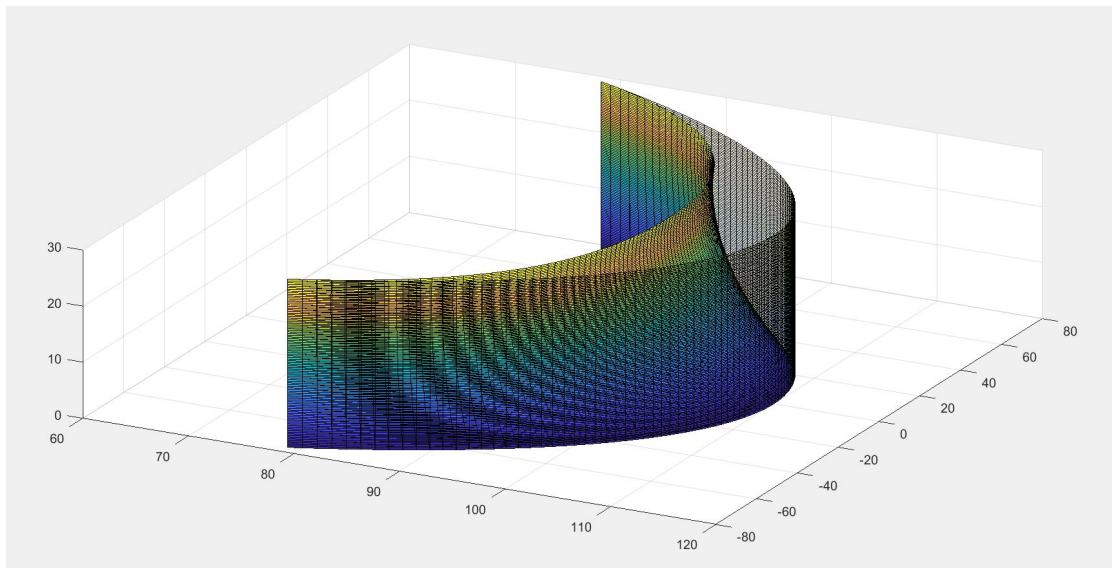


Figure 38: MATLAB-plot of the deformed and undeformed dam given as colored and transparent graph, respectively.

6 Results

In this chapter, the results from the four FE-models are given. These are presented with observations considered important. The results are divided into sections for each model, in addition to a final section where the results are compared.

6.1 Model I : Dam with fixed boundary conditions

Figure 39 and 40 show the absolute value of the dam displacement.

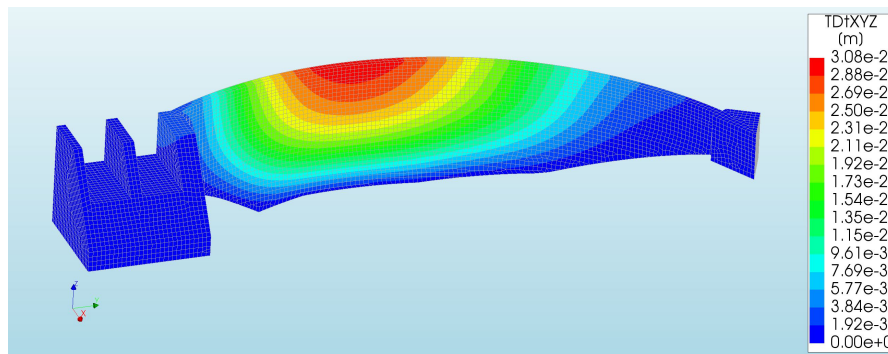


Figure 39: Total displacement contour plot for Model I.

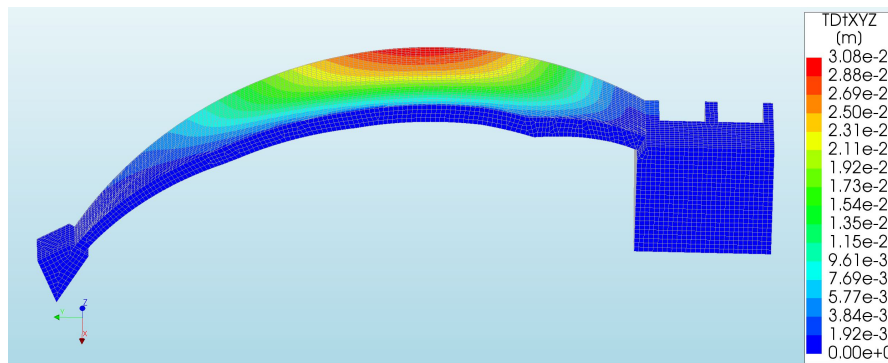


Figure 40: Total displacement of dam bottom for Model I.

Figure 39 shows a continuous and smooth displacement, which is consistent with the real response. Figure 40 shows that no base displacement occur.

Figure 41 and 42 show the reinforcement stresses in the vertical direction for a automatic and user defined stress interval, respectively.

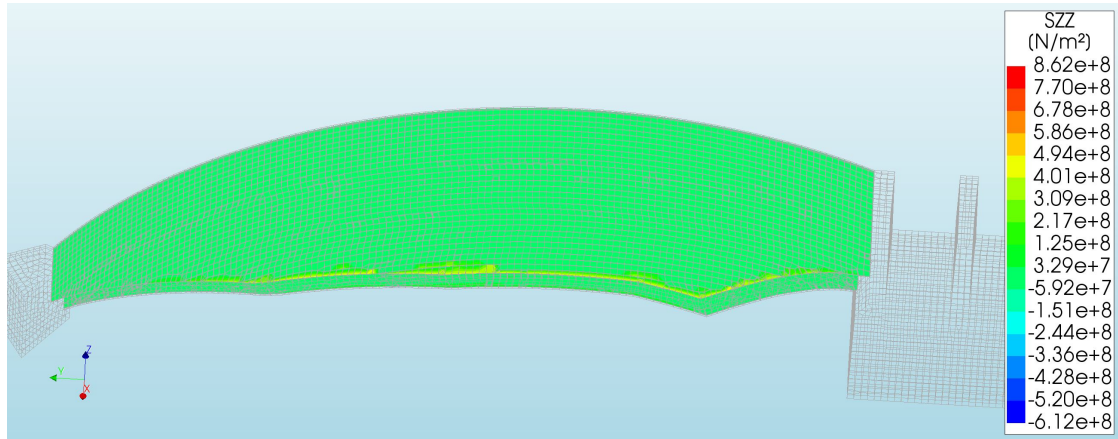


Figure 41: Reinforcement stresses in global Z-direction for Model I.

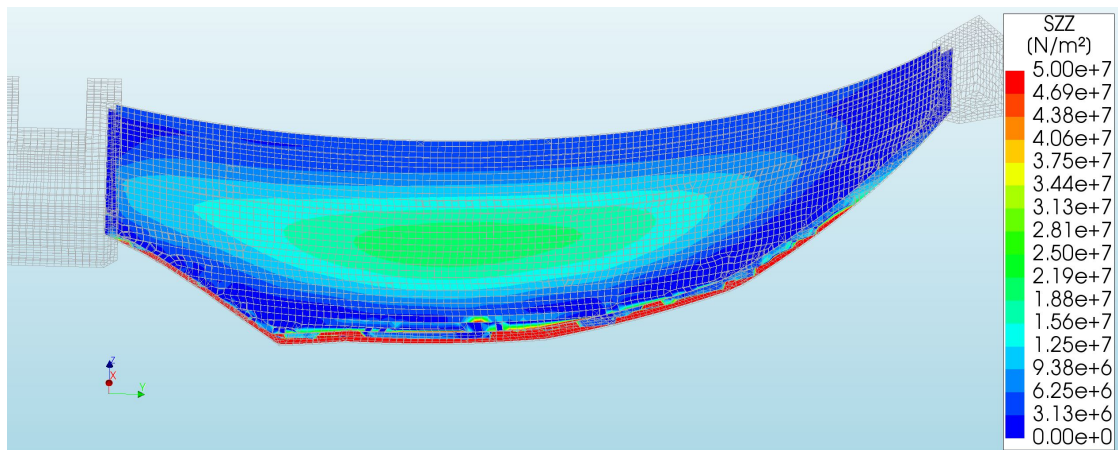


Figure 42: Scaled reinforcement stresses in global Z-direction for Model I.

Figure 41 and 42 show that the largest reinforcement stresses occur in the bottom upstream edge of the dam. The reinforcement stress variation in the rest of the dam is hard to trace from figure 41, making the scaling in figure 42 necessary.

Figure 43 and 44 show the normal crack strains in the dam. With this mesh the crack bandwidth, which relates crack strain and crack width in DIANA, is almost equal to unity. This means that crack strain and crack width have almost equal values.

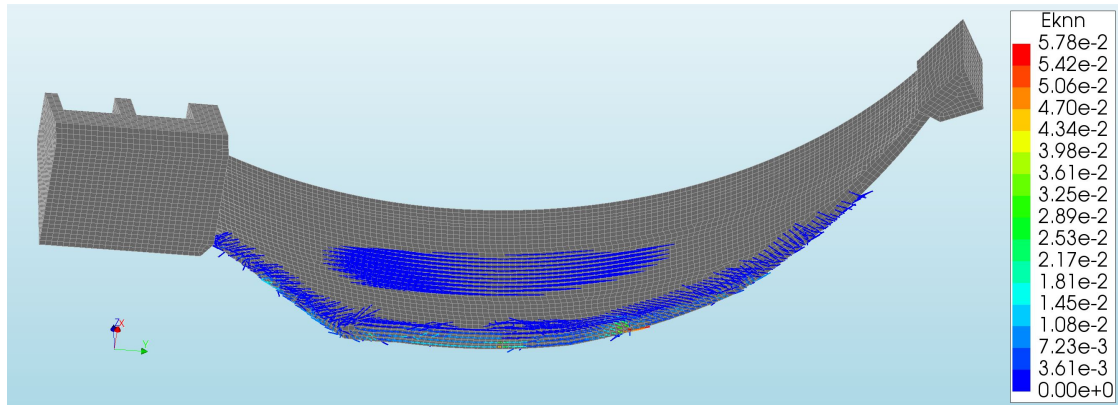


Figure 43: Crack strains on the downstream side in Model I.

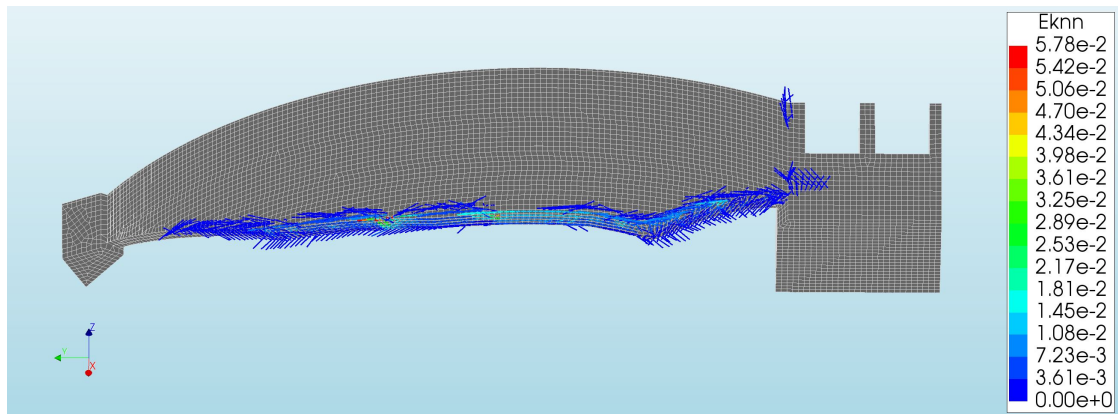


Figure 44: Crack strains on the upstream side in Model I.

It is evident from figure 43 and 44 that large and extensive cracking occurs at the bottom boundary of the dam. Some small cracks are also initiated at the middle of the downstream face of the dam, as seen from figure 43. The connection between the spillway and the dam arch are also prone to cracking, as seen from figure 44.

Figure 45 and 46 show the principal stress vectors projected onto the dam surface.

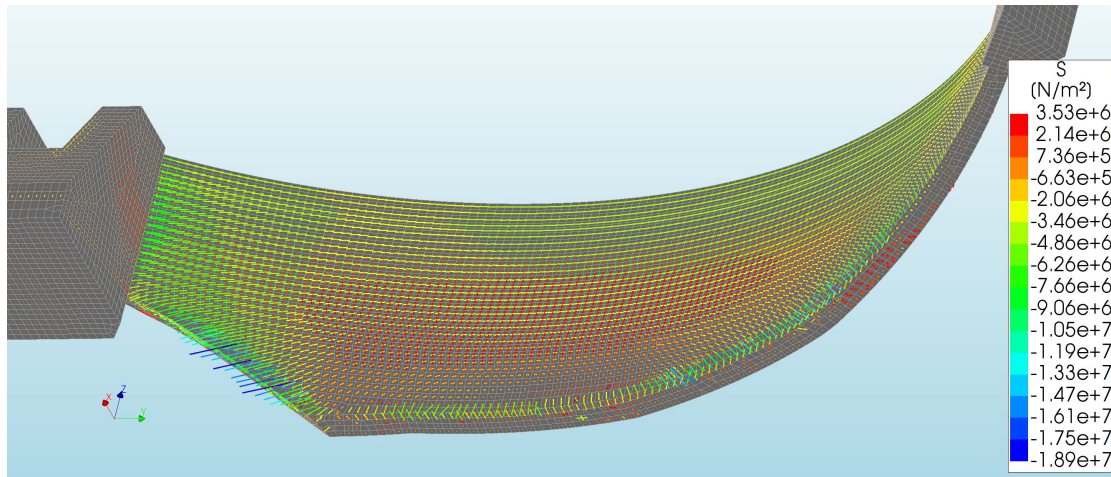


Figure 45: Principal stress field on the downstream side in Model I.

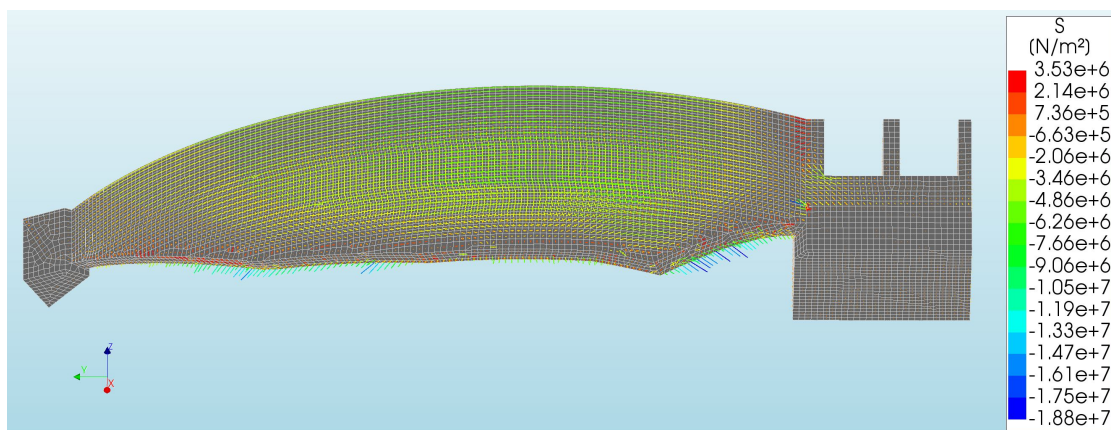


Figure 46: Principal stress field on the upstream side in Model I.

Figure 45 shows concentrations of compressive stress on the downstream bottom edge. From figure 46, the bottom of the dam are in tension, but the stresses are small due to extensive cracking. The stress field becomes more regular towards the crest, consistent with load carrying by arch effect. The clamping of the arch is also seen from the high stresses between the spillway and dam arch in figure 46.

6.2 Model II : Dam with boundary interface

Figure 47 shows the absolute value of the dam displacement.

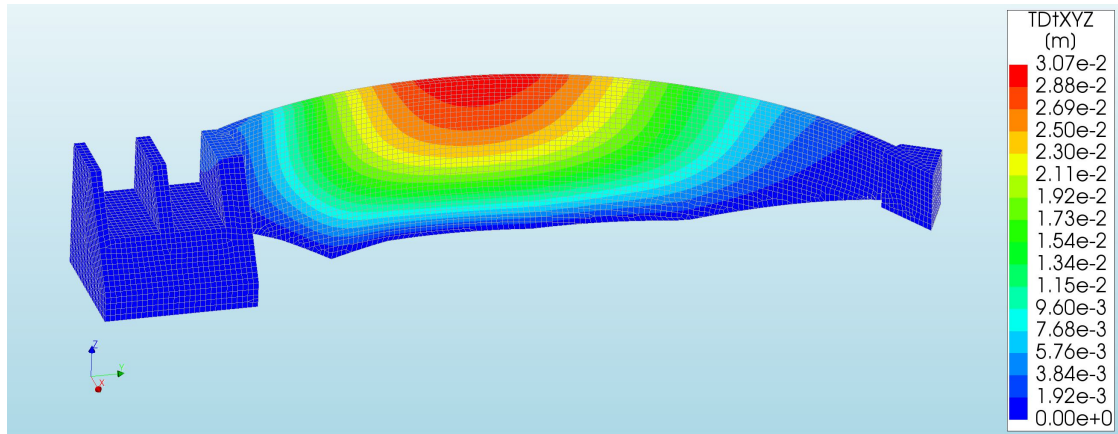


Figure 47: Total displacement contour plot for Model II.

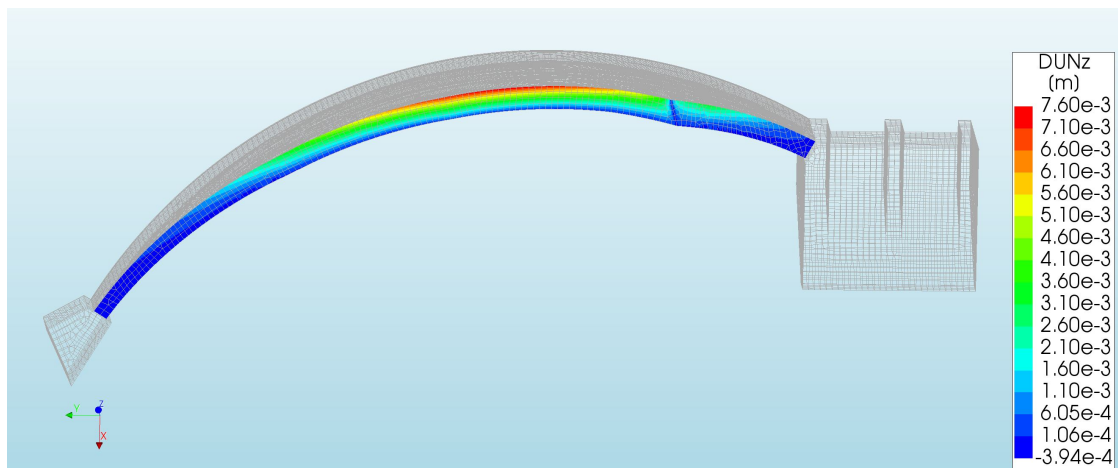


Figure 48: Interface relative displacement for Model II.

Figure 48 shows the relative displacement in the boundary interface. The interface allows only for a displacement component in the upward direction normal to the bottom, which is the one shown in figure 48. A discontinuity in the uplift, located at the sharp corner near the spillway, is seen from the figure.

Figure 49 and 50 show the principal stress vectors projected on the dam surface.

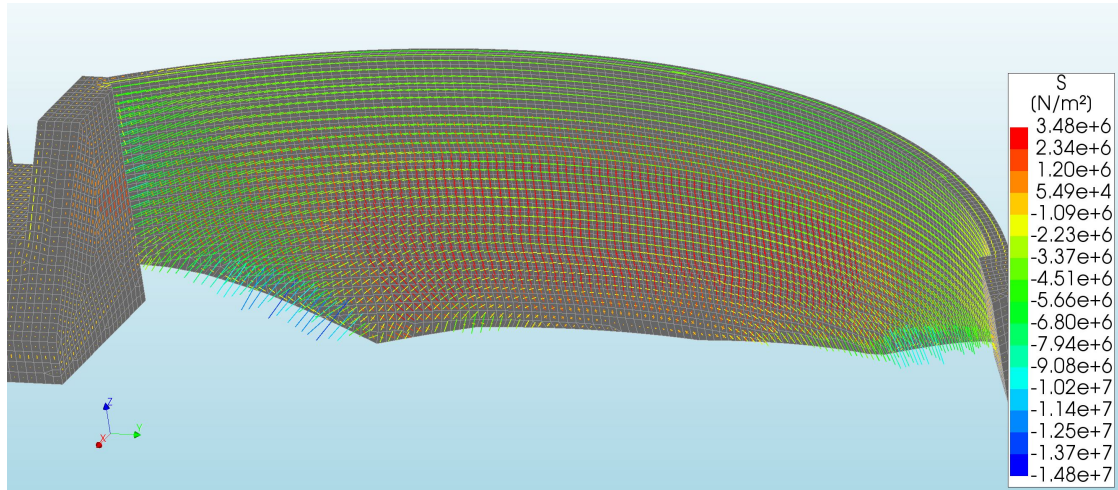


Figure 49: Principal stress field on the downstream side for Model II.

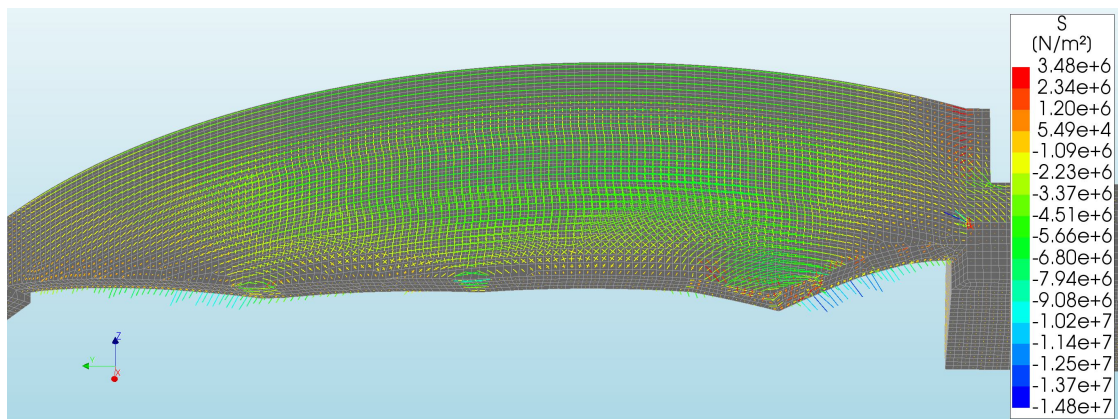


Figure 50: Principal stress field on the upstream side for Model II.

Figure 50 shows low stresses in the bottom boundary of the dam. However, near the sharp edges of the bottom, the stress concentrations become significant. Three such concentrations are observed from figure 50. It is noted from figure 49 that significant stresses on the downstream bottom edge occur only near the spillway and support. This figure also shows a large extent of tensile stresses on the downstream face of the dam.

Figure 51 and 52 show the normal crack strains for the dam.

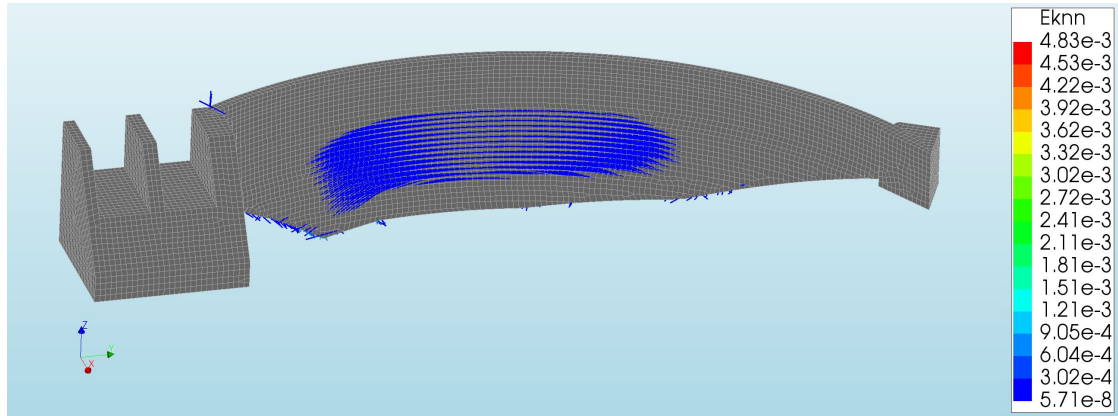


Figure 51: Crack strains on the downstream side for Model II.

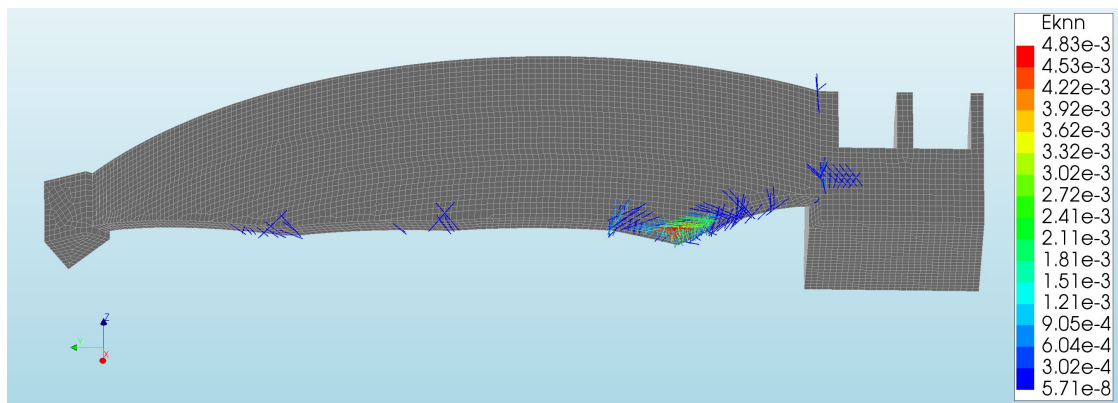


Figure 52: Crack strains on the upstream side for Model II.

Figure 52 shows cracking in all sharp edges of the dam bottom. The bottom corner near the spillway shows by far the largest crack strain in the dam. The middle of the downstream face of the dam in figure 51 is cracked, but the cracks are very small. Cracking occurs at the connection between the arch part of the dam and the spillway also in this analysis.

6.3 Model III : Dam and bedrock with interface

Figure 53 shows the absolute value of the dam and bedrock displacements.

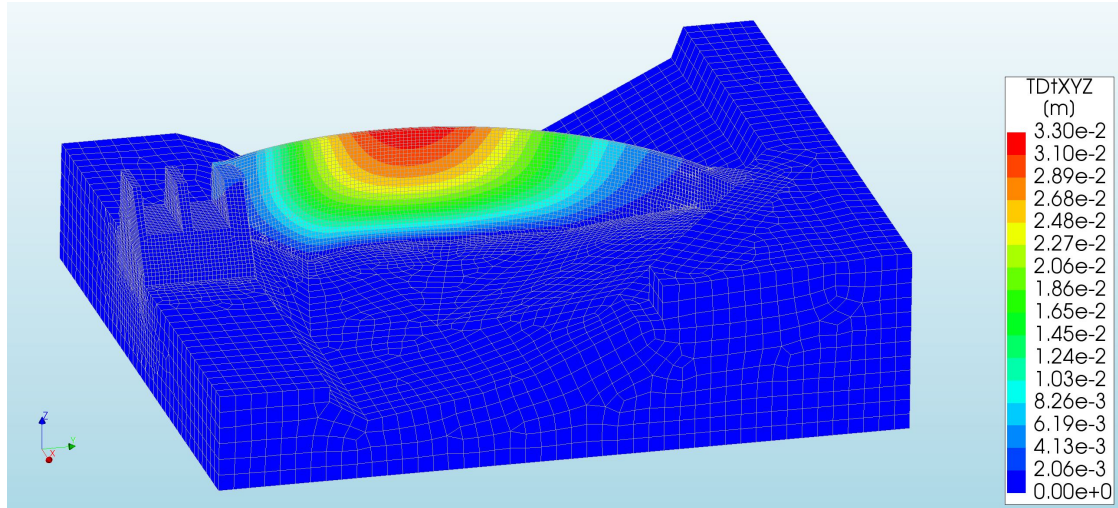


Figure 53: Total displacement contour plot for Model III.

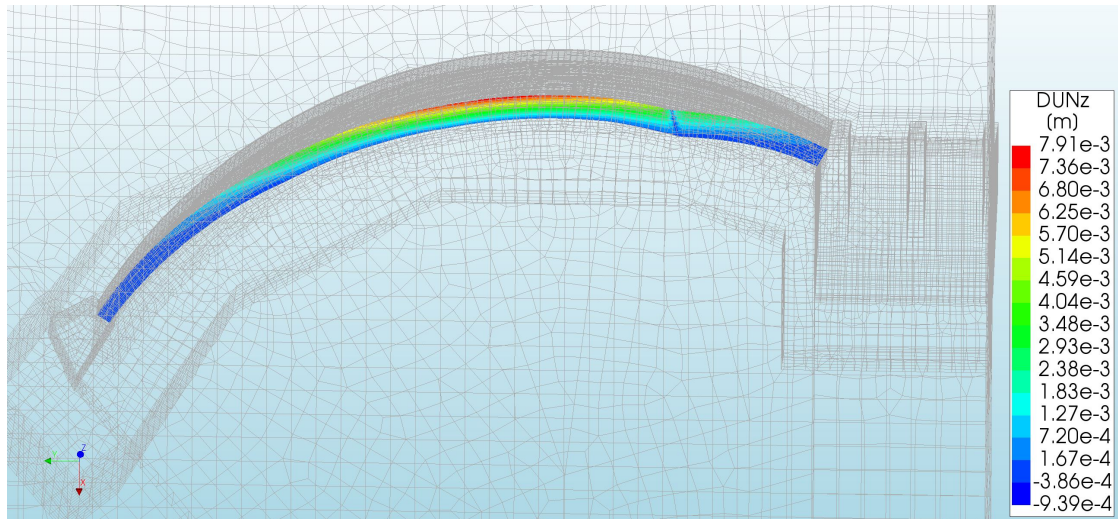


Figure 54: Interface relative displacement for Model III.

Figure 54 shows the relative displacement between the dam and the bedrock in a direction normal to the dam bottom. This is the only component of relative displacement allowed. A discontinuity in the uplift is also observed in this model, as seen in figure 54.

Figure 55 and 56 show the principal stress vectors projected on the dam and bedrock surfaces.

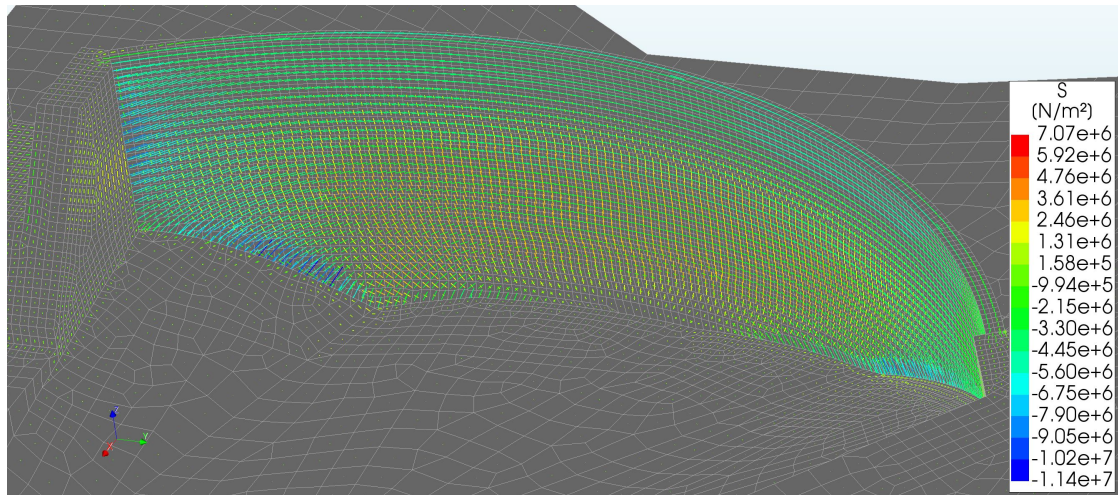


Figure 55: Principal stress field on the downstream side for Model III.

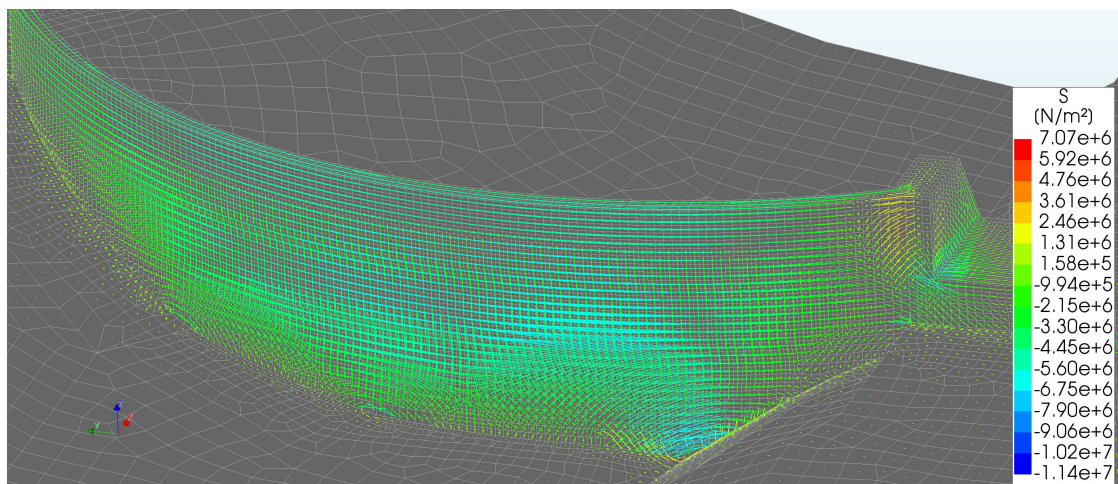


Figure 56: Principal stress field on the upstream side for Model III.

From figure 56, the most considerable stresses in the dam bottom seem to propagate from the corners in the geometry. Figure 55 shows small stresses in the middle of the downstream bottom edge, while larger stresses occur near the spillway and support. Figure 55 and 56 clearly show the disturbance in the stress field near the bottom boundary.

Figures 57 and 58 show the normal crack strains for the dam.

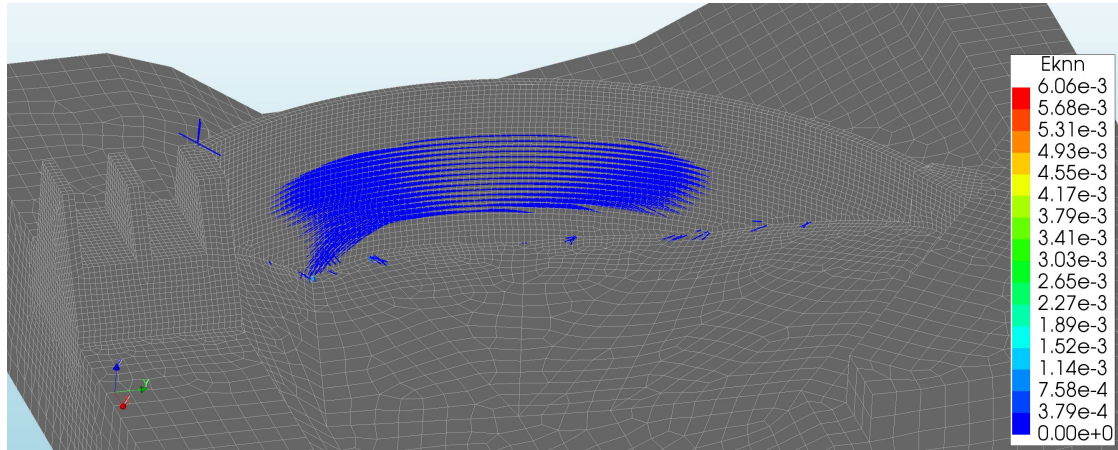


Figure 57: Crack strains on the downstream side in Model III.

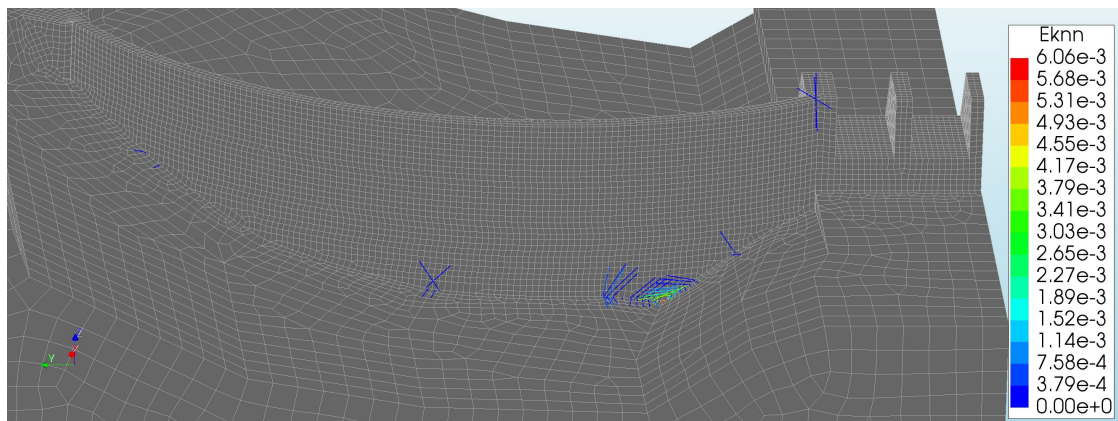


Figure 58: Crack strains on the upstream side in Model III.

Figure 58 shows significant cracks at the bottom corner near the spillway. Besides this, there are only a few cracks at the rest of the bottom boundary and on the upstream side. From figure 57, a large area in the middle of the downstream face is cracked, but the cracks are small. The cracks in this area will propagate to the bottom of the dam.

6.4 Model IV : Dam and bedrock with contact interface

Figure 59 shows the absolute value of the dam and bedrock displacements.

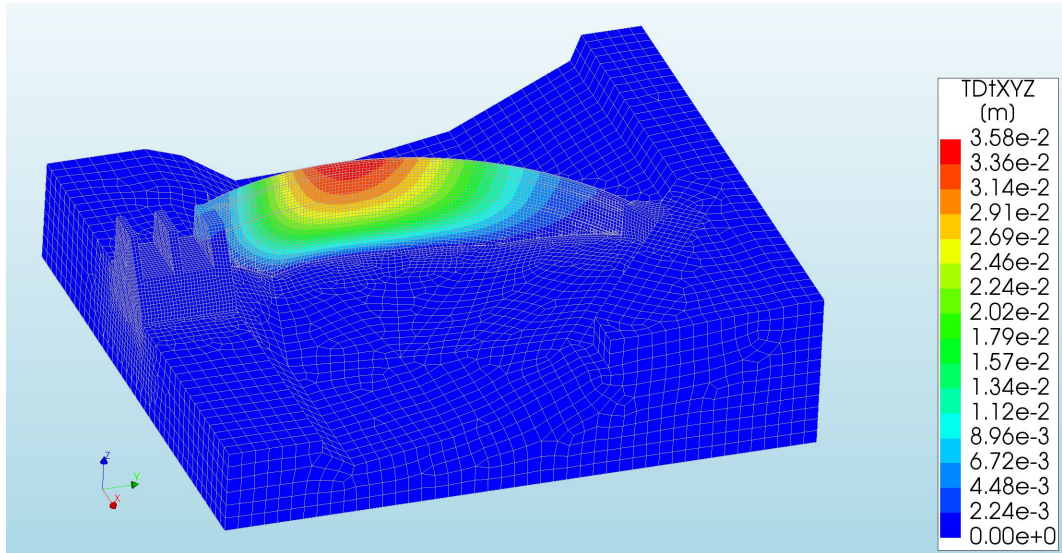


Figure 59: Total displacement contour plot for Model IV.

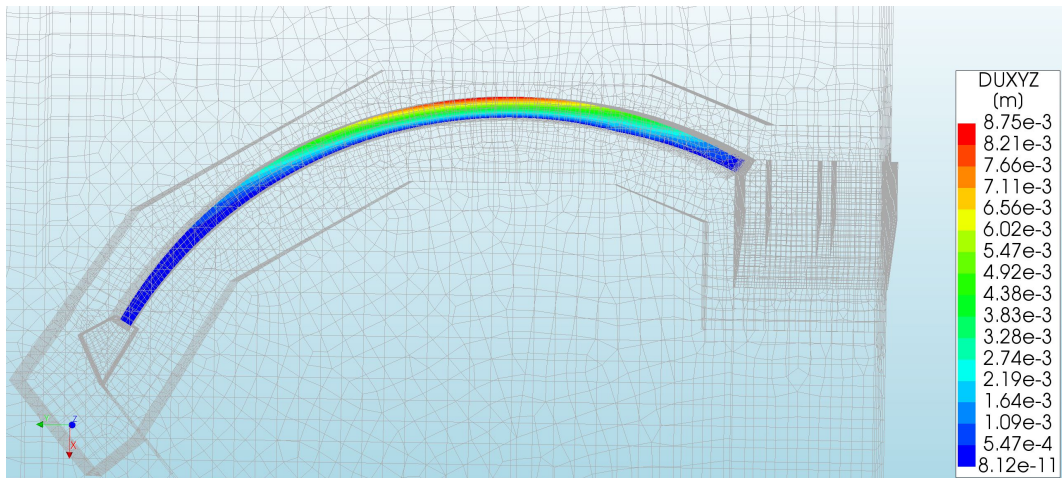


Figure 60: Interface relative displacement for Model IV.

Figure 60 shows a very smooth absolute value of the interface relative displacement. The absolute value almost coincides with the relative displacement in the upward vertical direction. However, when using the absolute value, the very small bedding of the dam shown by the blue area in figure 60 has a positive value.

Figure 61 and 62 show the principal stress vectors projected onto the dam and bedrock surfaces.

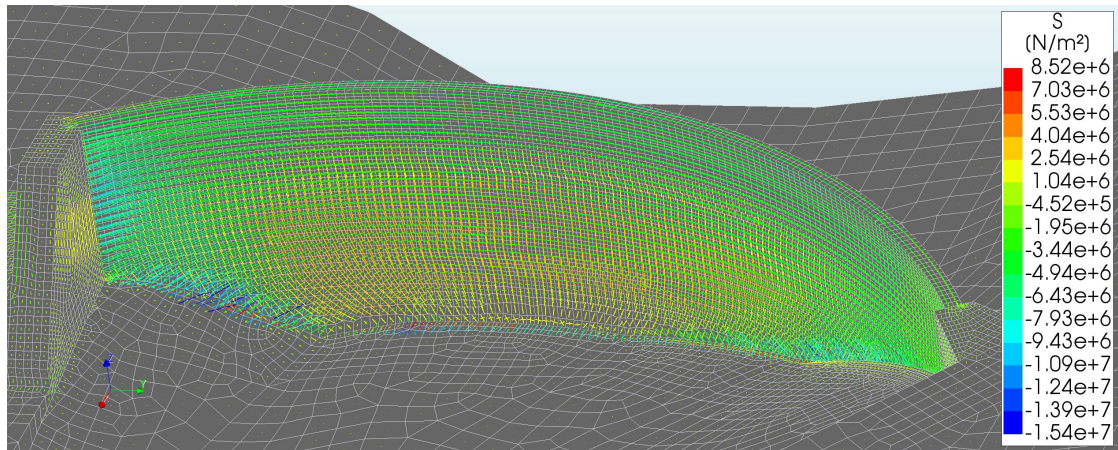


Figure 61: Principal stress field on the downstream side in Model IV.

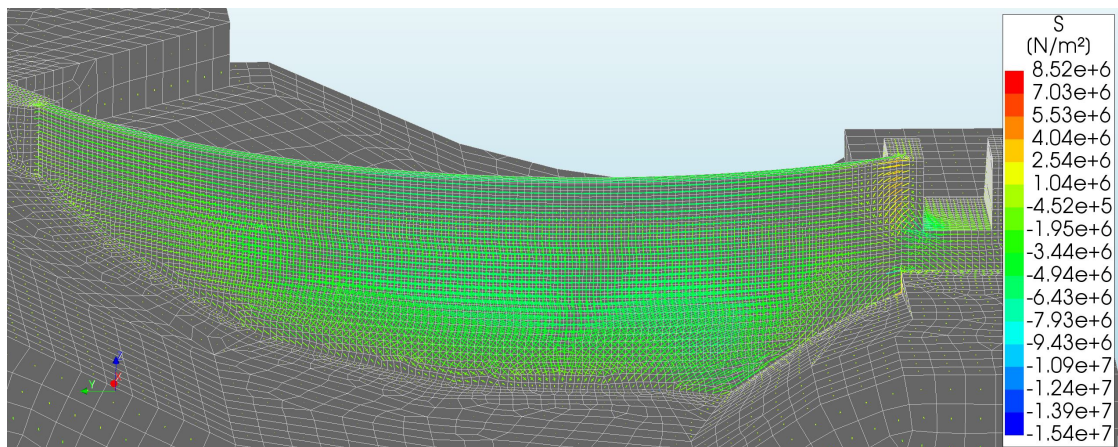


Figure 62: Principal stress field on the upstream side in Model IV.

From figure 62, it is evident that the stress field near the bottom boundary is smooth, and no apparent stress concentrations occur. Figure 61 shows large stress concentration at the downstream bottom dam edge, where the translation constraint is added.

Figure 63 and 64 show the normal crack strains for the dam.

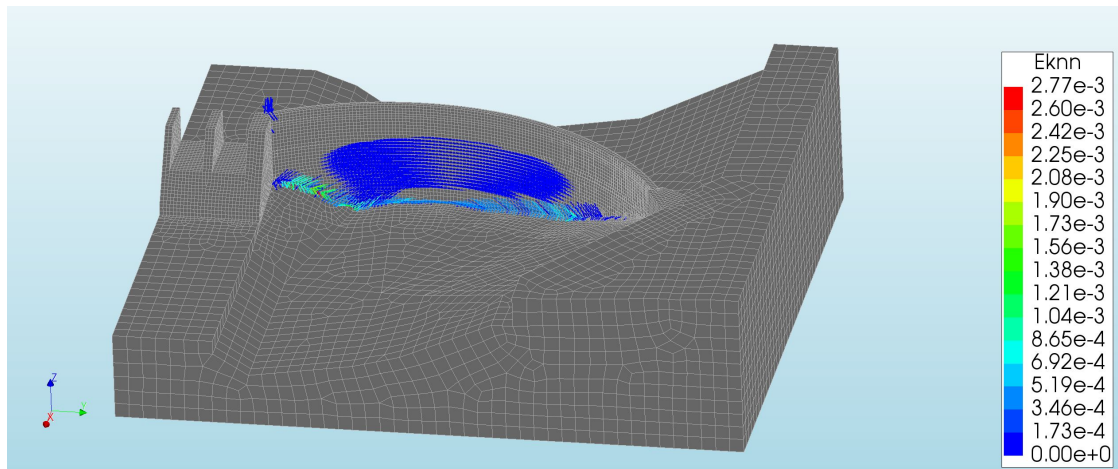


Figure 63: Crack strains on the downstream side in Model IV.

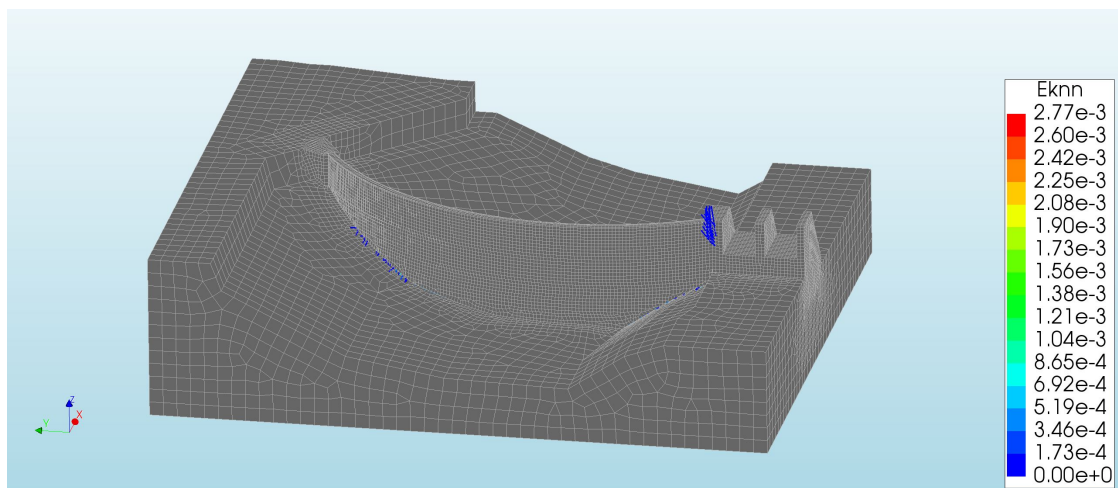


Figure 64: Crack strains on the upstream side in Model IV.

Figure 64 shows hardly any cracks at the upstream side of the dam. However, extensive cracking occur at the connection between the arch part of the dam and the spillway. On the upstream side, the bottom of the dam is almost free of cracks. From figure 63, extensive cracking occurs at the downstream side of the dam. Here, the most significant cracks occur at the bottom boundary, whereas the cracks at the middle of the dam are small.

6.5 Comparison of Results

Figure 65 shows the global X-displacement of the dam along the crest.

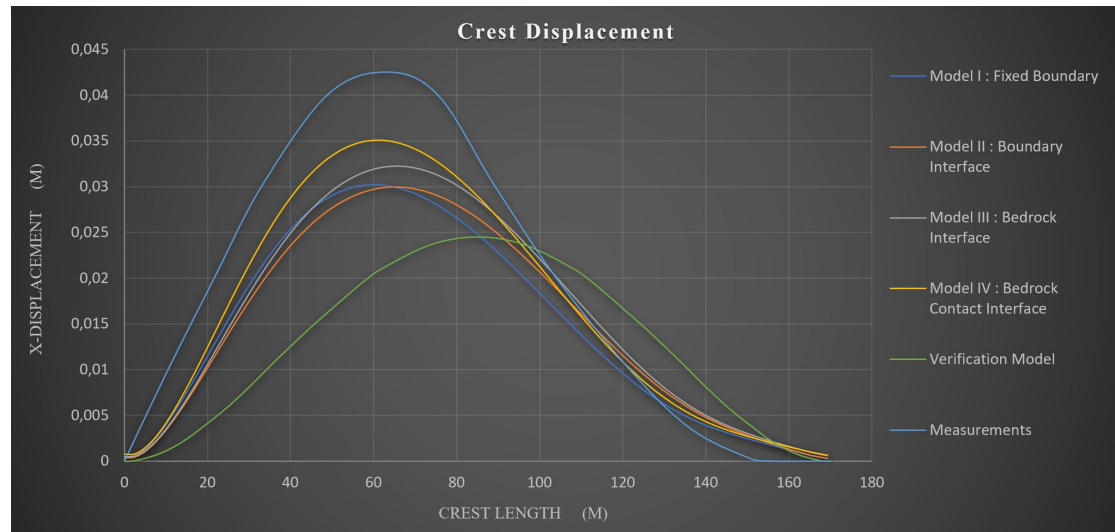


Figure 65: Global X-displacement along the dam crest for the different models. The spillway is at the origin.

In figure 65, Model IV shows an increase in crest displacement compared to the other three models, which are quite similar to each other. The displacement of Model IV is approximately 17 % higher compared to Model I. Model I and II show almost the same displacement response. Model I and IV, and Model II and III show similar displacement modes, but different magnitude. In figure 65, the real measured crest response of the dam from the winter of 2011 is included as well [17]. It is noted that the measured response is about 20 % larger than Model IV, but shows a quite similar displacement mode. This discrepancy in magnitude is most likely due to the neglecting of temperature load in the present work. The verification model presented in chapter 5 shows a very different displacement mode and magnitude compared to the FE-models. It predicts a maximum displacement which is about 80 % of Model II. It is noted that the radial displacement of the verification model is plotted, not the X-displacement. The difference between these is small since the arch is shallow.

Figure 66 shows the global displacement in X-direction, along a vertical section. The location of the section coincides with the maximum displacement point for each of the individual models. Thus, the location of the sections differs slightly among the models.

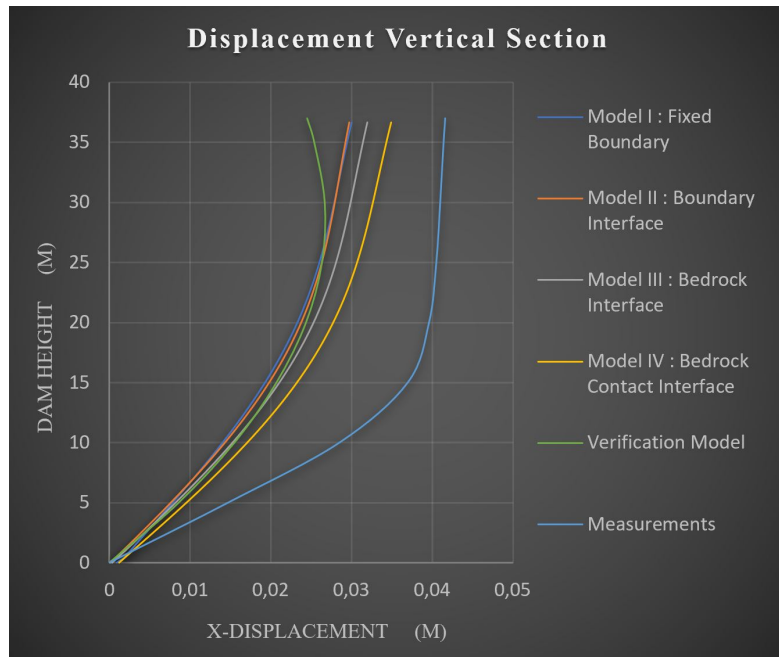


Figure 66: Global X-displacement along a vertical section for the different models.

Again, Model I and II are very similar, as seen in figure 66. There is an increase from these models to Model III. However, Model IV clearly shows the largest displacement. It is noted that the displacement modes are quite similar for all the four FE-models. The real measured displacement from the winter of 2011 [17] differ from the FE-models in both magnitude and mode. This difference is most likely due to the neglecting of temperature load in the present work. The analytic model is similar to the four FE-models but shows a discrepancy at the crest.

Figure 67 shows the displacement-load relationship in global X-direction for the four FE-models. The node in the dam crest with the largest displacement is used as basis for the plot. Hence, the position of this point varies slightly among the models.

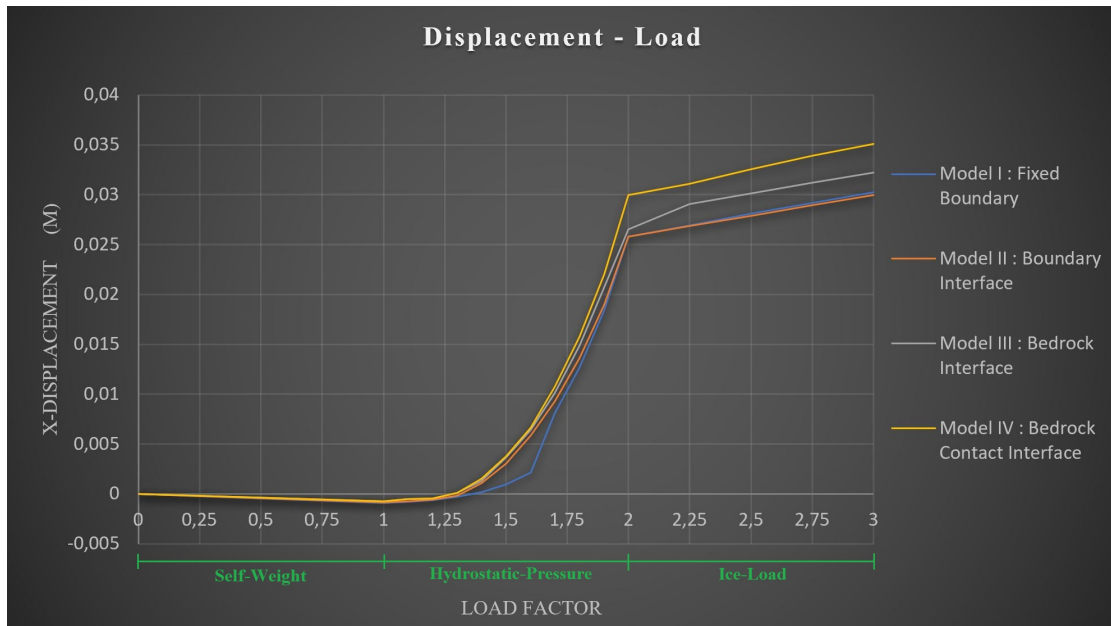


Figure 67: The displacement-load relationship for the different models.

The smoothness of displacement-load relation is dependent on the number of load steps used. For each load, the same number of load steps is used in all analyses. Hence, the different models becomes comparable in figure 67. In this figure, it is evident that Model I manage more water load than the other models, before the displacement starts a step increase when about 60 % of the hydrostatic-pressure is applied. The ice-load causes the largest difference in displacement between Model I/II and Model III, otherwise, these models are quite similar. Model IV and II show the smoothest displacement-load curves.

Figure 68 shows a comparison of the crack pattern from Model IV and the real crack pattern of the dam [17].

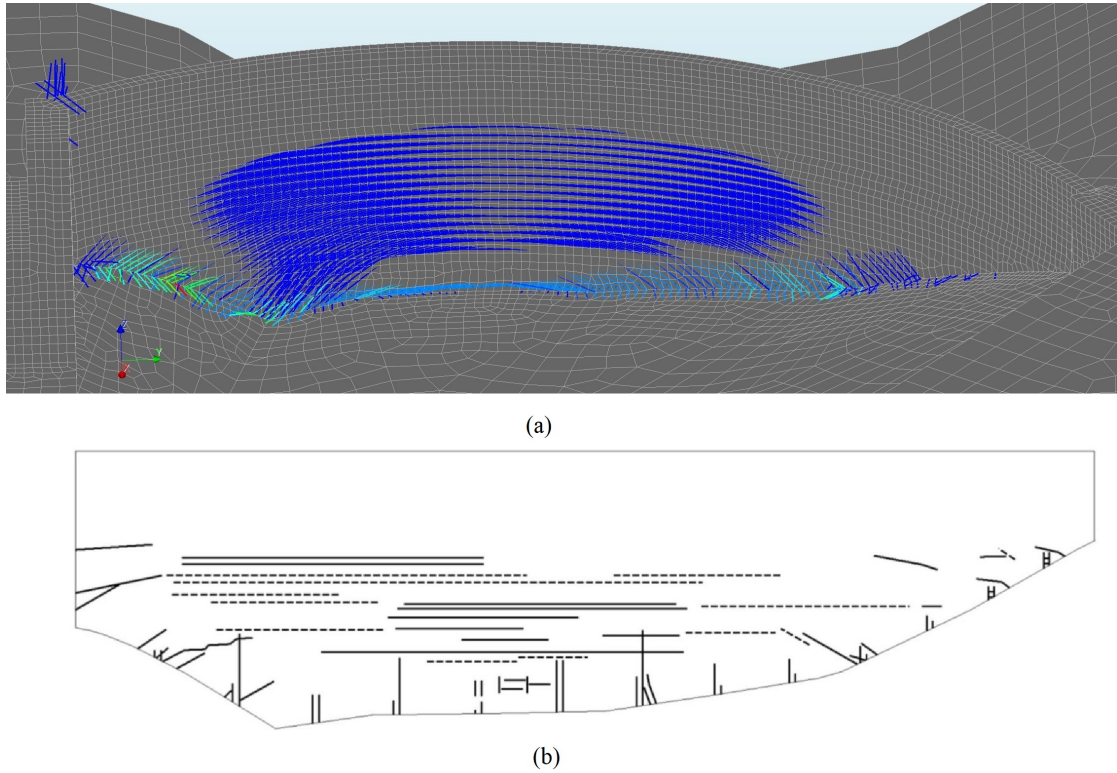


Figure 68: Crack pattern from Model IV (a) and the real crack pattern [17] (b).

The two patterns resemble, but some cracks near the spillway and some vertical cracks in the middle of the dam is not present in Model IV. It is also noted that the cracks from Model IV seem more smeared than the real crack pattern. Some real cracks near the spillway are not present in Model IV. However, Model IV shows initiated cracking at the top of the spillway.

Figure 69 shows the scaled principal stress field for all the analyses, seen from downstream.

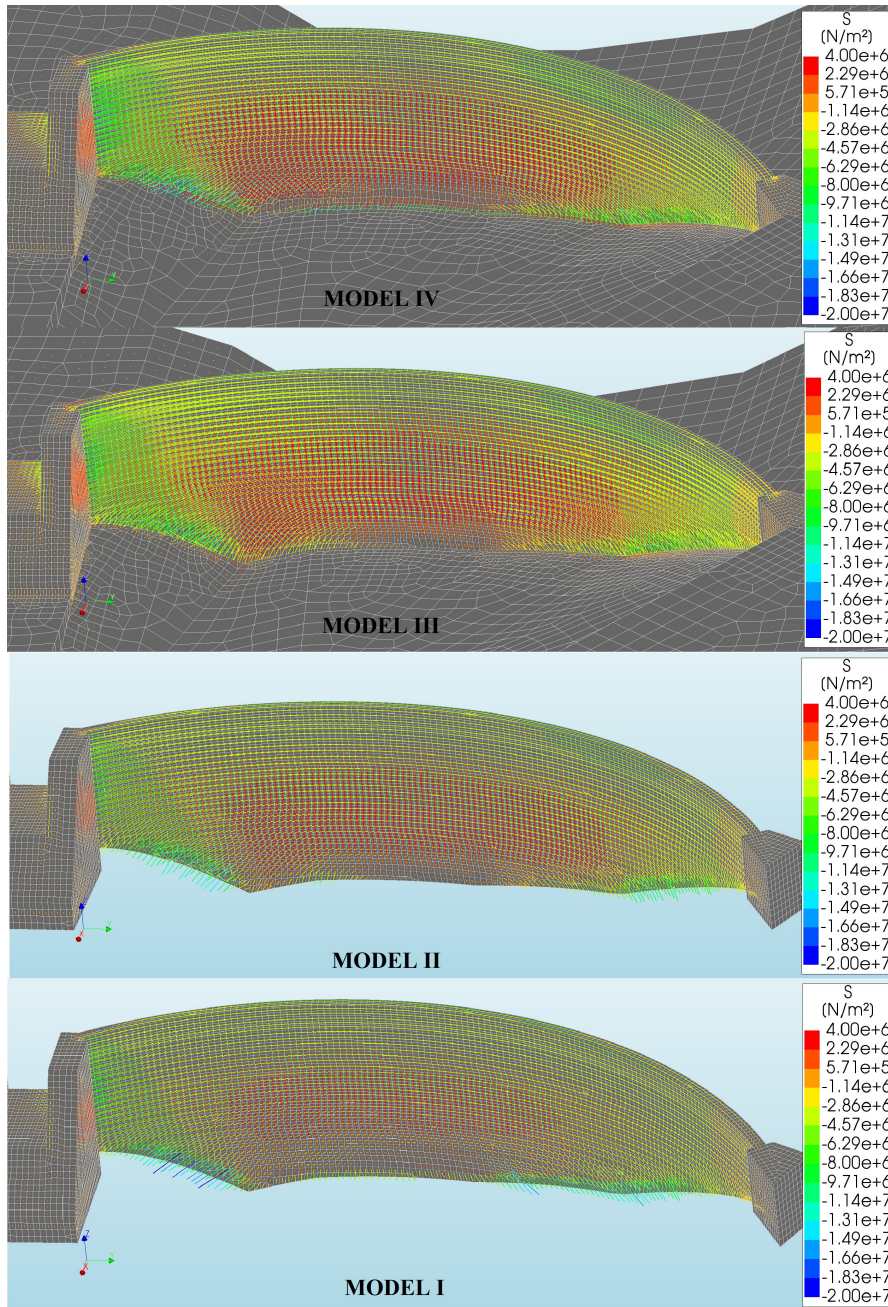


Figure 69: Stress comparison, downstream.

Figure 70 shows the scaled principal stress field for all the analyses, seen from upstream.

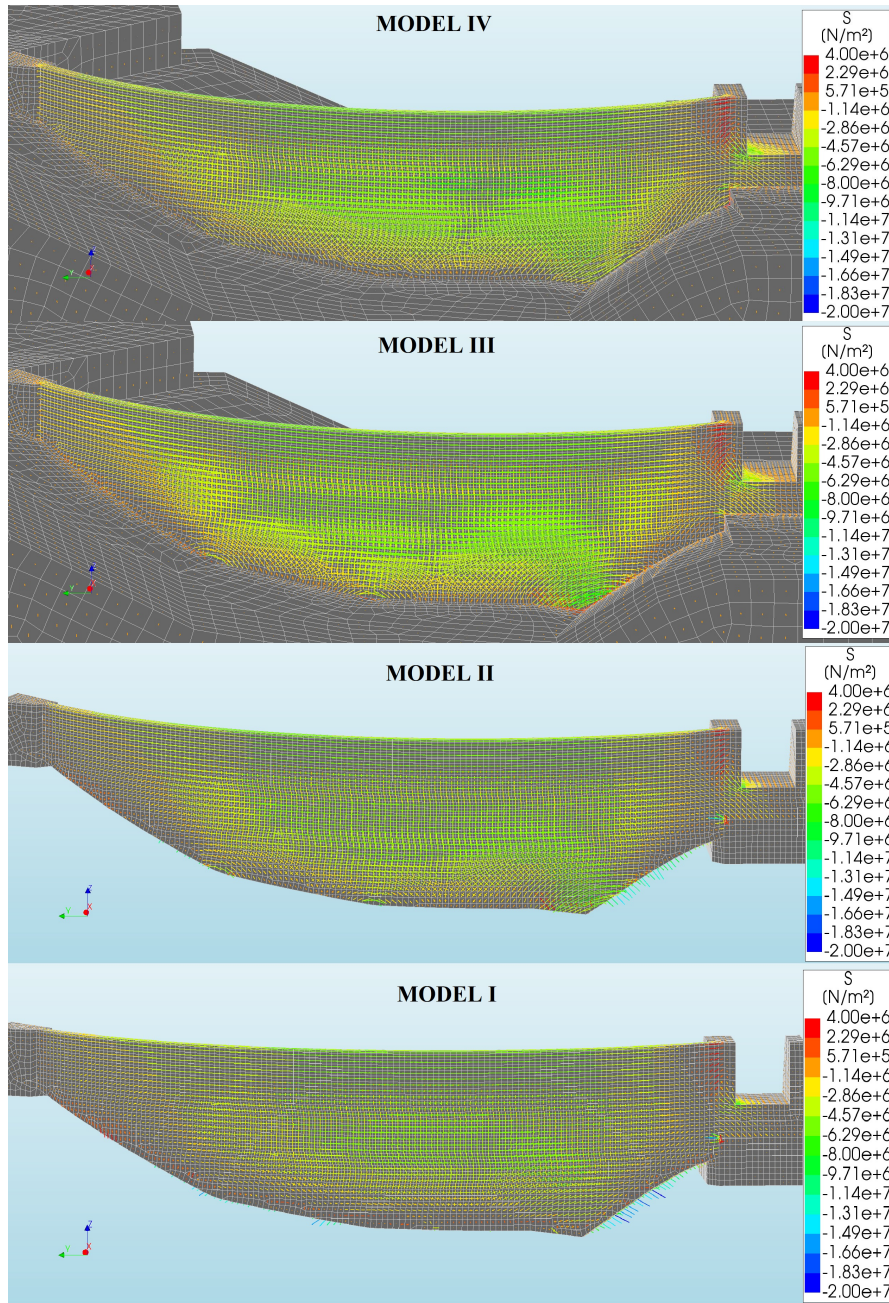


Figure 70: Stress comparison, upstream.

7 Discussion of individual analyses

In this chapter, the results from the individual analyses are discussed. The main goal of the discussion is to determine how the results from the models fulfill the criteria for realistic modelling. That is, if the models show an increasing compliance with the physical problem as intended.

For convenience, the criteria for realistic modelling from chapter 4.3.1 are repeated below:

1. Spillway and support should be elastically supported at the bottom, but is close to rigid at the base.
2. Low, but present, bedding of dam in bedrock.
3. No cohesion in the connection between the dam arch and the bedrock.
4. Reduced resistance for circumferential displacement of the dam in the connection between the dam arch and the bedrock.
5. No relative radial displacement in the connection between the dam arch and the bedrock.
6. The real stress field in the bottom of the dam arch should be approximated since the idealized geometric shape of the bottom is used.

7.1 Model I : Dam with fixed boundary conditions

Criteria 1 and 2 about elastic support are not satisfied since the dam is completely fixed at the base, as seen from figure 40. The reason for this is that all faces of the dam, which is shared by the dam and the bedrock, are fixed from all translation. The dam should be subjected to some base displacement in the physical problem, being elastically supported by the bedrock. This suggests that the model is too stiff, and thus underestimating the displacement response. Also, when the dam base is too rigid, the stresses might not be able to redistribute realistically.

The criteria of no cohesion and low resistance for circumferential displacement are not satisfied as seen in figure 40, which shows no translation of the dam bottom. The observation here is consistent with a boundary fixed from all translation, which is defined in the model. This modelling causes an infinite cohesion and resistance for circumferential displacement at the bottom of the dam arch. Also, by failing the no cohesion criterion, there will be an unrealistic large rotation stiffness about the circumferential axis of the dam arch. This will attract forces, making plate action dominate at the bottom. Cracking occurs when the moment capacity of the bottom is reached, as seen from figure 43 and 44, which allows for a global redistribution of forces. However, since bond slip and fracture of reinforcement are not modelled, there will be a significant rotation resistance even when the concrete is cracked. This is seen from the high reinforcement stresses in the upstream bottom, shown in figure 41. Therefore, the problem of infinite cohesion will influence the global response of the dam, not only cause cracking at the bottom.

No radial displacement of the dam arch bottom occurs, as seen from figure 40. The formulation of boundary conditions in this model causes no displacement, instead of no relative displacement. Thus, this criterion is therefore too strictly satisfied, due to the exclusion of bedrock. This might underestimate the dam displacement by making the model too stiff.

The criterion regarding the approximation of stress in the dam bottom is harder to assess from the results. However, from figure 45 and 46, it seems that the stresses are largest at the downstream edge of the bottom. This indicates that Model I satisfies the stress criterion. The reason for this is that the dam will likely behave as depicted to the left in figure 22. This will make most of the support forces transferred via the downstream side of the dam bottom in the physical problem. It was expected that the fixed boundary would show a more evenly distributed stress field in the bottom. However, it seems likely that the support forces will concentrate at the least cracked part of the bottom boundary, which is the downstream side as seen by comparing the strain values in the dam bottom in figure 45 and 46.

7.2 Model II : Dam with boundary interface

Criterion 1 about the spillway and support is not fulfilled, as seen from figure 47. This is by definition since the base of these are fixed from translation. The failing of this criterion has the same effect as in Model I. No information about the anchoring of the spillway and support is given in the benchmark description, making it challenging to model the boundary conditions in the bottom of these more realistic. The criterion for circumferential motion is not fulfilled. This is indirectly proved by figure 48, since the only displacement component of the interface is in the normal direction. The reason for failing criterion 4 is the high linear elastic tangential stiffness of the interface. By not allowing for circumferential motion, not even where uplift occurs, this can cause some unrealistic constraining forces. Circumferential contraction of the dam arch bottom can be constrained in a more uniform way, instead of constrained only at the support and spillway. This is assumed to be less realistic.

The criterion regarding the dam bedding is not fulfilled. This is seen from figure 48, showing a negligible bedding. The reason for the result is the large compression stiffness of the interface. The radial displacement criterion is also fulfilled too rigidly, for the same reason as for Model I. An effort was made to adjust the stiffnesses of the interface in tangential directions and in compression, to simulate the bedrock. To find the bedding stiffness of the bedrock, a DIANA model with extensive bedrock and a downward prescribed displacement on a small area at the top, was established. However, the normal contact stiffness of the bedrock varied too much with the shape of the area subjected to prescribed displacement, and the size of the prescribed displacement. Since the contact stiffness of the bedrock is large, the only reasonable approach was to take the stiffnesses of the interface large enough to almost brace the dam bottom. It is noted that the interface high compression and tangential stiffnesses are not equal to infinity, and the low tension stiffness is not equal to zero since this might cause numerical problems.

The criterion of stress approximation is not fulfilled. This is evident from figure 50, showing a low and uniform stress under a large area of the dam bottom. The reason for failing the criterion is the high and linear elastic tangential stiffness of the interface, which will cause the support forces to distribute uniformly. Since

extensive cracking in the bottom does not occur in this model, the forces are not able to redistribute more realistically to the downstream bottom edge in the same way as in Model I.

The cohesion criterion is only partly fulfilled. The dam shows a uniform uplift in figure 48, however, some cohesion occurs. This can be seen from figure 71, which shows the upstream bottom corner of the dam arch, and is a close-up of figure 47.

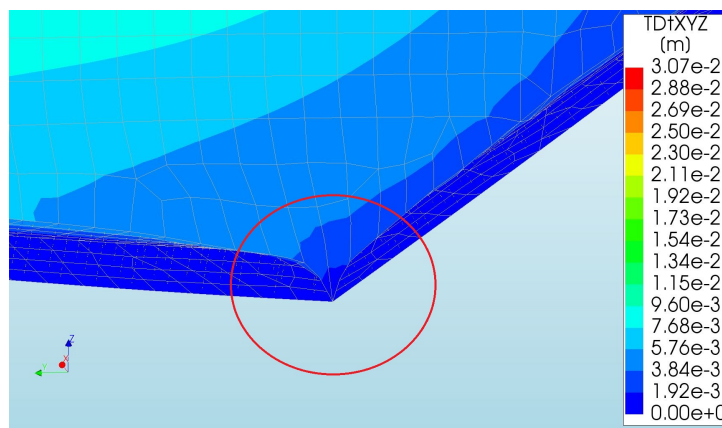


Figure 71: False anchoring

There is no apparent reason why this corner should be anchored in the physical problem. The irregular shape of the anchoring shown in figure 71, where only the corner shows no displacement, is not realistic. It is also not consistent with the requirement of no cohesion between dam and bedrock. A likely explanation for this observation is false anchoring due to poorly oriented interface local axis. By default in DIANA, the normal axis is perpendicular to the surface of the interface. The dam will tend to lift in a direction normal to the crest, which is the vertical direction. If the local interface normal axis is at a substantial angle from the global vertical axis, the real uplift of the dam will have a component along the tangential direction of the interface. Thus, some uplift will be constrained by modelling a high linear elastic tangential stiffness. This indicates that the failing to meet the low circumferential resistance criterion is the underlying reason for the problem in figure 71. The false anchoring also explains the discontinuity in the interface

relative displacement in figure 48, and the stress and crack concentrations of the three bottom corners shown in figure 50 and 52, respectively. Cracks and stress may have a tendency to concentrate at non-smooth areas like these corners in the physical problem as well, but most likely not in the extent shown in the present results. False anchoring of only the corners may not cause a significant change in the global response, but the underlying effect is more substantial. The problem is evident in the corners, but will occur every place where the interface normal axis is at an angle to the vertical axis. This is true for a significant portion of the bottom surface, and false cohesion will thus have an impact on the global response.

7.3 Model III : Dam and bedrock with interface

The cohesion criterion is not entirely fulfilled, and the circumferential criterion is not fulfilled, as seen from figure 54, by the same logic as in chapter 7.2. Model III also suffer from false anchoring, which is caused by the use of the same interface properties as in Model II. It is thus referred to the discussion of Model II for elaboration. The underlying reason for this problem was a large resistance for circumferential motion. To avoid this problem, an approach to isolate the radial and circumferential properties of the interface was attempted, to satisfy both of the corresponding criteria. The interface under the dam arch was divided into several sections with different interface local axis. Only one of the interface tangential directions is possible to specify in DIANA, and this was defined radial to each section. By specifying a low stiffness in both the other tangential direction and the normal direction of the interface, this should make the dam bottom free to move both in the circumferential and the normal direction to the dam bottom. The radial displacement criterion should be satisfied by modelling a high stiffness in this direction. The discretization of the interface with corresponding interface axis is shown in figure 72.

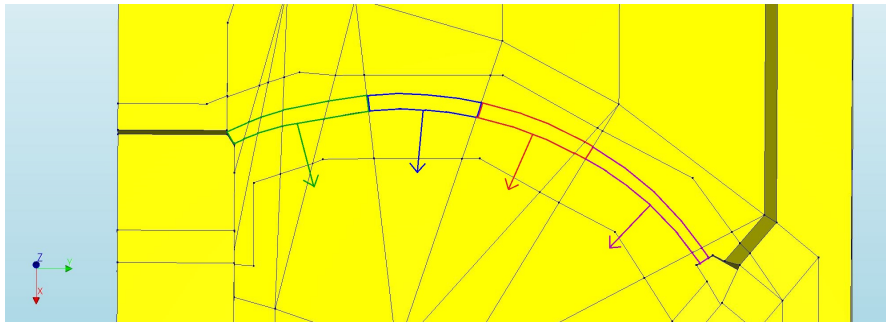


Figure 72: Discretization of the interface to isolate radial and circumferential properties

Unfortunately, this approach turned out to give poor results. The dam showed some slip in the radial direction, especially at the border between the areas with different interface orientation. The reason for this might be that the interface direction was discretized too coarse, and not updated to be radial to the dam at

each point. It was concluded that to get smooth and accurate enough results with this approach, the discretization of the interface area with corresponding element local axis would have to be very fine. Even this may not be adequate, and this approach was deemed not feasible. The upside of this failed attempt is that Model III is then very similar to Model II. The inclusion of bedrock is the only difference, which makes the effect of the bedrock easier to isolate.

Criteria 1 and 2 about elastic bottom support are satisfied since the bedrock is included. It is hard to see evidence of this in figure 53 and 54, since the base displacement of the dam is small, due to the predicted large contact stiffness of the bedrock. However, it is present since the bedrock is assigned realistic linear elastic material properties. Again, measures to make the spillway and support more realistic attached to the bedrock has not been taken due to lack of information. However, since these are surrounded by bedrock, it is assumed that approximating them as fixed to bedrock introduces negligible error.

The no radial displacement criterion is fulfilled as seen from the dam-bedrock connection in figure 53. It is noted that the total radial motion is small, not only the relative. This might suggest that Model I and II is closer to satisfying this criterion than initially assumed.

Whether the stress criterion is fulfilled is harder to assess from the results when the bedrock is included. However, since this model is very similar to Model II, also seen by comparing the stress fields in figure 69 and 70, it is assumed that the same logic as given in chapter 7.2 for Model II applies here as well. Hence, Model III does not satisfy the criterion.

7.4 Model IV : Dam and bedrock with contact interface

Similar to Model III, criteria 1 and 2 about elastic base support are fulfilled. This might not be clear by assessing the base displacement of the dam in figure 59, which shows almost no bedding. This observation is in accordance with the combination of a fixed connection between the support/spillway and the bedrock, and a high contact stiffness of the bedrock. However, it should be noted that the base of the dam has some small displacements downwards in the bedrock. These displacements are not visible in figure 59, due to the scaling, but they can be verified by investigating separate nodal displacements. The small bedding is of importance because it results in a softer structure causing force redistribution to a more realistic stress field.

The no-cohesion criterion is fulfilled, as seen from the continuous and smooth uplift of the dam bottom in figure 60. The stress field is also smooth, and neither stress nor cracks seem to concentrate near corners in the dam bottom on the upstream side, as seen from figure 62 and 64. Model II and III failed all of these observations due to false anchoring/cohesion. The no-cohesion criterion is fulfilled in this model because the tangential stiffness reduces to almost nothing where the interface is in tension. So when tension occurs, no contact is assumed, and the dam and bedrock become independent of each other. Thus, this will also fulfill the criterion of low resistance for circumferential motion, but only where there is uplift. The fulfilling of this criterion can be indirectly verified by fulfilling the no-cohesion criterion, since resistance for circumferential displacement was the underlying reason for why Model II and III failed the no-cohesion criterion.

The criterion of no relative radial displacement is fulfilled, as seen from figure 59. This is by definition since the translation constraint is used. The translation constraint was deemed necessary since only using a contact interface did not fulfill the no radial displacement criterion and produced slip. It was considered that using contact elements instead of interface elements would not change the result since the bedrock is relatively flat downstream. If the bedrock had a small incline in the downstream direction, the dam might stick to the bedrock when using contact elements allowed to lose connectivity in the mesh.

The stress criterion is approximately fulfilled, but probably too conservatively. As seen from figure 61 and 63, large stresses and corresponding cracks occur along the bottom downstream edge. The observation here is realistic, but the extent of stress and crack concentration might be too conservative. This is since the real curved bottom will likely transfer the support forces over a larger area of the dam bottom cross section. It is also noted that there are some direction changes of the cracks in the bottom boundary, as shown in figure 63. The cracks in the middle are horizontal, while the cracks become more vertical towards the spillway and the support. This observation could be explained by considering the downstream bottom edge of the dam as an arch. Since this part is constrained to have equal translation as the bedrock, it may show some constraint forces. In the middle, the circumferential displacement is low, such that cracks here are mostly due to radial forces between dam and bedrock. When moving towards the supports, the constrained circumferential expansion becomes larger, which will yield vertical cracks in combination with horizontal shear cracks. The above discussion suggests that totally constraining the downstream dam bottom edge to the bedrock might produce cracks and constraining forces, which are not present in the same degree in the physical problem. Also, if the stresses in the bottom should be more accurately predicted, the real bottom geometry would have to be implemented in the FE-model.

This model satisfies every criteria for realistic modelling and has the best compliance with the physical problem. To model the dam more realistic, the real curved bottom ought to be included in the geometry input files. An attempt was made to alter the benchmark files by modelling the dam bottom as curved. However, since the curvature of the bottom is unknown, the results would depend on this. It was thus concluded that this attempt was not feasible.

8 Discussion of results comparison

In this chapter, the response effect of how boundary conditions and connections are modelled will be discussed.

The basis for the comparison discussion is chosen to be the following:

- Displacement response
- Stress field
- Crack pattern

8.1 Comparison of displacement response

The bedrock affects the total displacement response by an increase of 7.5 % when included. This effect can be seen by comparing Model II and Model III, where the only difference is the inclusion of bedrock. The difference can be seen from figure 65, and by comparing figure 53 and 47. The bedrock will provide an elastic support under the dam arch, which causes larger motion. Motion of the spillway and support will also contribute. Since the base of these are fixed in Model II but are connected to the bedrock in Model III, the bedrock softens the dam behaviour. The difference in displacement response is not caused by translation of the spillway and support in the water pressure direction, as this should be seen in figure 65. Here, the ends of the graphs should then have different values, which is not the case. However, as arches tend to flatten out when loaded, the spillway and support may move in a direction normal to the water pressure. This motion may cause the difference in the magnitude of the modes between Model II and III and would not show in figure 65. This hypothesis is also supported by figure 67. Here it is shown that the ice-load causes the largest difference between Model II and III, and load carrying by arch effect will dominate where the ice-load is applied.

Another cause of the difference in displacement response between Model II and III is water intrusion. In Model III, water intrusion is modelled on the upstream side of the spillway and support, on the faces excavated down in the bedrock. In Model II, the spillway and the support are fixed, such that water intrusion load will go directly to the support. However, water intrusion on the spillway and support will likely have less effect, otherwise, a difference in crest displacement at the ends of the graphs should be observed in figure 65. It is noted that water intrusion in Model III and IV is applied only at the dam faces. This is because the forces would cancel out if water intrusion were applied to both the bedrock and the dam, when they share nodes.

The size of the displacement response is almost unaffected by the inclusion of an interface under the arch part of the dam. This can be seen by comparing Model I with Model II. The small difference is shown in figure 65 and 66, and by comparing figure 39 and 47. The reason why these models are so similar can be explained by the large extent of cracking of the dam bottom in Model I. When enough load is applied, the bottom of the arch part of the dam will be so cracked that it hardly resist additional rotation. A plastic hinge will thus be created, making the fixed boundary more similar to an interface allowing for uplift. This happens when about 60 % of the hydrostatic-pressure is applied, as seen in figure 67.

When avoiding false anchoring/cohesion in the transition from Model III to Model IV, the total displacement response increases with 8.5 %. This is a larger increase than from Model I to Model III, which indicates a great importance of details when modelling the connection between dam and bedrock. It is not immediately apparent that modelling of an interface with a tangential stiffness which vanish when tension occurs, should differ so much from an interface with constant tangential stiffness. However, the constant tangential stiffness restrains some displacement components in the dam bottom, causing a lower displacement response.

The measured results do not coincide with the results in the present work, as seen in figure 65 and 66. This is most likely due to the neglecting of temperature load in the FE-models. The measured results are from the winter of 2011, many years after the construction of the dam. These measurements were chosen since

temperature induced strain/stress will be damped over the years due to cracking [17]. The most recent measurements will thus be least affected by temperature and closest to the results in the present work. It is noted in figure 65 that the mode of the measurement is quite similar to Model IV. This might indicate that the FE-models will converge to the measured displacement. Near the origin in figure 65, the real measured crest displacement has a different angle than the FE-models and the verification model. This is most likely due to extensive cracking between the arch part of the dam and the spillway, making the crest act like a pinned supported arch rather than fixed, at this end. It is likely that this will happen when temperature load is included since cracks near the top of the spillway are already initiated, as seen from figure 64. The mode difference between the FE-models and the measured displacement in the vertical direction, seen from figure 66, is most likely caused by temperature-induced cracking. This cracking is seen initiated in all analyses at the middle of the downstream face of the dam. The cracking here will cause a loss of moment capacity for plate action in the water-pressure direction, giving the measured displacement a bend about 15 meters from the bottom as seen in figure 66. It should be noted that the measurements in figure 65 and 66 had to be extracted from a less accurate figure from Malm et al. [17]. This might lower the accuracy of the measurement curves in the present work.

The simplified analytic model does not show similar displacement response as the FE-models and the real measurement, as seen in figure 65. However, the value of the predicted maximum displacement is about 80 % of Model II. The necessary approximations done in the simplified analytic model is thus too severe to be able to predict the displacement pattern with acceptable accuracy. For instance, the assumption of a symmetric response of the crest is not valid, as seen in figure 65. This is natural since the dam is higher near the spillway than near the support. As a consequence, the peak displacement will shift position from the crest center towards the spillway. Even though the verification model does not show good compliance with the FE-models, the overall displacement mode from the verification can be useful. This is because the verification model shows some similarities with the real response, as seen in figure 38.

8.2 Comparison of stress fields

From figure 69 and 70, it is noted that the differences in the stress fields are mainly local. The global shape and values of the stress field are much similar for all the models. This result is explained by the use of a nonlinear material model. The forces will then be able to redistribute when cracking occurs, such that the effect of boundary conditions and connections will be damped. If a linear analysis had been performed, the differences would probably be substantially larger.

False anchoring/cohesion will affect the stress fields in the dam bottom considerably. This can be seen in figure 70. Here, Model II and III show stress concentration near corners in the bottom of the dam, while Model IV gives a much smoother and continuous stress field. This result is natural, since the parts of the bottom with false cohesion becomes stiffer and will attract load. As a consequence, stress and crack concentrations occur.

The difference in tangential properties of the connection under the dam affects the stress field. If a high linear elastic tangential stiffness between the dam and the bedrock is assumed, the support stress will be transferred more uniformly under the bottom of the dam. This is opposed to the downstream stress concentration that occurs when applying an interface simulating no-slip-contact. The difference in stress at the downstream bottom edge is observed in figure 69. These observations might seem obvious, but a higher redistribution of stresses was expected due to the use of a nonlinear material model, such that the stress distribution in the dam bottom would be similar for all models. However, this redistribution is present in Model I due to extensive cracking of the bottom. This will to some extent make the stress field in the bottom similar in Model I and IV, as seen in figure 69 and 70.

It is noted that many of the stress results show higher principal stresses than the concrete's tensile capacity. This should by definition not occur when using a rotating crack material model. This discrepancy is probably due to extrapolation error of stresses. When the stress fields have a substantial variation between integration points, the nodal values of stresses might be a bit off. This indicates a too coarse mesh in the bottom of the dam since the stress field should preferably not vary so much within a single element.

8.3 Comparison of crack pattern

The crack pattern is mainly locally affected near the connection between the dam and the bedrock. Besides this, all FE-models predict about the same crack pattern. Every model predicts that cracking will occur in the middle of the downstream side of the dam arch and in the crest between the spillway and the dam arch. However, the models show variation in the extent of cracking at these locations.

The inclusion of bedrock does not seem to affect the crack pattern to a notably extent. Model II and III show very similar crack pattern, and the only difference between these models is the inclusion of bedrock. In both models, the largest crack strains occur at the sharp bottom corner, as seen in figures 52 and 58. This is most likely due to false anchoring in both models, as stated in the previous chapter. The only difference between these models is that Model II shows more cracks along the bottom boundary, especially near non-smooth areas. This might be explained by the lack of bedding stiffness in Model II, which tends to make the dam settle on sharp part in the dam boundary where cracks will occur. These non-smooth areas would not be as rigid when there is bedrock underneath, which would allow for a redistribution of forces.

Cohesion between the dam and the bedrock has a substantial effect on the crack pattern near the bottom of the dam arch. Model I has an infinite cohesion, and the bottom attracts forces due to the increased moment capacity about the circumferential axis. When the moment capacity is reached, extensive cracking of the bottom occurs. In Model II and III, the cohesion is lower since the interface does not resist motion in the upward direction normal to the dam bottom. Thus, these models show much lower cracking of the dam bottom, but substantial crack concentrations in corners occur. In Model IV, the cohesion criterion is fulfilled, which almost makes the upstream side of the dam bottom free from cracks. This discussion indicate that the fulfilling of the cohesion criterion is essential for predicting the correct crack pattern in the bottom of the dam arch.

How the support forces are transferred between the dam and the bedrock, have a significant impact on the crack pattern. The contact interface in Model IV will cause most of the support forces to be transferred via a smaller area near the downstream bottom edge of the dam. This will cause more cracking at this area in Model IV compared to Model II and III. However, some of this cracking in Model IV may be caused by constraining forces from the translation constraint. Model II and III will transfer the support forces via a larger area of the dam bottom, due to the linear elastic tangential properties of the interface. This will cause low cracking of the downstream bottom of the dam. The physical problem will be somewhere between these two groups of models, due to the curved bottom of the dam arch. Thus, the idealization of the dam bottom in the geometry input file might not be ideal if the crack pattern of the dam bottom is to be studied.

9 Conclusion

It is concluded that the most realistic model of the dam includes bedrock and a connection between dam and bedrock consisting of interface elements combined with a translation line constraint. The interface elements simulates no-slip-contact, and the translation line constraint is applied between the bedrock and the downstream bottom edge of the dam arch. This model shows that attention to details when modelling the connection between the dam and the bedrock is important. Some unrealistic cohesion causes restraining of the bottom corners of the dam in the less realistic models. This has the most significant impact on the displacement response between all the models, and also causes significant stress and crack concentrations at the dam bottom. In the most realistic model, the false cohesion was avoided by specifying the dam-bedrock connection interface to have no tangential stiffness when tension occurs, instead of using a linear elastic tangential stiffness.

The response effect of the modelling of boundary conditions and connections is significant. The maximum displacement response increased about 17 % from the most simplified to the most realistic model. The local crack pattern and stress field near connections are significantly affected by how the connection is modelled. Unrealistic stress and crack concentrations caused by false anchoring / cohesion is an example of this. Also, the downstream side of the dam bottom shows larger stresses and more extensive cracking in the most realistic model compared to the other models. This is due to the modelling of force transfer between the dam and the bedrock. The effect of boundary conditions and connections on the global response is damped due to the redistribution of forces allowed when using a nonlinear material model. This is observed from the similar stress fields and crack patterns for the models, when disregarding the disturbances near the dam bottom.

The displacement response of the FE-models is verified both with the real measurements of the dam, and a simplified analytic model. The verification model managed to predict the overall displacement mode to some extent, but the accuracy is poorly. However, it showed an 80 % compliance with the maximum displacement from the two least realistic FE-models.

The FE-models predicted accurate displacement modes compared to the measurements of the dam, but the magnitude differed due to the exclusion of temperature load in the present work.

It is concluded that realistic modelling of boundary conditions and connections is of importance when analyzing this dam structure using NLFEA. A recommended procedure is that the most important properties of the physical connections should be listed as criteria for realistic modelling. Further, the results from the FE-model should be checked for compliance with these criteria.

10 Limitations and further research

The main limitation of the present work is that only one dam was analyzed to assess the effect of boundary conditions and connections. If several dams with different geometries were studied, more general conclusions could be drawn. There are also limitations on the loads applied, and dynamic analyses should be performed to see if this would change the results found in this thesis.

Suggestion for further research:

- Contact modelling using the real geometry:

It could be useful to make another model of the dam where the real bottom geometry was included, and contact elements were used between the dam and the bedrock. This was attempted in the present work, but the contact modelling resulted in a fixed connection between dam and bedrock. DIANA support could not find the modelling error, and user information on this subject was challenging to find. Thus, using a connection with no mesh connectivity was not pursued further. An improvement of the DIANA software would be the possibility to alter the connectivity of the interface elements easily, but this is for sure a difficult task.

- Assess the response effect of distorted elements and mesh size:

It could be useful to assess the effect of distorted elements and mesh size on the response variables, especially near the connections. This was a worrying subject in the present work, but was not pursued further due to time limitation.

- Study the necessary amount of bedrock included in the FE-model:

The bedrock is usually a large part of the FE-model when analyzing dam structures. Even though a recommended amount of included bedrock is given in the Energiforsk Guidelines [1], it could be useful to assess the response effect of the amount of bedrock included. The boundary conditions applied to the bedrock would probably also be more important when less bedrock is included.

References

- [1] R. Malm, "GUIDELINES FOR FE ANALYSES OF CONCRETE DAMS", Energiforsk, Sweden, 2016:270, 2016.
- [2] International Commission On Large Dams, *Why do we need dams*, Available: https://www.icold-cigb.org/GB/dams/role_of_dams.asp. Accessed on: Apr. 25, 2019.
- [3] Office of Energy Efficiency and Renewable Energy, *History of Hydropower*, Available: <https://www.energy.gov/eere/water/history-hydropower>. Accessed on: Apr. 25, 2019.
- [4] International Commission On Large Dams, *Dams' safety is at the very origin of the foundation of ICOLD*, Available: https://www.icold-cigb.org/GB/dams/dams_safety.asp. Accessed on: Apr. 25, 2019.
- [5] International Commission on large dams, mission, 2019. Available: <https://www.icold-cigb.org/>. Accessed on: Jan. 21, 2019.
- [6] DIANA FEA, DIANA, 2019. Available: <https://dianafea.com/>. Accessed on: Feb. 12, 2019.
- [7] M. Engen, "Aspects of design of reinforced concrete structures using nonlinear finite element analyses", Dr. Philos., Department of Structural Engineering, Norwegian University of Science and Technology, Trondheim, 2017.
- [8] J.A. Øverli, S.I. Sørensen, *TKT4222 Concrete Structures 3 Compendium*, Norway, NTNU 2018.
- [9] J. Lindemark, E. E. Aasheim, R. O. Mork, T. Bjønnes, "Sarvsfossen Dam - Design of a Norwegian Concrete Arch Dam", Hydropower'15, Norway, 2015.

- [10] Lovdata, *Forskrift om sikkerhet ved vassdragsanlegg*, 2009. Available: <https://lovdata.no/dokument/SF/forskrift/2009-12-18-1600>. Accessed on: Jan. 25, 2019.
- [11] NVE, *About NVE*, 2018. Available: <https://www.nve.no/about-nve/>. Accessed on: Jan. 20, 2019.
- [12] *Eurocode 2: Design of concrete structures - Part 1-1: General rules and rules for buildings*, NS-EN 1992-1-1:2004+A1:2014+NA:2018, Oct. 1, 2018.
- [13] FIB, *Model Code*, 2019. Available: <https://www.fib-international.org/publications/model-codes.html>. Accessed on: Jan. 21, 2019.
- [14] Y. Ghanaat, "Theoretical Manual for Analysis of Arch Dams", US Army Corps of Engineers, Washington DC, USA, 1993, Available: <https://apps.dtic.mil/dtic/tr/fulltext/u2/a269524.pdf>
- [15] R. Malm, M. Hassanzadeh and R. Hellgren, "14th International Benchmark Workshop on Numerical Analysis of Dams, Theme A : Thermal cracking of a concrete arch dam", KTH and ÅF, Stockholm, Sweden, 2017.
- [16] F. Hjalmarsson and F. Petterson, "FINITE ELEMENT ANALYSIS OF CRACKING OF CONCRETE ARCH DAMS DUE TO SEASONAL TEMPERATURE VARIATION", Master thesis, Department of construction sciences, Lund University, Lund, 2017.
- [17] R. Malm, M. Hassanzadeh and R. Hellgren, "Proceedings of the 14th ICOLD International Benchmark Workshop on Numerical Analysis of Dams", presented at the 14th ICOLD International Benchmark Workshop, Stockholm, Sweden, 2018.
- [18] R.D. Cook, D.S. Malkus, M.E. Plesha and R.J. Witt, *Concepts and Application of Finite Element Analysis*, fourth edition. USA: John Wiley & Sons Inc. 2002.

- [19] H.A.W. CORNELISSEN, D.A. HORDIJK and H.W. REINHARDT, "Experimental determination of crack softening characteristics of normalweight and lightweight concrete", 31, no. 2, pp. 45-56, 1986.
- [20] R. Malm, "Shear cracks in concrete structures subjected to in-plane stresses", TRITA-BKN Bulletin 88, Sweden, 2006.
- [21] Vecchio, F. J., and Collins, M. P. The modified compression field theory for reinforced concrete elements subjected to shear. *ACI Journal* 83, no.22, 1986, pp. 219–231.
- [22] DIANA FEA, Delft, The Netherlands. *DIANA User's Manual : Part V Analysis*. (2019) [Online]. Available: <https://dianafea.com/manuals/d103/Diana.html>
- [23] J.G. Rots, J. Blaauwendraad, "CRACK MODELS FOR CONCRETE: DISCRETE OR SMEARED? FIXED, MULTIDIRECTIONAL OR ROTATING?", *Heron*, vol.34, no.1, 1989, Available: <http://heronjournal.nl/34-1/1.pdf>.
- [24] M.A.N. Hendriks, A. de Boer, B. Belletti, "Guidelines for Nonlinear Finite Element Analysis of Concrete Structures", Rijkswaterstaat Centre for Infrastructure, Report RTD:1016-1:2017, 2017.
- [25] K.M. Mathisen, NTNU, TKT4197 Lecture Notes, 2018.
- [26] DIANA FEA, Delft, The Netherlands. *DIANA User's Manual : Part IV Materials*. (2019) [Online]. Available: <https://dianafea.com/manuals/d103/Diana.html>.
- [27] E. Chatzi, "The Finite Element Method for the Analysis of Non-Linear and Dynamic Systems", ETH Lecture Notes, 2015, Available: https://www.ethz.ch/content/dam/ethz/special-interest/baug/ibk/structural-mechanics-dam/education/femII/Lecture4_2015_PartB.pdf. Accessed on: May. 18, 2019.

- [28] K.M. Mathisen, "Solution Methods for Nonlinear Finite Element Analysis (NFEA)", Geilo Winter School, Norway, 2012, Available: <https://www.sintef.no/globalassets/project/evitameeting/2012/kmm-geilo-2012-lecture-11a.pdf>. Accessed on: May. 27, 2019.
- [29] N. Vasilos, Nonlinear Analysis of Structures: The Arc Length Method. Available: <https://scholar.harvard.edu/vasios/links/nonlinear-analysis-structures-arc-length-method>. Accessed on: Feb. 15, 2019.
- [30] The Hong Kong University of Science and Technology, Department of Mechanical and Aerospace Engineering, Lecture Notes on Elastic Foundation, Available: [https://www.mae.ust.hk/meqpsun/Notes/Chapter4\(202\).PDF](https://www.mae.ust.hk/meqpsun/Notes/Chapter4(202).PDF). Accessed on: Feb. 16, 2019.
- [31] R. de Borst, M.A. Crisfield, J.J.C. Remmers and C.V. Verhoosel, Non-Linear Finite Elements Analysis of Solids and Structures, Second edition. United Kingdom: John Wiley & Sons, 2012.
- [32] J. C. J. Schellekens and R. de Borst, "On the numerical integration of interface elements", International Journal for Numerical Methods in Engineering, vol. 36, pp. 43-66. doi: 10.1002/nme.1620360104
- [33] DIANA FEA, Delft, The Netherlands. *DIANA User's Manual : Part III Elements*. (2019) [Online]. Available: <https://dianafea.com/manuals/d103/Diana.html>
- [34] K. Bell, *An engineering Approach to Finite Element Analysis of Linear Structural Mechanics Problems*, 1st ed. Bergen: Akademika Publishing, 2013.
- [35] V.L. Popov, *Contact Mechanics and Friction*, Second Edition, Berlin, Germany, Springer, 2017.
- [36] The Norwegian Water Resources and Energy Directorate, *Retningslinjer for laster og dimensjonering*, 2003.

- [37] Swedish Hydropower companies guidelines for dam safety, application guideline 7.3 Concrete dams. Svensk Energi.
- [38] R. Lie, E. E. Aasheim, M. Engen, "Thermal Cracking of a Concrete Arch Dam", Norway, Multiconsult 2017.
- [39] K.M. Mathisen, NTNU, TKT4192 Lecture Notes, 2018.
- [40] C.L. Dym and H.E. Williams, "Stress and Displacement Estimates for Arches", Journal of structural engineering, vol. 137, no. 1, pp. 49-58, Jan. 2011, doi: 10.1061/(ASCE)ST.1943-541X.0000267.
- [41] S. Timoshenko and S. Woinowsky-Krieger, *Theory of Plates and Shells*, 2nd edition, McGraw-Hill, 1959.
- [42] M.Engen, NTNU, TKT4222 Lecture Notes, 2018.

Appendix

A MATLAB code for the verification model

This appendix contains the MATLAB script of the full calculations for the verification model.

```

close all
clear all
clc

% 2D-idealization of the dam

h= 20;           % Assumed 20 meter height section of dam
t = (3.56+2.5)/2; % Assumed average dam thickness
A = h*t;        % Cross-section area of the arch
a = (170/110)/2; % Half of opening angle of the arch
r = 110;        % Radius of arch part of the dam
E = 33*10^9;    % Young's modulus of linear B30 concrete
I = (1/12)*h*t^3; % Second moment of area

q = 200000 + 9.81*1000*20*20*1/2; % Load on the dam section treated as
% a line load

% Necessary Constants

I_s = I/(A*(r^2)); % Introduced calculation constant

% Clamped arch constants determined from boundary conditions
Dc = a^2 + a*sin(a)*cos(a)+cos(2*a) - 1 + I_s*(a^2 + a*sin(a)*cos(a));
C1_c = -(2*I_s*a*sin(a))/(Dc);
C2_c = -(2*I_s*(sin(a))^2)/Dc;
C3_c = -((1+I_s)*(a*sin(a)+(a^2)*cos(a)))/Dc;

% Define range of the arch angle
theta = linspace(-a, a);

% Horizontal shape function of the dam
w_H = ((q*r^4)/(E*I))*(((1+I_s)/2)*theta.*sin(theta))*C1_c-C2_c
+I_s*cos(theta)*C3_c+I_s);

% Maximum radial displacement:
Rad_Disp_Max = ((q*r^4)/(E*I))*(((1+I_s)/2)*0*sin(0))*C1_c-C2_c
+I_s*cos(0)*C3_c+I_s);

% 2D polar plot of crest displacement
M_2D = 1000; % Magnification factor
rho=110-M_2D*w_H; % Deformed radius
figure(1)
polarplot(theta,rho)
hold on
rho=110-M_2D*w_H+M_2D*w_H; % Undeformed radius
polarplot(theta,rho)
title('2D Deformation Mode')
grid on

%
%
```

```

% 2D plot of crest displacement
figure(2)
Rad_Disp_Crest=((q*r^4)/(E*I))*(((1+I_s)/2)*theta.*sin(theta))*C1_c -
C2_c+I_s*cos(theta)*C3_c+I_s);
plot(theta*r, Rad_Disp_Crest)
title('Crest Displacement')
xlabel('Crest length from center (m)')
ylabel('Displacement (m)')
grid on

% 2D plot of radial displacement along a centered vertical section
figure(3)
Height=linspace(0,37); % Assumed 37 m height
% Vertical shape function from plate-theory regression:
Rad_Disp_Vertical=(-0.0496*Height.*Height+2.8313*Height)*1/37;
plot(Rad_Disp_Vertical*Rad_Disp_Max, Height)
title('Displacement Vertical Section')
xlabel('Displacement (m)')
ylabel('Dam Height (m)')
grid on

% 3D plot of displacement in circular coordinates
[n, m] = size(r);
HEIGHT_Z = 30; % Approximated height of the dam when considered
               % uniform

z = linspace(0, HEIGHT_Z, length(theta));
[THETA, Z] = meshgrid(theta, z);

% Vertical shape function of the dam from plate-theory regression
w_v = -0.0573*Z.*Z+2.9467*Z; % Assumed an average height of 30 m

%Magnification factor of arch displacement;
M_3D = 10;

R = r*ones(size(Z));
figure(4)
surf(R.*cos(THETA), R.*sin(THETA), Z)
alpha(0.1)
hold on

R = r*ones(size(Z)) + M_3D*repmat(-w_H, length(Z), 1).*(w_v);
surf(R.*cos(THETA), R.*sin(THETA), Z)

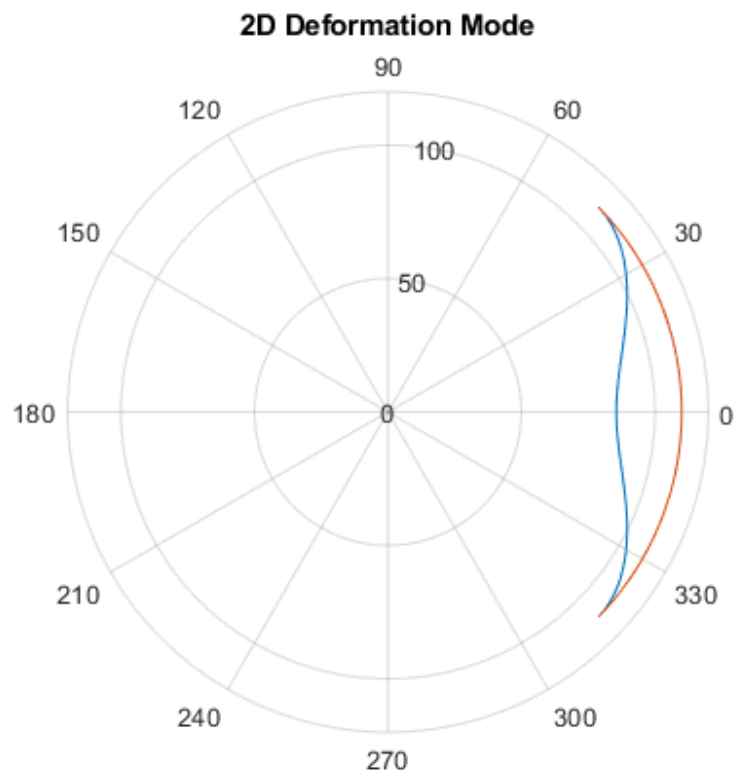
xlim([60 120])
title('3D Deformation Mode')

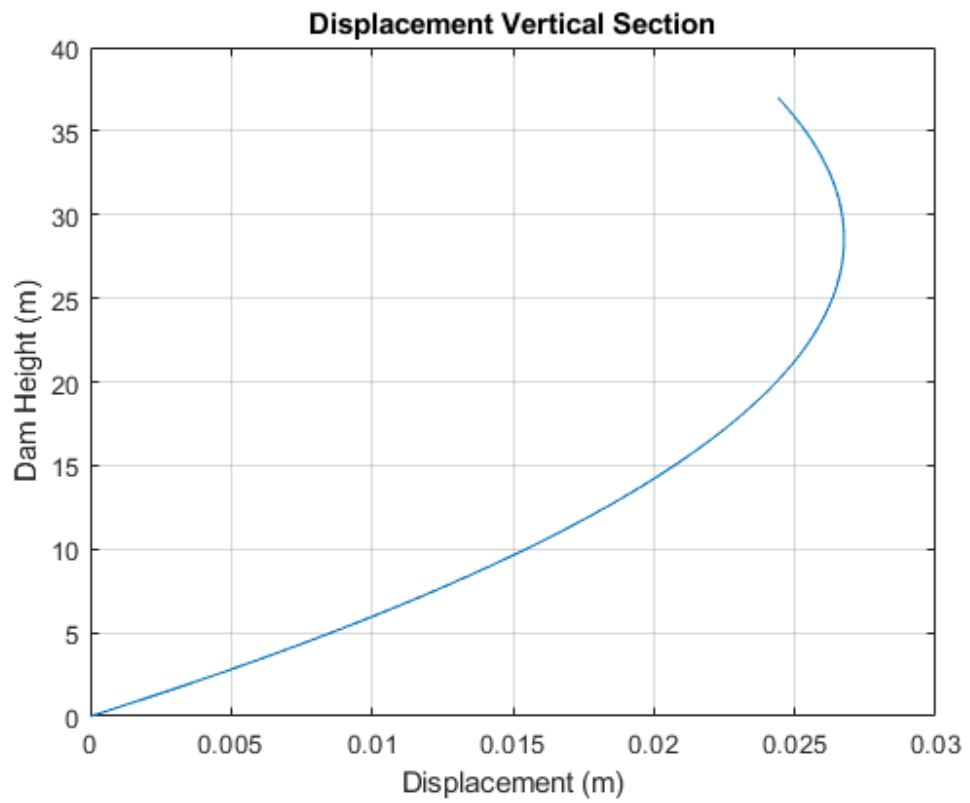
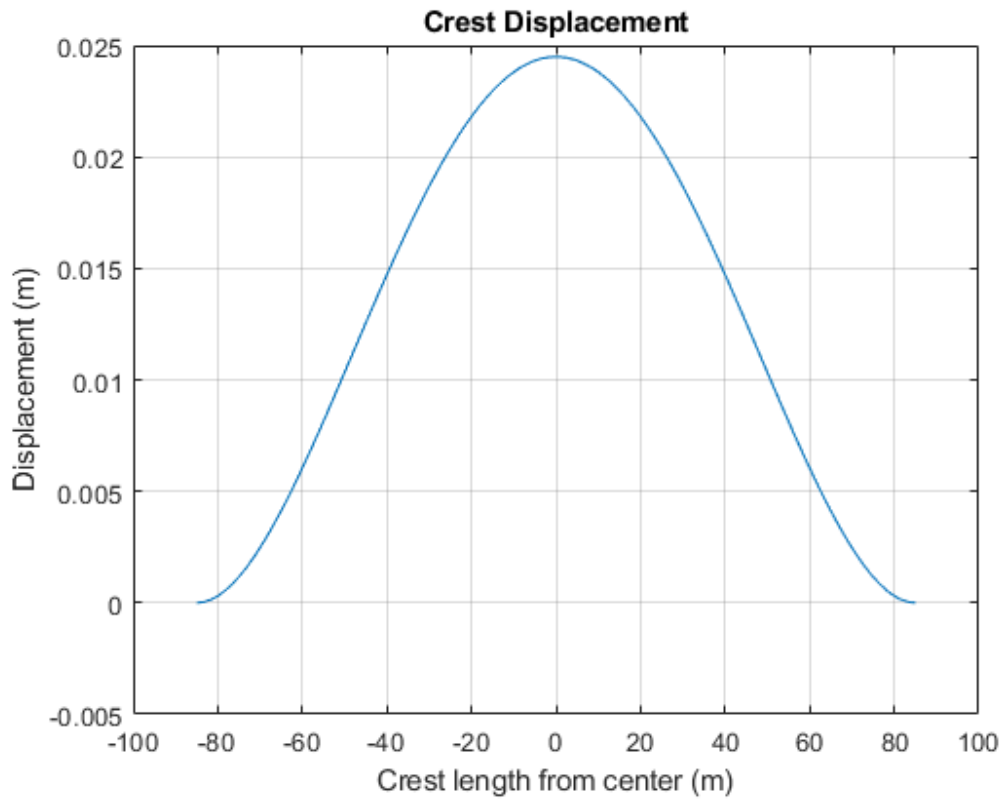
%
%

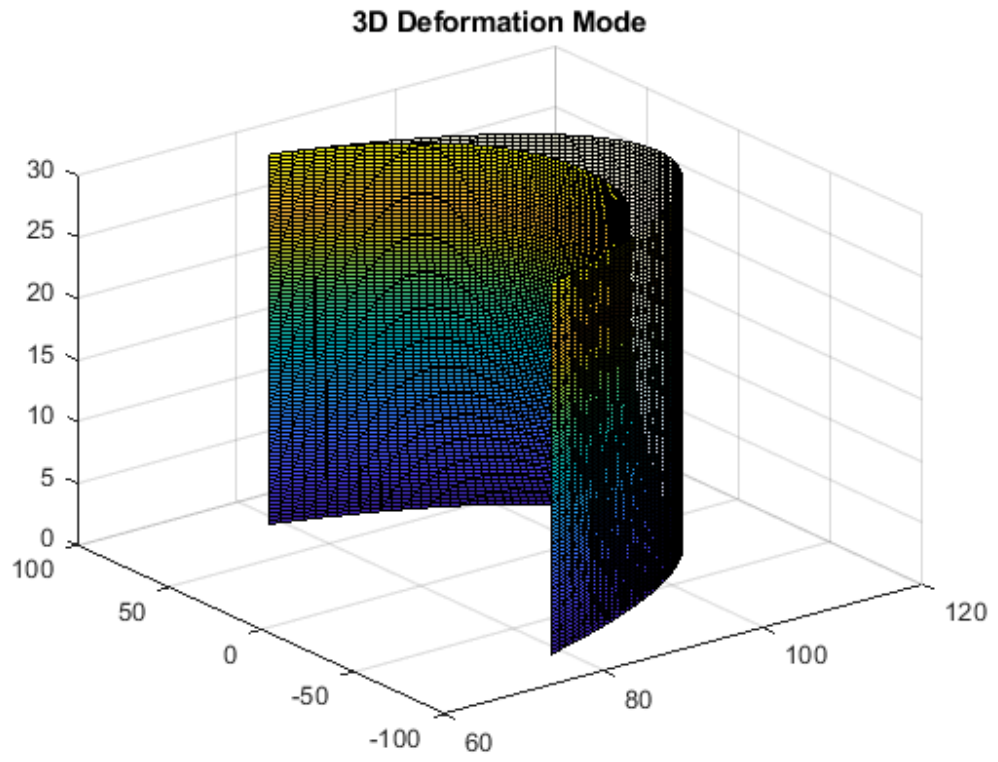
Rad_Disp_Max =

0.0245

```





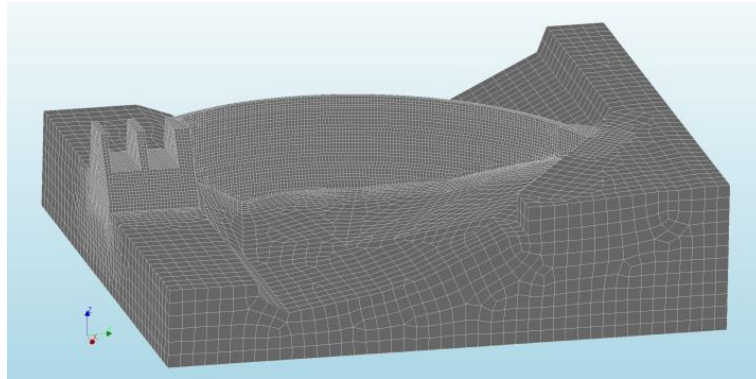


Published with MATLAB® R2018a

B DIANA Users Meeting presentation

This appendix contains a presentation of the present work, held at the DIANA International Users Meeting in Trondheim 23.05.2019.

Effect of boundary conditions and connections in NLFEA of a concrete dam



Master Thesis 2019

by

Lorents Flygansvær and Mathias Berg Rønning



1

Problem description and approach

- Importance of realistic modelling of concrete dams
- Emphasis on boundary conditions and connections when performing a NLFEA
- FE-models with increasing compliance with the physical problem
- Effect on displacement-, crack-, and stress response of the dam

2

ICOLD dam

- 14th ICOLD Benchmark Theme A
- Geometry files provided
- Idealized dam bottom in the geometry files

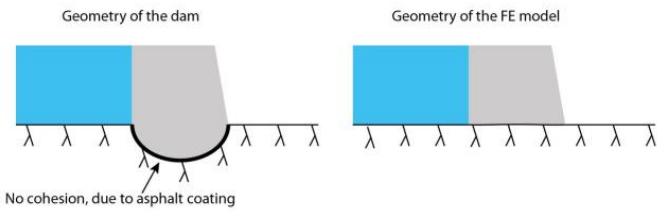


Figure: Malm, Hellgren, Ekstrøm and Fu 2017

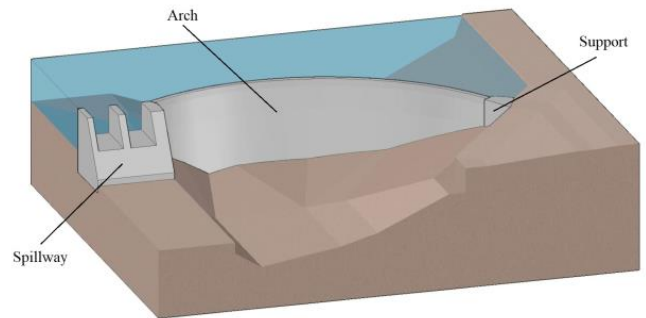
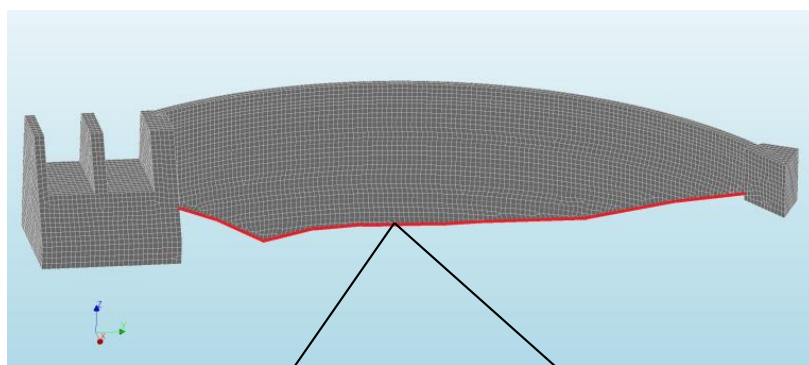


Figure: Hjalmarsson and Petterson 2017

3

The FE-models in DIANA (I and II)

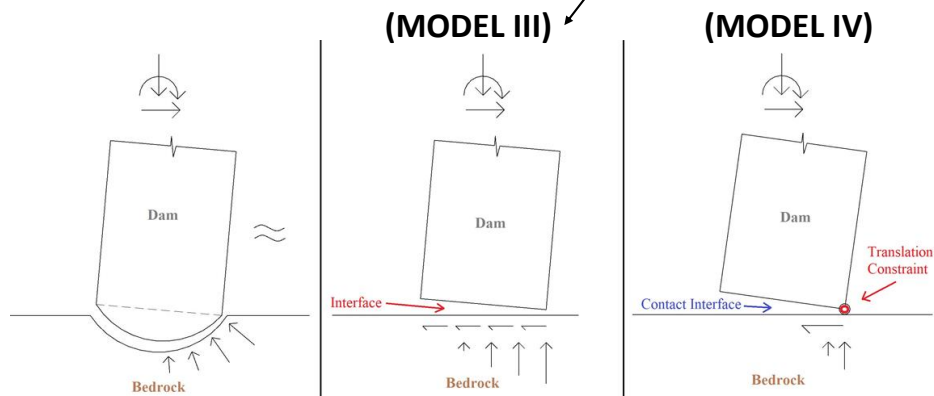
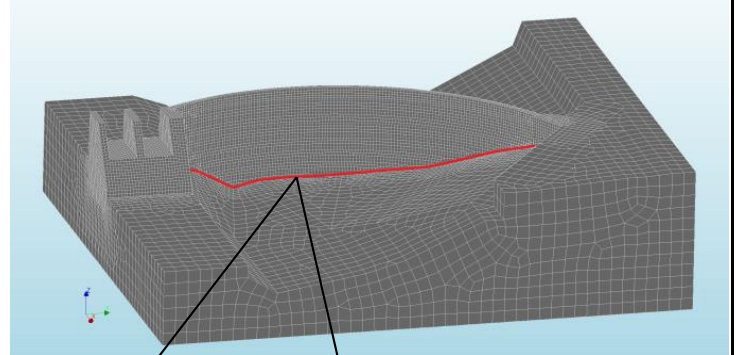


Fixed Boundary
(MODEL I)

Boundary Interface
(MODEL II)

4

The FE-models in DIANA (III and IV)



5

Common properties of the FE-models

- Loads: Selfweight, hydrostatic pressure and ice load (Loadsteps: 1+10+4)
- Material model: Smearred cracking and crushing, FIB Model Code 2010
- Reinforcement: Grids, elasto-plastic material model
- Element type: CHX60 (20-node solid element)
- Numerical solution method: Regular Newton-Raphson

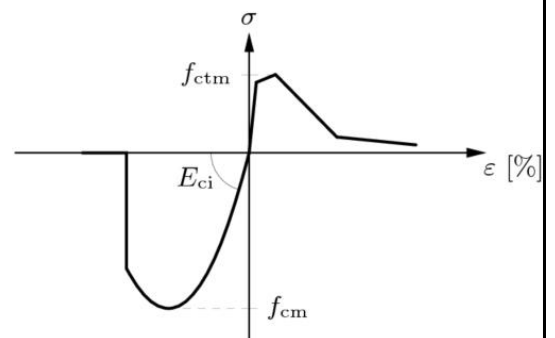
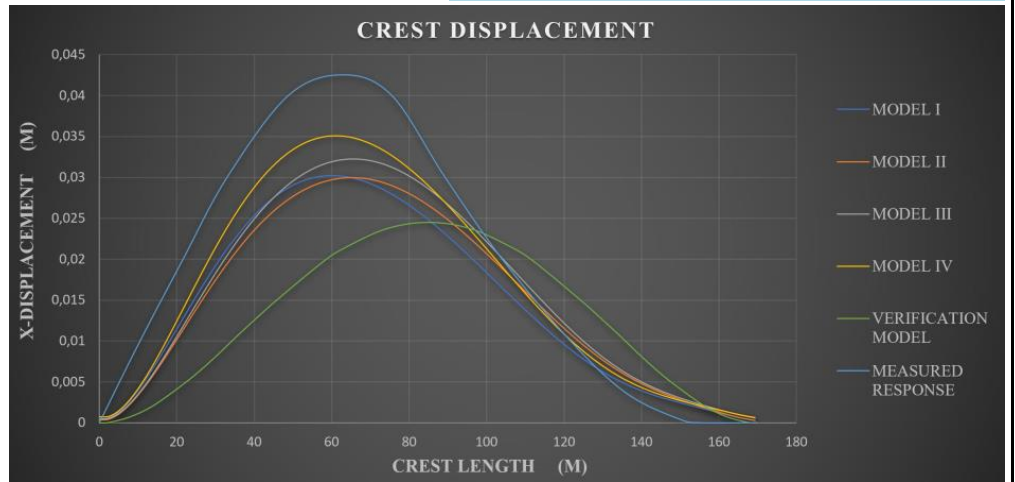
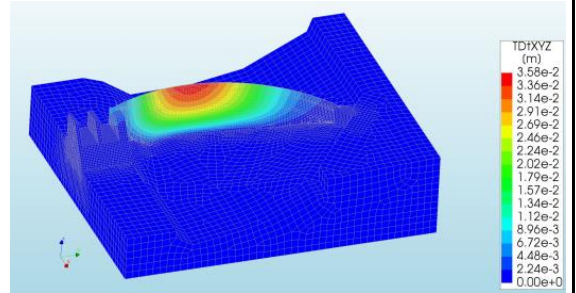


Figure: DIANA users manual

6

Difference in displacement response

- Importance of dam-bedrock connection
- Deviating measurements
- Verification model too idealized
- Redistribution of forces damp the effect

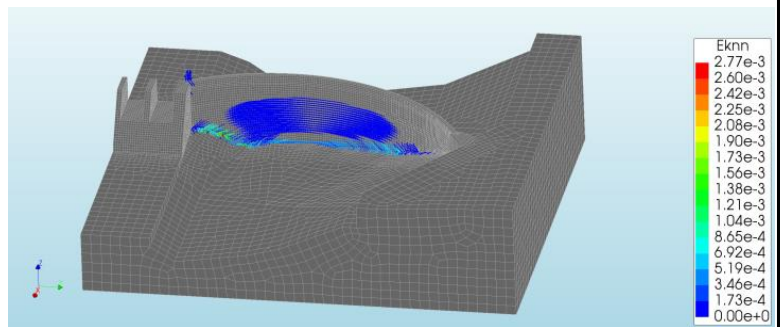


7

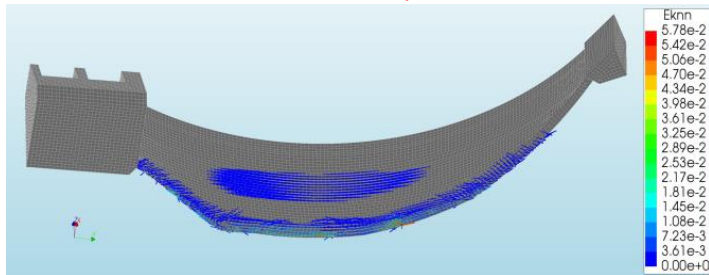
Difference in crack pattern

- Crack pattern depends on connection properties, mainly local variations
- Lowest crack strain value for the most realistic model

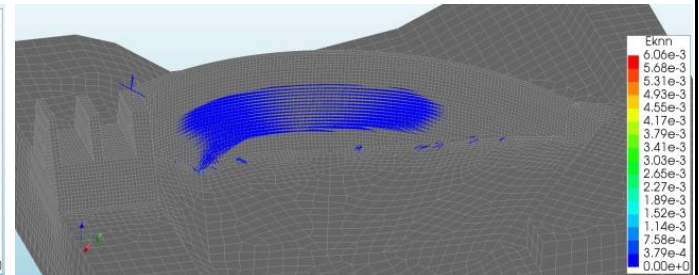
Bedrock Contact Interface + Translation Constraint (IV)



Fixed Boundary (I)



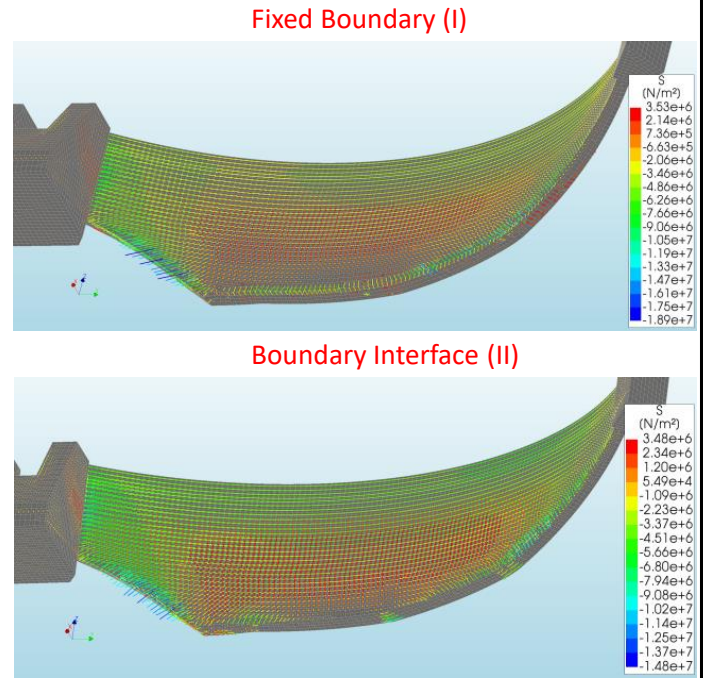
Bedrock Interface (III)



8

Difference in stress field

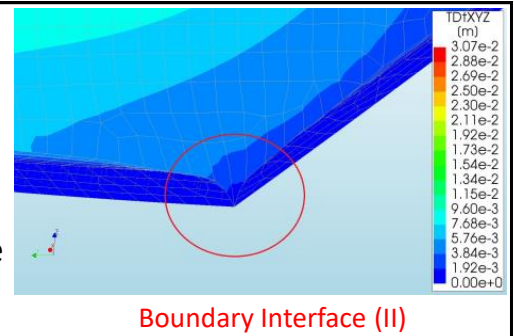
- Local effects more than global
- Difference in force transfer between dam and support/bedrock
- Model I and Model IV similar in the bottom



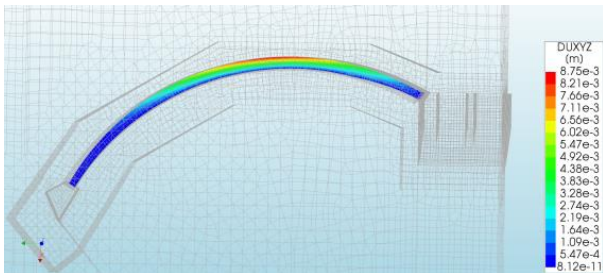
9

Unintended cohesion

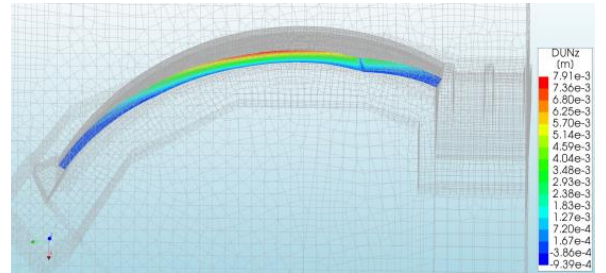
- Bracing displacement components
- Largest impact on the displacement response, 8 % increase
- Cause false stress- and corresponding crack concentrations
- Avoided in Model IV



Bedrock Contact Interface + Translation Constraint (IV)



Bedrock Interface (III)








10

Conclusions

- Displacement response increased 17 %
- Stress- and crack response mainly locally affected
- Avoid unrealistic cohesion
- Interface simulating no-slip-contact + translation line constraint is preferred in this case
- Make criteria for realistic modelling based on the physical problem

11

Our experience with DIANA

- Excellent definition of interfaces 
- Make real contact formulation as easy as interface formulation 
- Problem snapping when cutting geometry 
- Massive improvement of geometry import from 10.2 to 10.3 
- Safe software to use; user is made aware of important aspects 

12

Thank you for your attention!

